The six-bank multi-leaf system

A large field size, high resolution collimator for advanced radiotherapy

Rajko Topolnjak

Colofon:
This text was set using the freely available LaTeX 2_ε typesetting and text formatting system. The line drawings were made using the freely available Xfig program.

ISBN-10: 90-393-4363-2
ISBN-13: 978-90-393-4363-0
Druk: PrintPartners Ipskamp, Enschede

The six-bank multi-leaf system

A large field size, high resolution collimator for advanced radiotherapy

Het zes-bank multi-leaf systeem

Een collimator voor grote velden, en een hoge resolutie ten behoeve van geavanceerde radiotherapie

(met een samenvatting in het Nederlands)

Proefschrift ter verkrijging van de graad van doctor aan de Universiteit Utrecht
op gezag van de Rector Magnificus, prof. dr. W.H. Gispen
ingevolge het besluit van het college voor promoties
in het openbaar te verdedigen
op dinsdag 17 oktober 2006 des middags te 2:30 uur

door
Rajko Topolnjak
geboren op 25 januari 1974 te Zagreb, Kroatië

promotor:	Prof. dr. ir. J.J.W. Lagendijk Faculteit der Geneeskunde, Universiteit Utrecht
co-promotor:	Dr. U.A. van der Heide Faculteit der Geneeskunde, Universiteit Utrecht

Het beschreven werk werd verricht op de afdeling Radiotherapie van het Universitair Medisch Centrum Utrecht, participerend in het Image Sciences Institute en de onderzoekschool voor biomedische beeldwetenschappen ImagO en werd mogelijk gemaakt met financiële steun van Elekta Ltd. Deze uitgave is tot stand gekomen met financiële steun van ImagO en Elekta Ltd, Crawley, UK.

to Ivana and Ema

Contents

Chapter 1

General introduction

1.1 New developments in radiotherapy

The quality of radiotherapy for treating patients with cancer has improved significantly in the past couple of years due to technological developments in three areas. The use of multiple imaging modalities make it possible to visualize the tumor and define the target for irradiation. With intensity-modulated radiotherapy (IMRT) a dose distribution can be tailored to this target volume and with improved position verification technology it is guaranteed that the dose is indeed deposited in the right place.

Before the radiotherapy treatment, it is important to know the exact boundaries of volume to be irradiated. Therefore, the regions of interest (ROIs), such as target volumes and organs at risk (OAR) are delineated on a planning computer tomography (CT). This is particularly important for IMRT, because with this technique the dose distribution is shaped accurately around the target volumes. Consequently, if the targets and organs at risk are not delineated correctly, (Austin-Seymour *et al.*, 1995), the dose distribution will be inappropriate for the patient.

CT is most commonly used for radiotherapy treatment planning, but magnetic resonance imaging (MRI) is of increasing importance (Huch Böni *et al.*, 1996; Cruz *et al.*, 2002). The advantage of MRI is its good soft tissue contrast. CT provides information on the electron density and is therefore necessary for dose calculation.

Magnetic resonance spectroscopy (MRS) and positron emission tomography (PET) have the potential to characterize the tumor and provide information

about the tumor metabolism (Ling *et al.*, 2000). Application of multiple imaging modalities and subsequent registration of the obtained images, enables clinicians to define targets with higher reliability. This may lead to a reduction of margins around the target volumes and prescription of higher doses (Mohan *et al.*, 2000; Zelefsky *et al.*, 2000; Nederveen *et al.*, 2001; Vicini *et al.*, 2001) to certain parts of the target. At the same time, the organs at risk can be spared better.

With IMRT it is possible to shape the dose distribution to the anatomical and biological characteristics of the tumor, a concept called dose painting (Ling *et al.*, 2000; Webb, 2001b). To this end a non-uniform beam intensity is used. This variation in intensity can be achieved by using compensators that attenuate the beam at specific positions, or by using a multi-leaf collimator (MLC) with which a sequence of irregular field shapes can be delivered (Jordan and Williams, 1994; Galvin *et al.*, 1993b; Das *et al.*, 1998).

Determining the optimal way of modulating the radiation beams for IMRT is generally done by inverse treatment planning (ITP). ITP works backward through the complex range of radiation delivery options. The most important inputs for ITP are number of beams, their orientations, ROIs and prescriptions to the ROIs. The output is the calculated dose to the ROIs and a description of the treatment fields (beam segments) which have to be delivered.

The final important step in radiotherapy treatment is position verification during the therapy. To avoid underdosing the target volume due to geometrical uncertainties (Jaffray *et al.*, 1999; Langen and Jones, 2001) it is common practice to apply a margin around the target volume. A drawback of this approach is that healthy tissue is irradiated as well. To deliver the dose to the correct location it is essential that positions of the target(s) and OAR(s) during the treatment are the same as on the IMRT plan.

Stroom *et al.* (1999) and Van Herk *et al.* (2000) presented a 'margin recipe' in which the relation between random and systematic positioning errors and the required margin was established. In order to minimize the size of these margins in particular the systematic positioning uncertainty must be reduced as much as possible.

In adaptive radiotherapy (ART)(Martinez *et al.* (2001)) the target motion and systematic variation in patient setup is estimated by daily imaging during the

first few treatments fractions. Subsequently, a new treatment plan is made in which an individual margin is applied that encompasses the positions found in these treatment fractions.

Imaging during the treatment fraction has the possibility to recognize changes in patient anatomy due to internal organ motion. If the imaging technique provides sufficient soft-tissue contrast also the response of the tumor to the treatment can be observed. This approach is called image-guided radiotherapy (IGRT) and its potential is being explored clinically to date using a cone-beam CT mounted on an accelerator (Jaffray *et al.*, 2002) and with the tomotherapy system (Mackie *et al.*, 1993). Raaymakers *et al.* (2004) are working to integrate an MRI system with a linear accelerator so use the superior soft-tissue contrast of an MRI for treatment guidance in radiotherapy.

1.2 Design equipment

Technological improvements in design of linear accelerators have made IMRT and IGRT possible. Nevertheless, many linacs that are currently used have not been designed specifically for this purpose. In this paragraph we describe the available equipment for IMRT and IGRT and discuss possible improvements that would benefit the quality of the treatment.

1.2.1 Linear accelerator and multi-leaf collimator (MLC)

A linear accelerator (linac)(Khan, 1994) is the most commonly used device for treatment of patients with cancer in external beam radiotherapy (EBRT). The Linac delivers a high-energy ionization radiation (photons or electrons) to the region of the patient's tumor. The absorption of radiation in the treated area damages the diseased cells.

To minimize irradiation of healthy tissue beams should be shaped. Commonly, this is achieved by using an MLC. The MLC (Jordan and Williams, 1994; Galvin *et al.*, 1993b; Das *et al.*, 1998) is located in Linac's treatment head and is composed of computer controlled tungsten leaves. The various types of MLCs that are currently available commercially have different leaf widths and number of leaves. Originally, they have been introduced as a substitute for alloy block field shaping. Now, they are used for intensity modulated radiotherapy

as well. With an MLC IMRT can be performed in two ways (Chui *et al.*, 2001). A step-and-shoot approach of delivering IMRT can be applied (Bortfeld *et al.*, 1994; Webb, 2001b). This usually produces a big number of segments. Therefore, MLCs should be capable of delivering many segments quickly. A second approach is dynamic IMRT. Here, the MLC leaves need to allow fast movement and accurate positioning.

MLCs typically have leaves of 1 cm width projected at the isocenter and can produce a maximum field size of 40 x 40 cm^2 (Jordan and Williams, 1994; Galvin *et al.*, 1993b; Das *et al.*, 1998). While the field size is sufficient for most treatments, the leaf width limits the precision at which fields can be shaped. By introducing add-on mini-MLC (Meeks *et al.*, 1999; Xia *et al.*, 1999; Cosgrove *et al.*, 1999; Hartmann and Föhlisch, 2002) with leaf widths ranging from 1.6 to 4.5 mm at isocenter, the problem of undulations is decreased. However, a drawback is that none of them can achieve field sizes larger than 10 x 12 cm^2. Varian produces an MLC with 60 leaf pairs and a field size of 40 x 40 cm^2. In the central 20 cm of the field the leaf width is 0.5 mm while in the outer 10 cm on both sides of the field the leaf width is 1 cm. With such a design a high resolution is achieved in the central part of the field, but unfortunately not in the outer part. Elekta produces a mini-MLC integrated in the accelerator head with 40 leaf pairs and a field size of 16 x 21 cm^2. The maximum field size of the mini-MLCs is reduced because, at maximum overtravel and a 'horizontal' position the leaves may bend under their weight. The displacement is proportional to the fourth power of overtravel and inversely proportional to the square of the leaf width (Shigley and Mischke, 1989). Thus, by using 0.4 cm leaves rather than 1 cm the maximum overtravel for the leaf would be decreased by a factor 0.63 without increasing the inter-leaf distance. It is important to find the optimal balance between field size and leaf width.

Figure 1.1 shows an MLC manufactured by Elekta Ltd, Crawley, UK.

1.2.2 MRI-linear accelerator

From the currently available imaging modalities the MRI scanner has the best performance in soft tissue contrast. This is important in defining tumor boundaries relative to surrounding healthy tissue. Moreover, MRI and MRS can characterize the tumor itself. Hypoxia, vascularity or blood flow inside the tumor can be investigated and characterized.

Figure 1.1: The multi-leaf collimator manufactured by Elekta Ltd. (From Elekta website.)

From a clinical point of view having a precise on-line, soft-tissue based position verification system for IGRT would be greatly beneficial. The feasibility of integrating MRI system with a linear accelerator has been investigated by Lagendijk and Bakker (2000); Lagendijk *et al.* (2002); Raaymakers *et al.* (2002, 2003, 2004). Figure 1.2(a) shows an illustration of an integrated MRI accelerator. The system combines a 1.5 T MRI scanner and single energy (6 MV) radiotherapy accelerator rotating around it. Figure 1.2(b) shows a schematic view of such a system.

1.2.3 A six-bank multi-leaf system

We propose an alternative design for an MLC. The idea comes from the project at our department of integrating an MRI system with a linear accelerator. Figure 1.2(b) shows a schematic view of such a system. The space available for an MLC is small and the currently available MLCs are not compact enough or they do not have the necessary performance specifications.

The six-bank MLC is an alternative design of a multi-leaf collimator that combines high-resolution field shaping with a large field size. The system consists of three layers of bank pairs, positioned at 60^o relative to each other. The

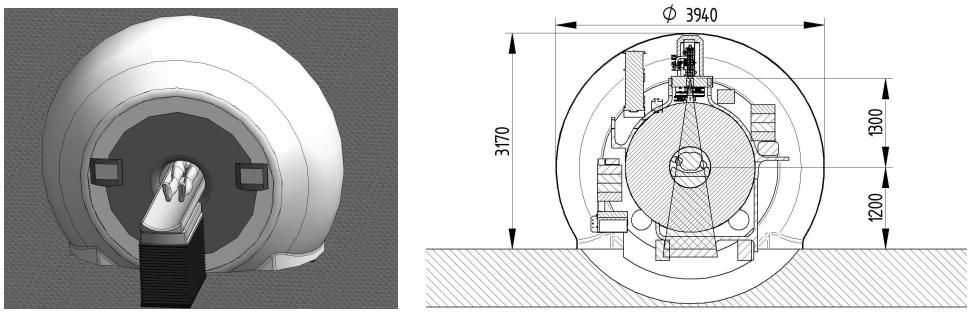

(a) (b)

Figure 1.2: (a) An illustration and (b) a schematic view of a MRI-linear accelerator.

bank pairs each have 40 single-focussed leaves with a standard 1 cm width at isocenter. With the three layers of leaf banks a field-shaping precision can be achieved comparable to that of mini-MLCs with a leaf width of 4 mm at isocenter. The distance between the leaves and the source vary for each layer, which will as a consequence produce a different geometric penumbra. Furthermore, by varying the leaf thickness the influence on transmission penumbra can be made in order to have the same total penumbra for each layer.

Although, the initial idea was to make MLC suitable for MRI-accelerator only, the MLC was developed further as a multipurpose MLC available for any Linac. It could be used as a conventional 1 cm leaf width MLC or as a mini-MLC. Furthermore, a six-bank MLC will have small transmission, and its compact size will allow more clearance for the patient. Collimator rotation would not be required and it will not suffer from the small maximal field sizes of conventional mini-MLCs. Figure 1.3 shows a six-bank MLC.

1.3 This thesis

1.3.1 Purpose

The purpose of this thesis is to investigate if linac/MLC design can be improved to achieve a better radiotherapy treatment of cancer patients. We will

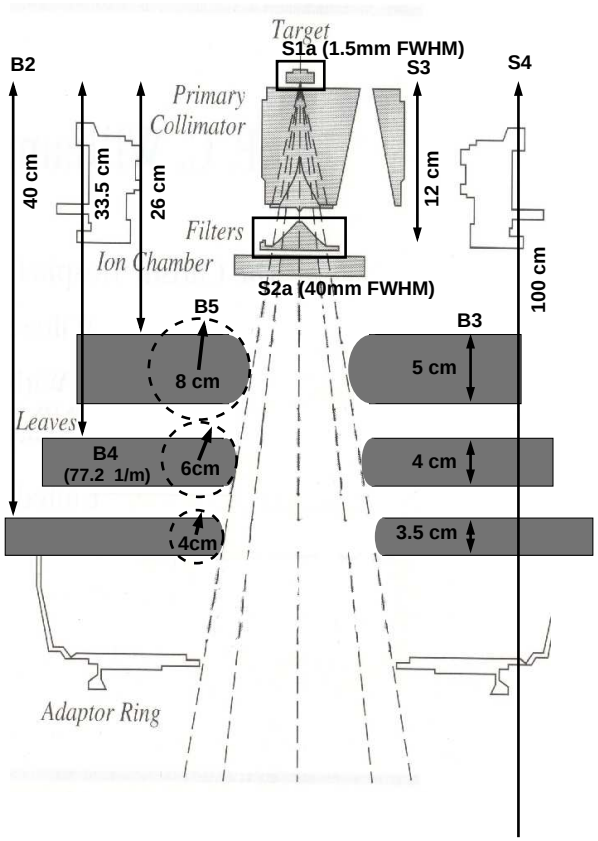

Figure 1.3: Schematic view of the six-bank MLC system and the computer simulation parameters from the lateral view (all parameters are listed in table 3.1).

examine which design parameters are the most important. Finally, we will propose a new design of MLC and investigate its feasibility.

1.3.2 Outline

In **chapter 2** we characterize and quantify the impact of linac/MLC design parameters on IMRT treatment plans. The investigated parameters were: leaf width in the MLC, leaf transmission related to the thickness of the leaves, and penumbra related primarily to the source size. We used CT scans from head-and-neck cancer patients. For each patient treatment plans were made with a different set of linac/MLC parameters. A hypothetical ideal linac/MLC was

introduced to investigate the influence of one parameter at the time without the interaction with other parameters. As a reference to clinical practice, we also optimized the plans with the clinically used Elekta SLi15.

In **chapter 3** we present a design of an alternative multi-leaf collimator, called a six-bank MLC, that combines high-resolution field shaping with a large field size. The six-bank collimator will enable shaping fields of about 40 cm diameter, with a precision comparable to that of existing mini-MLCs with a leaf width of 4 mm.

For the six-bank MLC which would function as a multi-purpose collimator, suitable for all types of treatments, it is important that IMRT can be delivered as well. **Chapter 4** presents a sequencer for delivering step-and-shoot IMRT using a six-bank MLC. Two methods for delivering IMRT with a six-bank MLC were developed. In a low-resolution mode similar segments can be delivered as with a conventional two-bank MLC with a leaf width of 1 cm. The performance in high-resolution mode is comparable to that of a mini-MLC with a leaf width of 4 mm, but a trade-off had to be made between accuracy and number of segments.

Chapter 5 presents an analytical model of an optimal MLC leaf design for a given setup of parameters. This was of importance because the six-bank MLC consists of three layers of two opposing leaf banks. The leaves in the banks that are closest to the source produce the largest geometric penumbra. This effect was compensated by reducing the transmission penumbra of the higher banks.

Summary and general discussion are presented in **chapter 6**. Here, we discuss benefit of using different Linac design on IMRT. We summarize the performance and characteristics of a six-bank MLC and IMRT sequencer developed for it. Finally, the analytical model for leaf design is discussed.

Chapter 2

Influence of the Linac design on intensity-modulated radiotherapy of head-and-neck plans

This chapter has been submitted as:
R. Topolnjak, U. A. van der Heide, G.J. Meijer, B. van Asselen, C. P. J. Raaijmakers and J. J. W. Lagendijk. Influence of the Linac design on intensity-modulated radiotherapy of head-and-neck plans.

Abstract
In this study, we quantify the impact of linac/MLC design parameters on IMRT treatment plans. The investigated parameters were: leaf width in the MLC, leaf transmission, related to the thickness of the leaves, and penumbra related primarily to the source size. Seven head-and-neck patients with stage T1-T3N0-N2cM0 oropharyngeal cancer were studied. For each patient nine plans were made with a different set of linac/MLC parameters. The plans were optimized in Pinnacle^3 v7.6c and PLATO RTS v2.6.4, ITP v1.1.8. A hypothetical ideal linac/MLC was introduced to investigate the influence of one parameter at the time without interaction of other parameters. When any of the three parameters was increased from the ideal setup values (leaf width 2.5 mm, transmission 0%, penumbra 3 mm), the mean dose to the parotid glands increased, given the same tumor coverage. The largest increase was found for increasing leaf transmission. The investigation showed that by changing more than one parameter of the ideal linac/MLC setup, the increase in the mean dose was smaller than the sum of dose increments for each parameter separately. As a reference to clinical practice, we also optimized the plans of the seven patients with the clinically used Elekta SLi 15, equipped with a standard MLC with a leaf width of 10 mm. As compared to the ideal linac this resulted in an increase of the average dose to the parotid glands of 5.8 Gy.

2.1 Introduction

A novel approach of delivering intensity-modulated radiotherapy (IMRT) is known as rotation IMRT or dynamic helical tomotherapy as presented by Mackie *et al.* (1993). The system is equipped with a multi-leaf collimator with leaves of 6.25 mm width and 10 cm thickness. Van Vulpen *et al.* (2005) compared step-and-shoot IMRT delivered by a conventional MLC with dynamic helical tomotherapy IMRT plans for patients with head-and-neck cancer. The results showed that the mean dose to the parotid glands can be reduced with about 6.5 Gy by using the tomotherapy system. This raises the question as to what is the influence of the linac/MLC design parameters on IMRT.

Several authors investigated the effect of the leaf width on IMRT plans (Fiveash *et al.*, 2002; Burmeister *et al.*, 2004; Leal *et al.*, 2004; Wang *et al.*, 2004, 2005; Nill *et al.*, 2005; Zhu *et al.*, 2005). An overall conclusion is that when the size of the target is small, it is beneficial to use MLCs with smaller leaf width. By using sampling theory Bortfeld *et al.* (2000) showed that optimum leaf width is 1.5-1.8 mm for the leaves without transmission.

The main purpose of this study is to extend the investigation of linac/MLC design to the impact of MLC leaf thickness and source size. As the starting point we chose a hypothetical ideal linac. By increasing the MLC leaf width and the source size, and by decreasing the MLC leaf thickness the impact of these parameters on the IMRT plans was characterized.

In this planing study CT scans of seven head-and-neck patients with stage T1-T3N0-N2cM0 oropharyngeal cancer were used. The first reason for this choice is that head-and-neck patients are complex and the dose requirements are challenging because of the variation in target dose and the overlap of targets with organs at risk (OAR). Secondly, five patients from our group of seven were already investigated (Van Vulpen *et al.*, 2005), which gave us the opportunity to compare our results with that study.

Two treatment planning systems (TPSs) have been used so that the bias of specific planning system on the results could be minimized. Computations were made on both Pinnacle^3 v7.6c (Philips Medical Systems, Best, The Netherlands) and on PLATO RTS v2.6.4 (Nucletron BV, Veenendaal, The Netherlands).

2.2 Methods and Materials

2.2.1 Patients

Seven head-and-neck patients with stage T1-T3N0-N2cM0 oropharyngeal cancer were studied. A planning CT scan (Philips Aura) with 3 mm slice thickness was made and CT-images were transformed to the treatment planing system (TPS).

The regions of interest (ROI) were split in two groups: the targets and the organs at risk (OAR). The primary tumor GTV_{prim}, the positive lymph nodes GTV_{nodes} and a volume for elective irradiation of lymph nodes were contoured by a physician as targets. $CTV_{prim/nodes}$ were defined at 10 mm around the $GTV_{prim/nodes}$. Organs at risks were the parotid glands and the spinal cord.

Five patients from our group of seven were already investigated in another study (Van Vulpen *et al.*, 2005). Two of them had positive lymph nodes on both sides and three on only one side. Two patients without positive lymph nodes were added to the investigation to obtain a complete range of indications.

2.2.2 Plan criteria

According to the protocol used clinically at our department, a dose of 66 Gy was prescribed to the $PTV_{66(prim/nodes)}$, extending 5 mm around the $CTV_{prim/nodes}$. The dose was boosted further to 69 Gy in the $PTV_{69(prim/nodes)}$, extending 5 mm around the $GTV_{prim/nodes}$. For the elective lymph nodes a dose of 54 Gy was prescribed to the $PTV_{54(elec.\ nodes)}$, extending 5 mm around the $CTV_{elec.\ nodes}$. Figure 2.1 shows the OARs, targets and the prescription to the targets for one patient.

In our investigation the mean dose to the parotid glands (Eisbruch *et al.*, 1999; Roesink *et al.*, 2001) was used as the quantitative measure for sparing of OARs and minimized as much as possible. In addition, the maximum volume of the spinal cord which received more than 46 Gy had to be smaller than 2 cc and care was taken to avoid 'hot spots' in the body. Because the $PTV_{54(elec.\ nodes)}$ and the parotid glands were overlapping, a trade-off between target coverage and parotid gland sparing had to be made. In order to quantitatively compare plans, hard constraints were imposed on the target coverage: 99% of the target

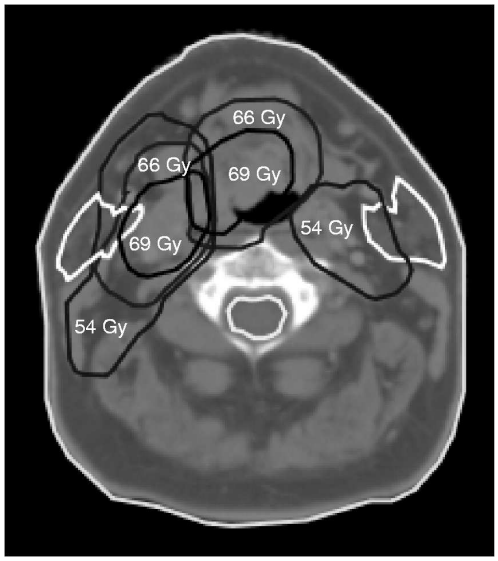

Figure 2.1: The ROIs for one patient. The prescribed dose to the primary tumor and positive lymph nodes in the boost region was 69 Gy, and 66 Gy elsewhere. For the elective lymph nodes the prescribed dose was 54 Gy. Note the overlap of the targets with parotid glands.

volume had to receive at least 95% of the prescribed dose. The volume that received more than 107% of the prescribed dose should be smaller than 2 cc.

With this procedure we had a well defined target coverage for all plans, so that the mean dose to the parotid glands could be used as a quantitative measure for comparing the plans.

2.2.3 Inverse treatment planning

The planning was performed on two different TPSs, Pinnacle^3 v7.6c (Philips Medical Systems, Best, The Netherlands) and PLATO RTS v2.6.4 with ITP v1.1.8 (Nucletron BV, Veenendaal, The Netherlands). The purpose of using two TPSs was to reduce the dependency of this planning study on one particular TPS. The modelling of the beam and the multi-leaf collimator is implemented differently in Pinnacle^3 and in PLATO. The optimization engine in the IMRT modules is different as well.

For both TPSs, all calculations were performed with an identical beam set-up.

Nine equidistantly spaced beams were used and sequenced with 15 intensity levels. The collimator angle was 0° for the first beam and it was increased for 5° in each following beam.

PLATO optimization.

The PLATO treatment planning system with its inverse treatment module ITP has several specific features to which the optimization approach must be tailored.

Some of the ROIs as defined above, are overlapping. In order to avoid inconsistent dose criteria to a voxel in an overlap region, an overlap priority can be defined. This allows the user to select to which ROI a voxel belongs.

In the dose prescription a maximum/minimum dose to a target can be defined in combination with a weight value. For organs at risk a maximum dose and weight are defined, but no prescription on the average dose is possible. In order to minimize the dose to the parotid glands, the maximum dose was set to 0 Gy, but a relatively small weight was applied. By using a maximum dose of 0 Gy, rather than a more realistic value, we ensure that there is always a benefit to reduce the dose to the organ at risk if this can be done without compromising the dose coverage of the target volumes.

The tools to optimize the dose in PLATO ITP are rather limited. In order to achieve a good tumor coverage combined with a better sparing of the OARs, artificial volumes were created so as to obtain a better control of the dose distribution. The parotid glands were split in an upper and a lower part. The upper part was defined as the volume on the CT slices where only the parotid gland and no target volumes were present. The rest of the parotid gland was defined as the lower part. As hard constraints are not available in PLATO ITP, the weight of the dose constraint in the upper part was always set to the maximum value of 100. The $PTV_{54(elec.\ nodes)}$ of the elective nodes were also split in an upper and lower part. The lower part was defined as the volume on the CT slices where no parotid gland was present and rest of the volume was defined as the upper part.

The fluence optimization was performed with resolution determined by the width of the leaves in the MLC, and the step size. The step size was fixed to 2.5 mm, the leaf width varied from 2.5 to 10 mm. After creating an optimal

fluence, it was sequenced with 15 intensity levels. A sliding window technique (Bortfeld *et al.*, 1994) was used and median filter of 5 voxels was applied. The dose calculation model in ITP is limited in order to enhance the calculation time. Therefore, the segments were exported to the RTS module where a full three dimensional (3D) pencil beam dose calculation was performed (Bortfeld *et al.*, 1993). A plan was accepted if it met the prescription criteria after this step.

Pinnacle^3 optimization.

Just as PLATO, the IMRT module in Pinnacle^3 has several specific features that require a specific approach to obtain the optimal treatment plans. The problem of conflicting criteria in overlapping regions of interest is solved in Pinnacle^3 by creating additional ROIs. Figure 2.2(a) shows two targets where T_1 has a higher prescription dose than T_2. Subsequently, T_1 is higher in hierarchy, meaning that the prescription dose in the overlapping region is dictated by the prescription dose of T_1. In order to steer the dose distribution on the remaining part of T_2, two new ROIs are generated (T_2' and T_2'+). T_2' (figure 2.2(b)) is a copy of T_2, but without T_1 and a minimum dose objective is applied in that region. Furthermore, to realize a fairly homogeneous distribution a uniform and a maximum dose objective are applied on the remaining part of T_2 (T_2'+). T_2'+ (figure 2.2(c)) is defined as a copy of T_2, but it has a margin of 5 mm to T_1. The 5 mm margin serves as a transition zone to build up the dose to the target T_1. This procedure is applied to all overlapping structures with different hierarchies starting with the highest priority for the targets with the highest dose and ending with the OARs.

In Pinnacle^3 prescriptions were used in terms of a maximum/minimum dose, a uniform dose and a mean dose. For each target (T) two additional ROIs were created (T' and T'+) (figure 2.2(b)–(c)). For T'+ maximum (107% of the prescribed) and uniform (prescribed) dose prescriptions were used. For T' only minimum (95% of the prescribed) dose prescription was applied. Finally, maximum dose and mean dose prescriptions were applied for the regions of the spinal cord, parotid gland and the body which do not overlap with the targets.

The fluence optimization was performed with a voxel resolution of 5 mm. After creating an optimal fluence map a K-means Clustering (Wu *et al.*, 2001)

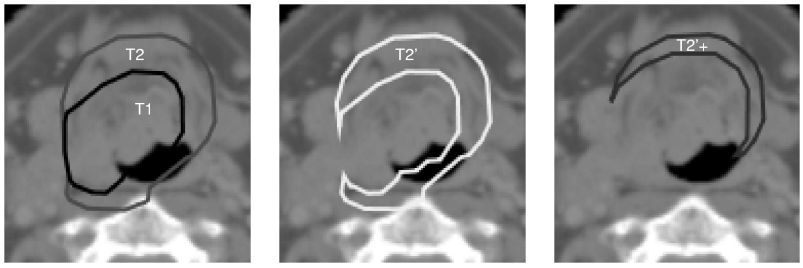

(a) (b) (c)

Figure 2.2: Additionally created ROIs in Pinnacle^3 TPS: (a) two targets where T_1 has a higher prescription dose than T_2, (b) T_2' is a copy of T_2, but without T_1, (c) T_2'+ is a copy of T_2, but it has a margin of 5 mm to T_1.

sequencer with 15 intensity levels was used to obtain field segments. Subsequently, direct machine parameters optimization (DMPO) was applied to the sequenced segments in which the position of the leaves could be modified with a precision of 1 mm.

A plan was accepted if the prescribed dose criteria were met in an accurate dose calculation using the convolution/superposition algorithm (Mackie *et al.*, 1987).

2.2.4 Linac/MLC design parameters

In order to investigate the influence of a single linac/MLC design parameter without the interaction of other parameters, we took a hypothetical ideal linac as the starting point. For this linac the values of MLC leaf width, leaf transmission and source size are listed in table 2.1. All other linac/MLC parameters were set to the values of the Elekta SLi15 accelerators used in our clinic.

The values for the MLC leaf width could easily be defined in both TPSs. The leaf step in PLATO was 2.5 mm. In Pinnacle^3 it was set to default value of 1 mm in the final DMPO phase of the optimization. In PLATO the size of the voxel in a fluence grid was defined by the size of a leaf step. We used the smallest leaf step possible, given the limitations of hardware memory.

Table 2.1: Hypothetically ideal and middle linac/MLC design parameters.

design parameter	hypothetically ideal linac/MLC	middle linac/MLC
MLC leaf width (mm)	2.5	5
MLC transmission (%)	0	0.75
source size (mm)	0.1	2

Defining the MLC leaf transmission was straightforward in both TPSs. The transmission of backup jaws in PLATO was set to 100% so that it was possible to investigate the effect of MLC leaf transmission only. In Pinnacle^3 it was not possible to set the transmission of the backup jaws higher than 20% or to remove them completely. However, their position could be fixed to the biggest aperture for each beam.

In PLATO it was not possible to modify the source size directly. Therefore we had to mimic this indirectly. The effect of a specific source size on the fluence matrix in PLATO is implemented by blurring the fluence with a Gaussian function. For the ideal linac/MLC design we used a Gaussian with a full-width-half-maximum (FWHM) of 0 mm. In Pinnacle^3 TPS the source size is a parameter which can be set directly.

All calculations were performed with a photon energy of 6 MV, which is the standard energy for head-and-neck patients at our department. The investigation was performed by changing only one of the parameters in the ideal linac/MLC. The values for the leaf widths were 2.5, 5 and 10 mm. Furthermore, the values for transmission were 0%, 0.75% and 1.5%. Finally, the source sizes were 0.1, 2 and 4 mm in Pinnacle^3, and FWHM values of Gaussian function in PLATO were 0, 5 and 10 mm.

In addition, we performed computations for a linac/MLC design with the median values of each of the investigated parameters. They are listed in table 2.1. We will refer to the linac/MLC with these parameters as the 'middle' linac/MLC. Finally, to have a clinicly relevant reference for the calculations, we performed computations for the Elekta SLi15 accelerator equipped with 1 cm leaf width MLC (Jordan and Williams, 1994) used at the Catharina Hospital (Eindhoven, The Netherlands) and at our department.

Table 2.2: Input and calculated transmission (trans) parameters for Pinnacle^3 and PLATO TPS.

Pinnacle^3		PLATO	
input trans (%)	calculated trans (%)	input trans (%)	calculated trans (%)
0	0	0	0
0.75	0.83	0.75	0.78
1.5	1.59	1.5	1.5

2.3 Results

2.3.1 Parameters check

The leaf width was verified by visual inspection of the fluence maps. In all created segments the leaf width was in agreement with the input values of both TPSs.

To be able to check the other design parameters a water equivalent phantom (40x40x40 cm^3) was created in both TPSs. The source-surface distance (SSD) was 1 m and a 6 MV open field of 10x10 cm^2 made by MLC leaves only was created. A dose profile was taken at D_{max}=1.6 cm, from which transmission and penumbra data were calculated.

The transmission of the leaves was checked by comparing the intensity at the center of the field at D_{max} when the field was opened, with the intensity for the situation of a field closed entirely by the MLC leaves. In both cases the same number of monitor units (MU) was delivered. In both TPSs the calculated transmission of the leaves was in agreement with the input transmission set in the TPSs. The check was performed for 0%, 0.75% and for 1.5% transmissions. Table 2.2 lists the input parameters and calculated transmissions.

The effect of the finite source size in Pinnacle^3 or the effect of blurring the fluence matrix with different Gaussian functions in PLATO has influence on the dose penumbra (80-20%). Therefore, by measuring the dose penumbra (80-20%) we were able to check if the chosen values for the source size in Pinnacle^3 and the FWHM of the Gaussian function in PLATO matched. Table 2.3 lists the input parameters and calculated dose penumbra (80-20%) for both TPSs.

Table 2.3: The source size values used in Pinnacle^3, FWHM values of Gaussian function used in PLATO TPS and calculated penumbras (80-20%) for both TPSs.

Pinnacle^3		PLATO	
source size (mm)	penumbra 80/20 (mm)	Gauss (FWHM) (mm)	penumbra 80/20 (mm)
0.1	3	0	2.6
2	5	5	6
4	8.5	10	9.8

2.3.2 Ideal plans

The plans obtained for the ideal linac/MLC (chapter 2.2.4) all met the required plan criteria (chapter 2.2.2) for all patients in both TPSs. The dose gradients in the direction of OARs were steep. We did not find a significant difference in steepness of the dose gradient to the parotid glands from contralateral or the ipsilateral (Spiessl *et al.*, 1985) side.

Figure 2.3 shows a typical dose distribution calculated by PLATO for one patient. Figure 2.4 shows the dose volume histograms (DVHs) obtained for the

(a) (b) (c)

Figure 2.3: The dose distribution obtained by a hypothetically ideal linac/MLC in PLATO TPS for one patient: (a) transversal, (b) coronal and (c) sagital view.

same patient in Pinnacle^3 and PLATO. From the DVHs good target coverage can be observed as well as sparing of the OARs. For some of the ROIs the

DVH curves differ between Pinnacle^3 and PLATO TPS, indicating differences in the dose distributions.

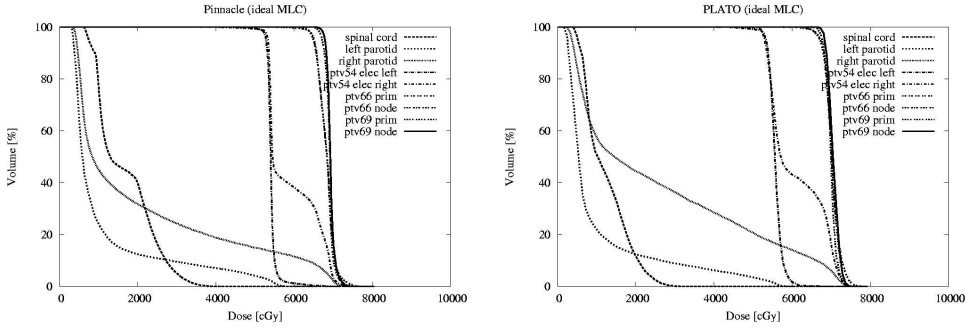

(a) (b)

Figure 2.4: DVHs obtained by a hypothetically ideal linac/MLC for one patient in (a) Pinnacle^3 and (b) PLATO.

The mean dose to the parotid glands for all patients achieved with the ideal linac/MLC was 16.2 ± 8.7 Gy in Pinnacle^3 and 17.6 ± 9.1 Gy in PLATO. The large variation in mean dose between the patients is explained by variations in size of the parotid glands and their overlap with the targets. The results of the two TPSs were compared using a paired samples T-test. A p-value of 0.126 was found, indicating that the difference in the mean dose to the parotid glands between the two TPSs was not significant. While the individual dose distributions differed between Pinnacle^3 and PLATO (figure 2.4), the similarity in mean dose to the parotid glands is understandable as the goal of the optimization was specifically to minimize this dose, rather than to obtain identical dose distributions.

As there was no significant difference between the mean dose to the parotid glands obtained in Pinnacle^3 and PLATO we will present the data of both TPSs combined in the remainder of this paper. Thus, in total we have seven patients and fourteen mean dose values to the parotid glands obtained by Pinnacle^3 and fourteen mean dose values obtained by PLATO.

2.3.3 Leaf width

Figure 2.5 shows the result of increasing the leaf width on the dose to the parotid glands for one example. By increasing the leaf width, the dose to the parotid glands was increased mainly in the intermediate dose region.

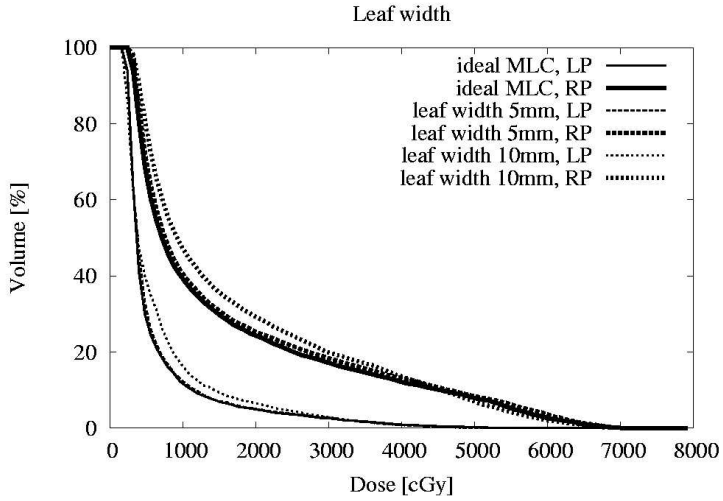

Figure 2.5: DVH of the left (LP) and the right (RP) parotid glands for one patient. Calculations were obtained for MLC's leaf width 2.5, 5 and 10 mm in PLATO TPS.

The increase of the mean dose to the parotid glands for all patients due to increasing MLC leaf width from 2.5 mm to 5 mm and from 5 mm to 10 mm was 1.6 Gy and 1.7 Gy, respectively. Table 2.4 lists the mean dose and standard deviations for each leaf width.

The paired samples T-test comparing the mean dose for an MLC leaf width of 2.5 mm with 5 mm and of 5 mm with 10 mm showed that the observed increase in the mean dose to the parotid glands is highly significant with p-values smaller than 0.001.

2.3.4 Transmission

The consequence of the increase in leaf transmission on the dose to the parotid gland is shown in figure 2.6 for one patient. The dose to the parotid glands increased mainly in the low dose region.

Table 2.4: The mean dose to the parotid glands obtained by Pinnacle^3 (Pin) and PLATO (PL) combined. Mean doses and standard deviation (SD) to the parotid glands. ^{a}: A paired samples T-test showed a significant ($p<0.001$) increase of the mean dose to the parotid glands comparing the linac/MLC design setup with the ideal linac/MLC. ^{b}: A paired samples T-test showed a significant ($p<0.001$) decrease of the mean dose to the parotid glands comparing the linac/MLC design setup with the middle linac/MLC design.

		ideal	leaf width		transmission		source size		middle	Elekta
TPSs	dose	lin/MLC	5mm	10mm	0.75%	1.5%	2mm	4mm	lin/MLC	lin/MLC
Pin+PL	mean (Gy)	16.9	$18.5^{a,b}$	20.2^{a}	$19.0^{a,b}$	20.8^{a}	$18.0^{a,b}$	20.4^{a}	20.2^{a}	22.7
	SD (Gy)	8.8	9.4	10.0	8.4	8.5	9.1	9.5	9.0	10.0

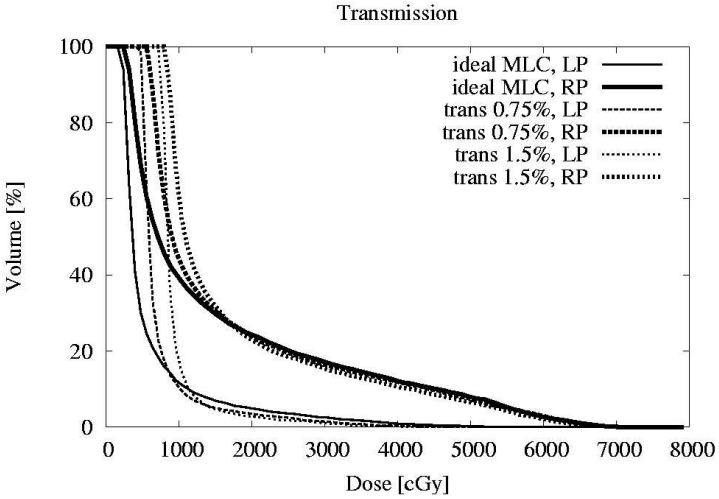

Figure 2.6: DVH of the left (LP) and the right (RP) parotid glands for one patient. Computations were obtained for MLC's with transmissions of 0%, 0.75% and 1.5% in PLATO TPS.

The paired samples T-test showed a significant increase in mean dose ($p<0.001$) when increasing the transmission from 0% to 0.75% and from 0.75% to 1.5%. Increasing the transmission of the leaves from 0% to 1.5% resulted in an increase of the mean dose to the parotid glands of 3.9 Gy (table 2.4).

2.3.5 Source size

An increase of the source size had a similar effect on the dose to the parotid glands as an increase in leaf width. The dose increased mainly in the intermediate dose region (figure 2.7).

Again, the paired samples T-test showed a significant increase in mean dose ($p<0.001$) when increasing the source size from 0.1 mm to 2 mm and from 2 mm to 4 mm. Increasing the source size from 0 mm to 4 mm resulted in an increase of the mean dose to the parotid glands of 3.5 Gy (table 2.4).

2.3.6 Middle linac/MLC

By using the middle linac/MLC (chapter 2.2.4) instead of the ideal linac/MLC the dose to the parotid glands increased mainly in the low and intermediate

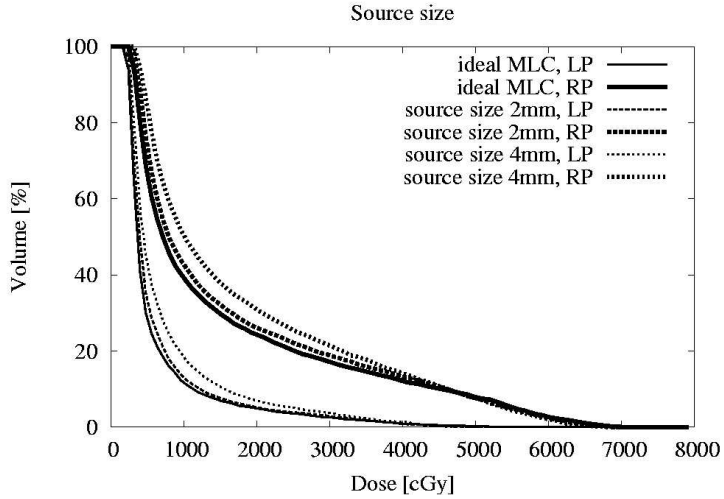

Figure 2.7: DVH of the left (LP) and the right (RP) parotid glands for one patient. Calculations were performed for linac's source size of 0.1, 2 and 4 mm in PLATO TPS.

dose regions. Figure 2.8 illustrates an effect of increasing the dose for one patient. Quantitatively, the average mean dose to the parotid glands of all patients increased by 3.3 Gy. This shows that the increase of the dose for middle linac/MLC was smaller than the sum of increases for all parameters separately and bigger than the square root of sum of squared increases. For our setup of parameters the transmission had the most dominant effect on the dose. Actually, the mean dose was 1.2 Gy higher than obtained by only increasing the transmission (table 2.4).

2.4 Discussion

In this investigation we studied the impact of three parameters in linac design on dose distributions for complex IMRT treatment plans. In order to isolate the influence of one parameter without the interaction of the others, we started with the hypothetical ideal linac/MLC design (chapter 2.2.4). By using sampling theory, Bortfeld *et al.* (2000) showed that the optimum MLC leaf width is 1.5-1.8 mm. The value of 2.5 mm used in this study, was close to the ideal

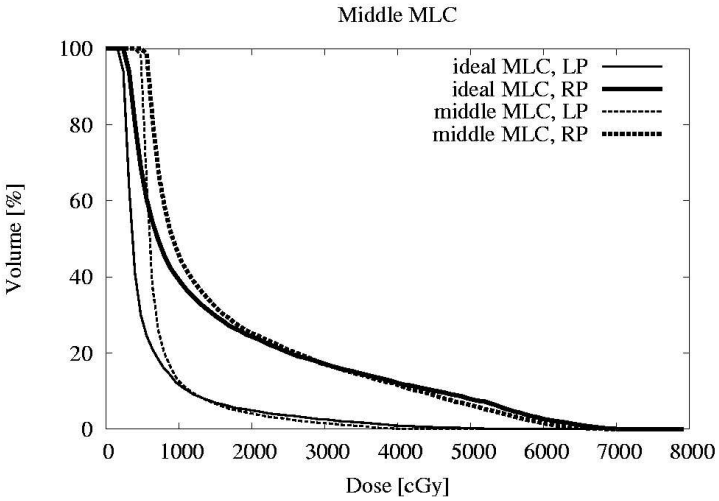

Figure 2.8: DVH of the left (LP) and the right (RP) parotid glands for one patient. Calculations were performed with hypothetically ideal and middle linac/MLC design (chapter 2.2.4) in PLATO TPS.

value. The transmission of 0% was ideal and also the source size of 0.1 mm was considered to be close enough to the ideal value of 0 mm.

Other parameters in the linac design, such as the source-isocenter distance and the distance between the source and the MLC were not included in this investigation. However, both parameters impact mainly on the dose penumbra, so that changing their values will have a similar effect as changing the source size.

In our optimization procedure we used hard constraints for the dose coverage of the targets. By having a well defined target coverage for all plans, the mean dose to the parotid glands could be used as a quantitative measure for comparing the plans. In order to facilitate the steering of the dose in both TPSs, specific artificial volumes were defined. To ensure, that the best possible plan for a particular set of linac design parameters was made, at least one plan was made where the targets were slightly underdosed (99% of the volume not receiving the prescribed dose) and one where they were slightly overdosed (99% of the target receiving more than the prescribed dose). The plan obtained at intermediate values of the dose prescription parameters in the TPSs yielded

the required dose coverage in combination with the lowest average dose to the parotid glands possible.

In studying the effect of changing the design parameters, we could have preserved the dose prescription parameters in the two TPSs constant. While this is a commonly used approach (Fiveash *et al.*, 2002; Wang *et al.*, 2004, 2005; Nill *et al.*, 2005), we found that our hard constraints would not be met in all cases. Indeed, by modifying the dose prescription parameters in the TPSs, we were able to improve the quality of the plans by meeting the constraints to target coverage and limiting the average dose to the parotid glands. Using this approach, the plans made with the ideal linac yielded similar results for both planning systems. Indeed, no significant difference was found in the average dose to the parotid glands for the plans generated in Pinnacle^3 and PLATO.

In this investigation the number of beams was fixed to nine. While this was the maximum number achievable, due to memory limitations of our PLATO system, it may be considered sufficient for most IMRT applications (Bortfeld *et al.*, 1990; Mohan *et al.*, 2000).

Five of the patients studied here, were also used in the study by Van Vulpen *et al.* (2005), in which conventional IMRT was compared with tomotherapy. In that study the mean dose to the parotid glands was 30 Gy with a conventional Elekta SLi15 accelerator and using PLATO for treatment planning. The mean dose to the parotid glands was 24 Gy with the Tomotherapy system. In our investigation, for the same patients, we found out that the theoretical limit of the mean parotid gland dose for an ideal linac/MLC was 18.3 Gy using PLATO. For the conventional Elekta linac/MLC we found a mean dose of 24.4 Gy. This is about 6 Gy less compared to conventional Elekta linac/MLC design in the investigation of Van Vulpen *et al.* (2005) and it is comparable to the results with the Tomotherapy system in the same study. This shows that our elaborate strategy of dose optimization indeed has the potential to provide better treatment plans. Nevertheless, the difference found by Van Vulpen *et al.* (2005) between the conventional IMRT and the Tomotherapy system seems quite plausible. The Tomotherapy system has a leaf width of 6.25 mm, a leaf thickness of 10 cm, and a source-isocenter distance of 85 cm. Consistent with our findings, these parameters should result in better IMRT distributions as compared to the conventional Elekta linac/MLC design.

Our study showed that by changing more than one parameter from the ideal linac/MLC setup, a smaller increase in the dose to the parotid glands was observed than the sum of the individual contributions. The transmission of the MLC leaves had the most dominant effect. Consequently, by manufacturing MLCs with thicker leaves as suggested earlier Topolnjak *et al.* (2002, 2003b,a, 2004a,b, 2005) , the IMRT treatment of head-and-neck cancer patients could benefit. An improvement of 2.5 Gy of the mean parotid gland dose was found when going from the conventional Elekta linac/MLC to the middle linac/MLC. An improvement of 5.8 Gy was possible by going to the ideal linac/MLC. The clinical impact of these differences can be assessed by observing the normal tissue control probability (NTCP) curves as proposed by Roesink *et al.* (2001) and Eisbruch *et al.* (1999). A complication is defined as a reduction of the stimulated parotid flow rate one year after a radiotherapy treatment to less than 25% of the of flow before the treatment. Depending on the model used (Roesink *et al.* (2001) or Eisbruch *et al.* (1999)), the dose reduction found between Elekta and middle linac/MLC results in an average decrease of the NTCP between 4% and 9%. Likewise, the dose reduction between Elekta and ideal linac/MLC results in the decrease of the NTCP between 8% and 17%.

2.5 Conclusion

In this study, the impact of the MLC leaf width, MLC leaf transmission and linac's source size on IMRT treatment plans of seven patients with head-neck cancer have been investigated. By increasing those parameters from their ideal values to the the clinically used Elekta SLi 15, equipped with a standard MLC with a leaf width of 10 mm, an increase of the mean dose to the parotid glands of 5.8 Gy was observed. The investigation showed that by changing more than one parameter from the ideal linac/MLC setup, a smaller increase in the the mean dose to the parotid glands was observed than the sum of the contributions of each parameter separately. The dose increased mainly by increasing the transmission of the MLC leaves.

Acknowledgment

This study is supported by Elekta Ltd, Crawley, UK.

Chapter 3

A six-bank multi-leaf system for high precision shaping of large fields

This chapter is based on the article:
R. Topolnjak, U. A. van der Heide, B. W. Raaymakers, A. N. T. J. Kotte, J. Welleweerd and J. J. W. Lagendijk. 2004. A six-bank multi-leaf system for high precision shaping of large fields. *Phys Med Biol.* **49** 2645–56.

Abstract
In this study, we present the design for an alternative MLC system that allows high precision shaping of large fields. The MLC system consists of three layers of two opposing leaf banks. The layers are rotated 60° relative to eachother. The leaves in each bank have a standard width of 1 cm projected at the isocenter. Because of the symmetry of the collimator set-up it is expected that collimator rotation will not be required, thus simplifying the construction considerably.

A 3D ray tracing computer program was developed in order to simulate the fluence profile for a given collimator and used to optimize the design and investigate its performance. The simulations show that a six-bank collimator will afford field shaping of fields of about 40 cm diameter with a precision comparable to that of existing mini-MLCs with a leaf width of 4 mm.

3.1 Introduction

Accurate field shaping is becoming increasingly important in radiotherapy. While alloy blocks allow high precision field shaping, it is quite time consuming to make them for each individual field. For this reason modern linacs are equipped with a multi-leaf collimator (MLC). These MLCs typically have leaves with a width of 1 cm at the isocenter and can produce a maximum field size of 40 cm (Jordan and Williams, 1994; Galvin *et al.*, 1993b; Das *et al.*, 1998). While the field size is sufficient for most treatments, the leaf width limits the precision with which fields can be shaped. In a comparison between MLCs with 1 cm leaves and alloy blocks, Galvin *et al.* (1998) noted that the effect of high-precision field shaping is often blurred by the use of multiple beams and by set-up variations. Nevertheless, the undulations of the 1 cm leaves become problematic in particular when sharp dose gradients are required and the distance between target and organ at risk is small. Thinner leaves improve this, although no further benefit is expected for leaf widths below 1.8 mm because of the width of the dose deposition kernel (Bortfeld *et al.*, 2000). Otto *et al.* (2002) investigated dose conformity and found that complex and small shapes are more sensitive to the leaf width.

Nowadays, several types of mini-MLCs are on the market that can be attached below the conventional linac head. The leaf widths range from 1.6 to 4.5 mm at isocenter. The physical characteristics of mini-MLCs, such as the penumbra, the transmission and leakage and the field-shaping precision were determined in various studies (Meeks *et al.*, 1999; Xia *et al.*, 1999; Cosgrove *et al.*, 1999; Hartmann and Föhlisch, 2002). These studies showed both the improved field shaping by reduced undulation and the reduced penumbra of the individual leaves. The latter mainly because the distance of the add-on mini-MLC to the source is larger. The precision of field shaping with a mini-MLC was found sufficient for radiosurgery and small-field intensity modulated radiotherapy (IMRT).

However, a drawback is that none of them can achieve field sizes larger than 10x12 cm^2. Varian produces a MLC with 60 leaf pairs and a field size of 40x40 cm^2. In the central 20 cm of the field the leaf width is 0.5 mm while in the outer 10 cm on both sides of the field the leaf width is 1 cm. With such a design a high resolution is achieved in the central part of the field, but

unfortunately not in the outer part. Elekta produces a mini MLC integrated in the accelerator head with 40 leaf pairs and a field size of 16x22 cm^2.

The key problem is realizing a large field-size MLC with a high resolution field shaping ability. Several approaches have been proposed to tackle this problem. The effective field shaping resolution can be improved by superimposing two MLC-shaped fields with a small shift of the isocenter or a rotation of the collimator between them (Siochi, 1999a; Evans and Partridge, 2000; Bortfeld *et al.*, 2000; Otto and Clark, 2002). Also, considerable research was done in direction of radical alternative designs of MLCs and delivery techniques. Webb (2001a) investigated the concept of a shuttling MLC in which small elements in the collimator can swap to an adjacent position instantaneously. A similar idea by Lagendijk using a checkerboard was presented in the same paper. Webb (2002) also developed the idea of using only jaws and a mask for IMRT. Williams and Cooper (2000) presented a method of high-resolution beam collimation by using tertiary grid collimator situated below the conventional MLC.

In this study, we present the design for an alternative MLC system that allows a high precision shaping of large fields. We took the existing MLCs with 1 cm wide leaves as the starting point. The new system consists of three layers of bank pairs positioned at 60° relative to eachother. The bank pairs each have a standard 1 cm leaf width projected at the isocenter. With the three layers of leaf banks, a field-shaping precision can be achieved comparable to that of mini MLCs with a leaf width of 4 mm at isocenter.

In order to study the physical properties of such a design, a computer program was developed that simulates the fluency profile for a given collimator set-up. The program uses three-dimensional (3D) ray tracing in similar way as presented by Chen *et al.* (2000) and takes into account the geometry of the system, the transmission through the leaves and the leaf tips.

The program was validated by comparing calculations for the Elekta MLC with measurements. Typical tests are the penumbra profile and the output as a function of the field size (Huq *et al.*, 2002; Jordan and Williams, 1994). For these tests, the calculations showed good agreement with the measurements. The program was then used to characterize the penumbra, transmission and beam-shaping precision of the six-bank MLC.

Table 3.1: The computer simulation parameters.

Collimator set-up	Number of bank pairs (C1)
	Angles between bank pairs (C2)
Bank pair	Number of leaves (B1)
	Distance source-bank (B2)
	Leaf thickness (B3)
	Coefficient of attenuation in leaves (μ) (B4)
	Radius of tip curvature (B5)
	Offset of tip curvature (B6)
	Leaf width at isocenter (B7)
Source	Size (S1a), distribution (Gaussian) and resolution (S1b) of primary
	Size (S2a), distribution (Gaussian) and resolution (S2b) of secondary
	Distance primary-secondary source (S3)
	Distance source-isocenter (S4)
	Ratio in contribution primary-secondary source (S5)
Fluence plane	Size (F1)
	Resolution of calculating (F2)
	Distance source-plane (F3)

3.2 Ray tracing

3.2.1 Computer simulation

In order to investigate the performance of a six-bank collimator and to find the optimal design, we made a computer program simulating existing and new collimators. It is based on a 3D ray tracing algorithm similar to that described by Chen *et al.* (2000). Ray lines are cast from a two-dimensional (2D) source to a fluence plane. The attenuation of each ray line is calculated from the path length through the collimator leaves and the corresponding linear attenuation coefficient. We used a single attenuation coefficient of $\mu = 77.2 \ \ \mathrm{m}^{-1}$ corresponding to the attenuation of 4 MeV photons in tungsten. At this energy the attenuation exhibits a minimum (Bureau of Radiological Health, 1970). The collimator is defined analytically and the surface of every leaf is specified, including a rounded leaf tip. The parameters describing the collimator set-up are listed in table 3.1 (see also figure 3.1).

The source was modeled as a matrix describing a 2D Gaussian intensity dis-

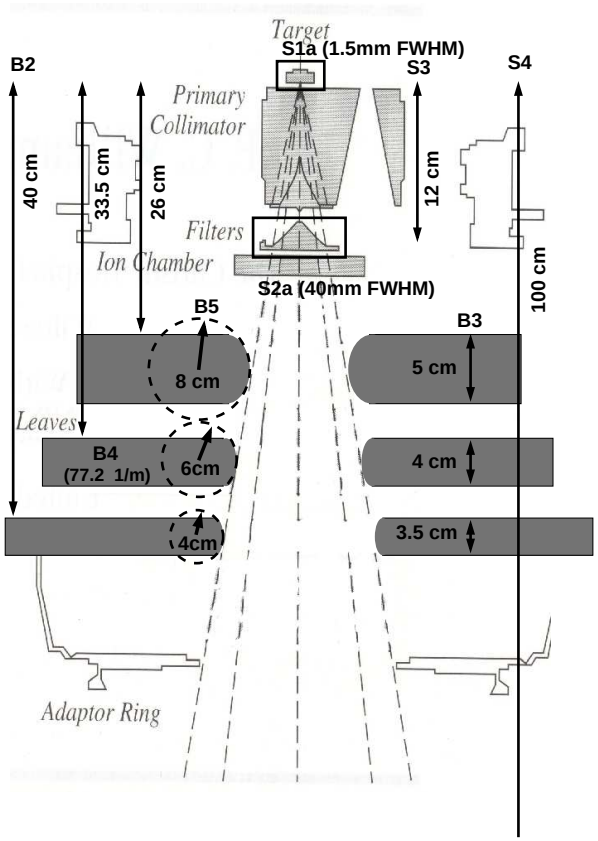

Figure 3.1: Schematic view of the six-bank MLC system and the computer simulation parameters from the lateral view (all parameters are listed in table 3.1).

tribution. From each matrix element radiation is emitted isotropically, so that a flat fluence distribution for an open field is obtained. The size of the primary source has been studied in detail for various linear accelerators (Jaffray *et al.*, 1993; Loewenthal *et al.*, 1992). Typically values for the full-width-half-maximum (FWHM) were found between 1 and 2 mm. For this reason we have carried out our calculations using a FWHM of 1.5 mm. A secondary source is implemented similarly, to account for the scatter produced in the flattening filter (Liu *et al.*, 1997; Chen *et al.*, 2000). We used a FWHM of 4 cm and a relative intensity contribution of 10% based on simulation of the collimator scatter factor as a function of the field size (Zhu *et al.*, 1995).

Table 3.2: Elekta MLC parameters.

Number of leaves pair	40
Distance source-bank	29.8 cm
Leaf thickness	7.5 cm
Radius of tip curvature	11.9 cm
Leaf width at isocenter	1 cm
Primary source size (FWHM)	1.5 mm
Secondary source size (FWHM)	4 cm

All calculations were done using a primary and secondary source of 30x30 pixels and a fluence plane of 400x400 pixels. The fluence plane has a size of 40x40 cm^2 resulting in a fluence resolution of 1 mm. Calculations performed at a higher resolution showed no further change in the fluence profile. For this configuration the calculation time was approximately 1 h on a 2.8 GHz Pentium 4 PC operating under the Linux operating system.

3.2.2 Validation of the computer simulations

The computer simulation program described above was tested with a series of simulations based on the geometry of an Elekta SLi20 accelerator, equipped with an MLC. Table 3.2 shows the parameters used, and a detailed description of the collimator is given in Jordan and Williams (1994). All measurements were done using a beam energy of 10 MV, with a photon energy spectrum peaking around 1/3 of that energy.

The first test was the simulation of the collimator scatter factors (Sc). The fluence was calculated for a series of square fields, with sizes ranging from 2 to 28 cm. The value at the center of the field is a combination of the contribution of the primary and secondary source. The fluence intensity at the center drops sharply for small field sizes and this relation strongly depends on the size and relative contribution of the primary and secondary sources (Zhu *et al.*, 1995). Normalizing the center field values to that of the 10x10 cm^2 field, a curve appears that can be compared to the collimator scatter factors as measured with an ionization chamber (ionization chamber 2571, Saint Gobain Crystals & Detectors Ltd, Reading, UK) in a mini phantom (figure 3.2(a)). While the correspondence between measurement and simulation is good, small differences

must be attributed to the simple model used for the primary source as well as the scatter contribution of the flattening filter.

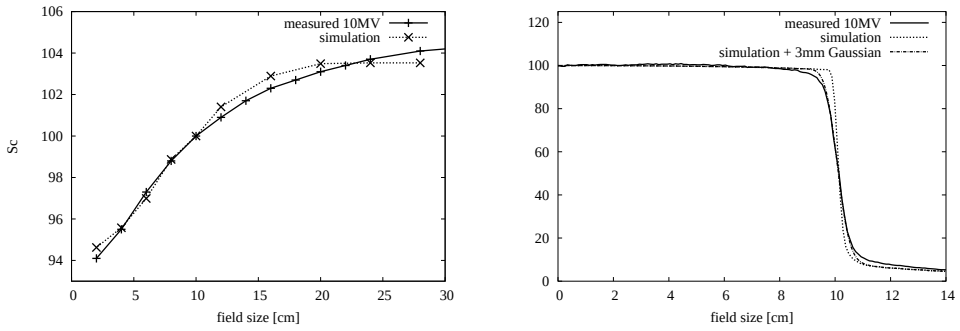

(a) (b)

Figure 3.2: Validation of the computer simulations. (a) The collimator scatter factor as a function of field size. (a) The half profile for a 20x20 cm^2 field in water phantom at d_{MAX}=2 cm.

The second test was the simulation of the profile across a square field of 20x20 cm^2 in a water phantom. The profile was measured at d_{MAX}=2 cm using an IC15 type ionization chamber (Wellhöfer, Schwarzenbruck, Germany) (figure 3.2(b)). The simulation yields fluence, without considering the effects of scatter inside the water phantom.

In the region inside the field all radiation from the primary and secondary sources reaches the surface of the phantom. The calculated fluence profile shows a flat area within the beam, a sharp penumbra and a gradual decline outside the beam. However, the fluence falls off more steeply than the measured dose. This suggests that the phantom scatter and the measurement probe cause a more gradual fall-off.

The connection between the fluence and the dose is a complex issue. In the Bortfeld *et al.* (1993) model a convolution with three pencil beams is used to calculate the dose. The three kernels represent the primary radiation and scatter for small and for big fields. At d_{MAX} the contribution of the first kernel, which can be described by a Gaussian with σ approximately 3 mm, is dominant. For the sake of simplicity we convolved the fluence profile with this

Gaussian function (dashed curve in figure 3.2(b)). In the penumbra region this curve indeed shows good agreement with the measurement.

These two tests show that the simulation program predicts both collimator scatter and fluence profile of an Elekta accelerator in reasonable agreement with experimental data.

3.3 The six-bank multi-leaf system

For simulating the six-bank multi-leaf system, we have used the parameters for primary and secondary sources as specified in the previous section. We have left out the wedge and replaced Elekta's collimator set-up (including MLC) by a six-bank MLC. Thus, the space available for a six-bank collimator in the Elekta-accelerator geometry lies below the ionization chamber. Although room is left for the X-collimator, it can be removed as the three MLC layers produce sufficient attenuation. We have chosen not to lower the collimator down to the adaptor ring, as the lowest pair of leaf banks would become unpractically large. Figure 3.1 shows a schematic view.

3.3.1 Design

Our goal for designing this collimator is to achieve a large field size (40 cm in diameter) in combination with the ability of high resolution field shaping, comparable with mini MLCs with a leaf width down to 4 mm at isocenter. The six-bank collimator has three layers of two banks, each with a width of 1 cm at isocenter. The leaf motion directions of the three layers are separated by 60°. Because of this three-fold symmetry, the need for collimator rotation is reduced. In fact, we propose to abolish collimator rotation completely, thus simplifying the collimator head manufacturing considerably. In our simulations we choose the top pair of leaf banks to travel perpendicular to the axis gun to target. The middle pair will be rotated 60° anti-clockwise, as seen from the source, the lowest pair is rotated another 60°.

Each leaf bank has 40 leaves and is single focused, with the sides of the leaves diverging from the source. The leaves move in one plane. Interleaf transmission in one leaf bank will be blocked by the two other banks. For this reason we

Table 3.3: Parameters for the six-bank MLC.

Banks pair	Distance from the source (cm)	Leaf thickness (cm)	Tip curvature (cm)
High	26	5	8
Middle	33.5	4	6
Low	40	3.5	4

expect that a tongue-and-groove design will not be required, thus simplifying the design of the leaves.

We believe that it is convenient if the size of the penumbra does not depend on the orientation of the field or the field size. In the absence of collimator rotation, the penumbra will be determined by different leaf banks, depending on the field orientation. Therefore, the design should be such that the three layers of banks produce more or less the same penumbra.

Several physical effects contribute to the penumbra: geometry, transmission and scatter. The scatter is primarily produced in the phantom or patient. Its contribution to the penumbra depends on the field size, photon energy, phantom/patient and depth. The phantom scatter does not depend on the specific MLC design. The size of the geometric penumbra linearly depends on the source size, and is inversely proportional to the distance between the source and the leaf bank. The leaf thickness and curvature influence the transmission penumbra. A thicker leaf with less curvature will attenuate a ray more quickly and thus result in a smaller transmission penumbra. The curvature of the leaf tips is used to create a transmission penumbra that is independent of the position of the leaf tip in the field (Jordan and Williams, 1994).

The leaves in the banks that are closest to the source will produce the largest geometric penumbra. This effect is compensated to some extent by reducing the transmission penumbra of the higher banks. To this end the leaf thickness is chosen 3.5 cm, 4 cm and 5 cm from the lowest to the highest bank respectively. There is a 2.5 cm clearance between the layers for a mechanism to drive the leaves. The parameters for the three layers of leaf banks are listed in table 3.3. A patent application based on the described different leaf thickness has been made by Elekta Ltd.

3.3.2 Characteristics

For characterizing the performance of the six-bank MLC and comparing it with conventional MLC systems, we chose to calculate the fluence. Although dose is the clinically relevant quantity, fluence profiles are less blurred and thus pose a more stringent test of the performance.

The penumbra for each layer of leaf banks.

For each layer of leaf banks the variation of the penumbra width with leaf position was investigated. The fluence was calculated for rectangular fields with leaves of one bank at a position between -20 and +20 cm at the isocenter plane. The midline of the field is at 0 cm, and a negative sign indicates overtravel. The penumbra (80-20%) was calculated from a profile along the center of a leaf in the bank (figure 3.3).

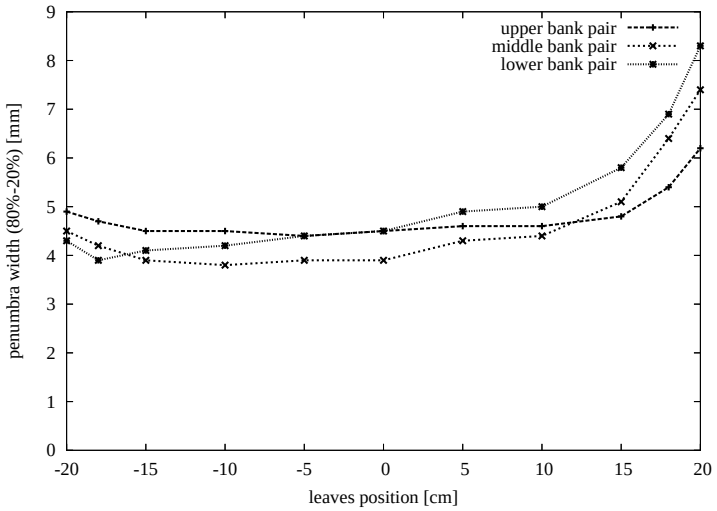

Figure 3.3: The penumbra width for each layer of leaf banks separately.

The curves for all pairs of leaf banks are similar at the value of about 4.3 mm, and vary less than 0.7 mm with the leaf position between -20 and +15 cm. The penumbra width (80-20%) for the leaf position at +18 and +20 cm increases for all three layers. The reason for increasing penumbra is a flattening filter, which has a contribution to the penumbra with its full size for those leaf positions. The effect is the most dominant for the lowest layer because, the

leaves in that layer are the thinnest and have the biggest transmission (6.5%). Furthermore, a small contribution of irradiation from the flattening filter has a significant influence on the penumbra width (80-20%).

The penumbra of rotated fields.

The edge of an arbitrary field will be made by a combination of the three layers of leaf banks. As our design will have a non-rotating head, we have investigated the size of the penumbra for different orientations of a straight field edge. A half field was rotated from 0° to 180° in 10° steps. For the three layers of leaf banks, the leaves were positioned such that the leaf tips touch the intended field edge. Profiles were taken perpendicular to the field edge. A total of 50 of such profiles were generated along the length of the field edge and the average width of the penumbra (80-20%) and the standard deviation was calculated. The average is plotted in figure 3.4 as a function of the angle between the gun-target direction and the field edge. The standard deviation was found to vary typically from 0.3 to 0.7 mm depending on the angle. All three leaf banks will produce an undulation around the field edge. The combination of the three patterns is quite irregular and causes variations in the resulting penumbra width along the edge. This effect is reflected in the standard deviation. If the half field is positioned exactly in the center the it can be matched precisely with diverging side of the leaves at the 90°, 150° and 30°, respectively, from the highest to the lowest bank. In figure 3.4, two minima are found at 150° and 30° as a result of this effect. There is no minimum at 90° because at that angle, the field was matched with diverging part of the leaves in the highest bank with a relatively large geometric penumbra. In general, such a precise match will not occur. We shifted the half field by 3.5 and 7 mm and repeated the test. Now the minima have disappeared. In fact, for a shift of 7 mm some maxima appear as a large mismatch between the leaves and the field edge results in effective blocking by only two of the three layers of leaf banks.

For comparison, we calculated the penumbra width for an Elekta MLC. Because collimator rotation is possible, the penumbra will not depend on the field angle. Overall, the penumbra generated by the six-bank MLC is similar to that of the Elekta MLC. As the top leaf bank creates a larger penumbra than the lower two, some angle dependence is found.

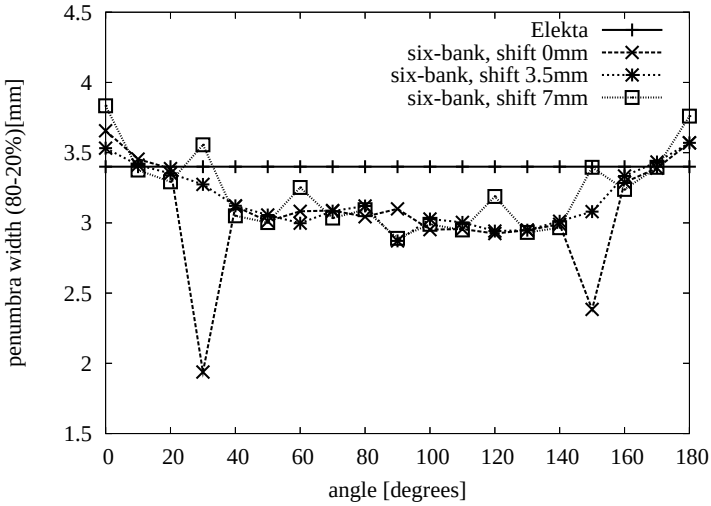

Figure 3.4: The penumbra width for the entire collimator as a function of field angle.

Undulation test.

A MLC will approximate an irregular field shape by creating an undulating pattern around the desired shape. The amount of undulation is an indication for the precision of the MLC field shaping. To quantify the performance of the six-bank collimator for high resolution field shaping, we used the profiles perpendicular to the intended field edge as described in the previous section. The half field was shifted by 3.5 mm, as described above, to avoid specific matches between the field and the diverging part of the leaves. The results for the six-bank MLC were compared to the conventional Elekta MLC (table 3.2, Jordan and Williams (1994)). For comparison with a mini MLC, we also simulated a collimator with the same parameters as the Elekta MLC, except using 100 leaf pairs with a width of 4 mm at isocenter. In contrast to the previous section, collimator rotation was not allowed for the Elekta and mini MLCs. As in the previous section, the leaves were positioned such that the leaf tips touch the intended field edge.

The degree of undulation was quantified by calculating the distance between the intended field edge and the 50% fluence line (the actual field edge) (figure 3.5). The average distance reflects the degree to which the field is enlarged

by the undulations. The standard deviation is a measure for the degree of undulations. In figure 3.6(a), the average distance is plotted as a function of the field rotation angle. The solid line for the conventional Elekta MLC shows a minimum at 0°. Here we can match the field edge with the leaf tips. The value at 0° is the distance between the tip of the leaf and the actual 50% decrement line, used in radiotherapy practice as the reference position of a leaf. Another minimum is found at 90° because we match a field with the diverging side of a leaf. That extreme depends on the distance of the side to the field edge.

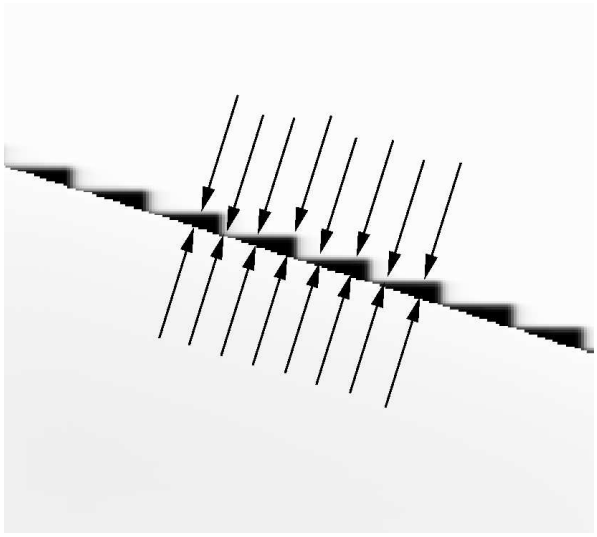

Figure 3.5: The overdose area and average distance between the intended field edge and the 50% fluence line.

The mini MLC shows a similar curve but at a lower level, indicating the reduced undulations. At 90°, a maximum is found as the match between the side of a leaf and the field edge is unfavorable. The curve for the six-bank collimator exhibits three minima made by the leaf tips at 0°, 60°, 120°. Overall the curve lies around that of the mini-MLC, indicating that the degree of undulation is comparable.

Figure 3.6(b) shows the standard deviations as a function of the field orientation. The curves for the Elekta and mini MLCs show a value of 0 for orientations of 0° and 90°, indicating the absence of undulations. The standard deviation for the six-bank MLC lies mostly above that of the mini MLC, but below 0.9 mm for all angles.

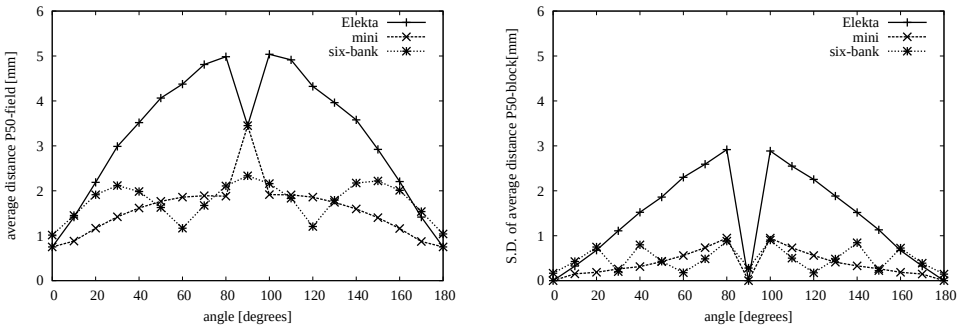

(a) (b)

Figure 3.6: The results of undulation test, 3.5 mm shifted field. (a) The average distance between the 50% isodose line and the intended field edge, as a function of field angle. (b) The standard deviation of the distance between the 50% isodose line and the intended field edge, as a function of field angle.

Conformity of circular fields.

The precision of field shaping was characterized further by creating circularly shaped fields (Zhu *et al.*, 1998; Xia *et al.*, 1999; Otto and Clark, 2002; Killoran *et al.*, 2002), ranging from 4 to 16 cm in diameter. The conformity of the resulting fluence compared to the intended field was determined as the difference in surface area divided by the area of the intended field. The leaves were positioned such that the leaf tips touch the intended field edge. As shown in the previous section, the 50% decrement line lies at some distance from the leaf tip, so that a slightly larger field is created. For the Elekta and the mini MLC this shift is about 0.7 mm, and for the six-bank MLC it is about 1 mm. Figures 3.7(a)–(c) show the calculated fluence for a circle with the contour of the intended field. For the Elekta and mini-MLCs the leaf-travel direction is horizontal in the figure. The conformity as a function of the circle diameter is plotted in figure 3.8. For all diameters the six-bank MLC shows a better performance than the Elekta and mini-MLCs. The wiggle in the curve of the mini-MLC at a diameter of 6 cm is an artifact caused by a mismatch of the 4 mm wide leaves and the radius of 3 cm. In particular at the top and bottom of the fluence graphs, the Elekta and mini-MLCs show a large area outside the intended circle getting a high fluence. In practice, one could position the

leaves slightly more inward, so that the midline of the leaves touch the circle. The area outside the circle would be reduced at the cost of underdosing a small area inside it. For the six-bank MLC this would not be a good approach. Leaves of one bank pair could block part of the circle, in order to minimize the area outside the circle. However, this area is blocked already by the two other pairs of banks.

(a) (b) (c)

Figure 3.7: The simulation of the fluence of a field conforming to a circle with radius 12 cm. (a) Elekta. (b) Mini. (c) Six-bank.

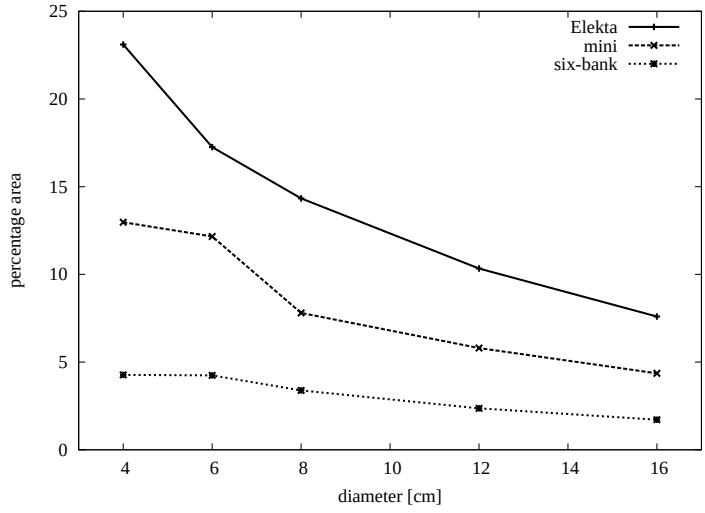

Figure 3.8: Conformity as a function of circle diameter.

3.4 Discussion

In this study, we propose a six-bank multi-leaf collimator assembly that combines a large field size with a high precision field shaping ability. The design is based on a conventional MLC with a leaf width of 1 cm, typically creating maximum field sizes of 40x40 cm^2. By creating three layers of bank pairs, at 60° relative to eachother, a polygon field shape is created with 12 sides and a distance of 40 cm between the opposite sides. At maximum overtravel and a 'horizontal' position the leaves may bend under their weight. The maximum tolerated displacement at the leaf tip is limited by the interleaf distance. Thus, the maximum overtravel that can be achieved will depend on the stiffness of the leaves. The displacement is proportional to the fourth power of overtravel and inversely proportional to the square of the leaf width (Shigley and Mischke, 1989). Thus, by using 1 cm leaves rather than 0.4 cm the maximum overtravel for the leaf can be increased by a factor of about 1.6 without increasing the interleaf distance. Based on Elekta's beam modulator with 0.4 cm leaves and a full travel of 21 cm at isocenter, the maximum travel in horizontal position for 1 cm leaves is estimated to be at least 38, 34 and 32 cm, respectively, from the highest to the lowest layer. However, because the six-bank MLC will be non-rotating, the leaves will not move horizontally so that even an larger travel will be feasible.

A six-bank MLC will not have the physical wedge. As a straight field edge can be achieved in any direction with the combination of the three banks, a virtual wedge can be created by moving this edge in defined steps from one to the other side of the field.

The concept of a six-bank MLC was tested in this study with a series of computer simulations. The results indicate that indeed a field shaping precision can be achieved that is similar to or better than a mini-MLC with a leaf width of 4 mm. Due to the combined behavior of the three leaf layers the undulation of the field edge around the desired shape is reduced. While the penumbra that can be realized will depend on the detailed parameters of the leaf banks, our study shows that for a reasonable set of parameters a penumbra can be achieved similar to that of a conventional MLC. For the six-bank collimator, a penumbra is formed in varying degrees by all three banks. We studied the variation of the penumbra width as function of angle and shift of the field edge and found it to be sufficiently stable. As a consequence, collimator rotation

would not be required, so that the construction of the accelerator head could be simplified considerably. This MLC construction itself may be simplified because we expect that the leaves will not require a tongue-and-groove design, since interleaf transmission is always blocked by the leaves from at least one other layer.

Future work involves the development of an IMRT sequencer for the six-bank MLC and the study of the system in a variety of clinical examples. In collaboration with Elekta we will work towards a prototype for further testing.

Acknowledgment

This work on the six-bank MLC arose out of discussions with Dr. P. Williams, Christie Hospital, Manchester and Elekta. We also acknowledge Dr. K. Brown, Elekta, Crawley, for many useful discussions.

Chapter 4

IMRT sequencing for a six-bank multi-leaf system

This chapter has been published as:
R. Topolnjak, U. A. van der Heide and J. J. W. Lagendijk. 2005. IMRT sequencing for a six-bank multi-leaf system. *Phys Med Biol.* **50** 2015–31.

Abstract

In this study, we present a sequencer for delivering step-and-shoot IMRT using a six-bank multi-leaf system. Such a system was proposed earlier and combines a high-resolution field-shaping ability with a large field size. It consists of three layers of two opposing leaf banks with 1 cm leaves. The layers are rotated relative to each other at 60°. A low-resolution mode of sequencing is achieved by using one layer of leaves as primary MLC, while the other two are used to improve back-up collimation. For high-resolution sequencing an algorithm is presented that creates segments shaped by all six banks. Compared to a hypothetical mini-MLC with 0.4 cm leaves, a similar performance can be achieved, but a trade-off has to be made between accuracy and number of segments.

4.1 Introduction

Multi-leaf collimators (MLC) with small leaf widths are available allowing high-precision field shaping. Unfortunately, they suffer from small field sizes, thus limiting their use to specific cases. For machines that are dedicated primarily to stereotactic applications mini-MLCs have been incorporated into the head of the accelerator. An example is the Elekta beam modulator. Alternatively, add-on MLCs are used that allow a temporary conversion of an accelerator with a conventional MLC (Meeks *et al.*, 1999; Xia *et al.*, 1999; Cosgrove *et al.*, 1999; Hartmann and Föhlisch, 2002). Varian produces a MLC with 60 leaf pairs and a field size of 40x40 cm^2. In the central 20 cm of the field the leaf width is 0.5 cm, while the outer 10 cm on both sides have a leaf width of 1 cm. While such a design provides a high resolution in the central part of the field, the field shaping in the outer part has a low resolution.

In a previous study, we proposed an alternative design for a multi-leaf collimator that combines high-resolution field shaping with a large field size (Topolnjak *et al.*, 2004a). In this way a multi-purpose collimator can be created that can be used for both common applications and high-precision treatments. The system consists of three layers of bank pairs, positioned at 60° relative to each other. The bank pairs each have 40 single-focussed leaves with a standard 1 cm width at isocenter. With the three layers of leaf banks a field-shaping precision can be achieved comparable to that of mini-MLCs with a leaf width of 4 mm at isocenter. At the same time the mechanical rigor of the conventional MLC is maintained so that large fields can be realized. Because of the threefold symmetry of the system, collimator rotations are not required, so that a substantial simplification of the design can be achieved.

For the six-bank MLC to function as a multi-purpose collimator, suitable for all types of treatment, it is important that intensity-modulated radiotherapy (IMRT) can be delivered as well. In this study we focus on step-and-shoot IMRT. One way of delivering IMRT would be to use only one layer of two leaf banks as a primary collimator for IMRT sequencing. The two other layers are then used as backup collimators to reduce transmission through the primary MLC layer. While this approach is straightforward, the resolution of IMRT sequencing would then be limited by the leaf width of the primary leaf bank. It has been argued that high-resolution fluence distributions can improve a dose distribution further (Bortfeld *et al.*, 2000; Kubo *et al.*, 1999; Shepard

et al., 1999). Therefore, we have developed a sequencer for the six-bank MLC system that allows the delivery of large IMRT fluence distributions with a resolution comparable to a mini-MLC with a leaf width of 4 mm.

4.2 Materials and Methods

4.2.1 Conventional sequencing

With the six-bank MLC IMRT fields can be delivered in a conventional as well as a high-resolution mode of operation. In the conventional mode, the two leaf banks in one of the layers are used as the primary MLC used to shape the segments. The leaf banks in the other two layers are used as back-up for reducing the transmission through the leaves of the primary MLC. We use an iterative algorithm similar to that proposed elsewhere (Convery and Webb, 1998). We have chosen to use fixed numbers of monitor units for the segments. Thus a threshold is defined at half this number of monitor units. The sequencing procedure starts with closed leaf pairs at one extreme of the field. From the input fluence a segment is derived by pushing the trailing leaves forward until a fluence bixel is found above the threshold. From that point on the leading leaves are retracted until a fluence bixel is found below threshold. The leaves are allowed to touch each other, but interdigitation is prohibited. The fluence delivered in such a segment is calculated and subtracted from the input fluence. If the remaining fluence is above the threshold, it is used as input for deriving the next segment. For this study, we have not considered tongue-and-groove effects. Nonetheless, this can be easily included if required (Van Santvoort and Heijmen, 1996).

For a conventional collimator set-up, back-up collimators are positioned just around the aperture made by the MLC. For the six-bank MLC in low-resolution mode, the back-up MLC layers are positioned such that the leaves touch the field edge formed by the primary MLC. In this way, the transmission of the MLC outside the open field is minimized.

Figure 4.1 shows the collimation of an aperture in low-resolution mode.

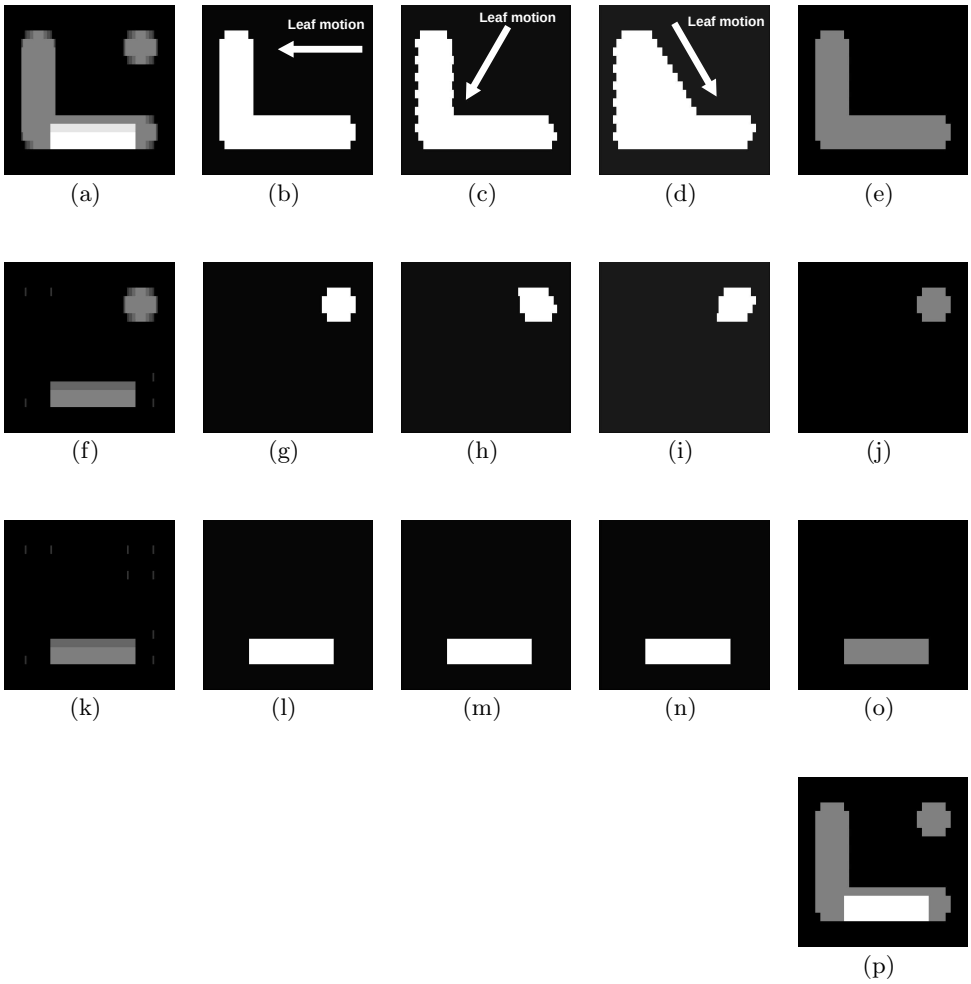

Figure 4.1: Example of the low-resolution sequencing; the sequencing was done using two fluence levels. (a) Input fluence, leaves positions in the (b) first, (c) second and (d) third layer, (e) first segment. (f) Input fluence for the second segment, leaves positions in the (g) first, (h) second and (i) third layer, (j) second segment. (k) Input fluence for the third segment, leaves position in the (l) first, (m) second and (n) third layer, (o) third segment. (p) All segments added together.

4.2.2 High-resolution sequencing

The algorithm for sequencing the fluence for a six-bank MLC in the high-resolution mode differs in several respects from the conventional approach. A flow diagram of the sequencer is shown in figure 4.2, an example of the sequencing procedure in figure 4.3 and a description of the main steps is given below.

The three layers of leaf banks cannot be sequenced independently as this might result in apertures in the three layers that do not overlap. Therefore, a connection between the layers has to be established in the sequencing process. We propose the use of masks for each layer of leaf banks to indicate which part of the fluence matrix is included in the aperture created by the other layers. The aperture is represented in a matrix with a value of 1 for a bixel in the open field and 0 for a bixel blocked by one of the leaves.

Step 1.

Figure 4.3(a) illustrates an input fluence and starting point for sequencing algorithm. The initial set-up of the leaves in a layer is found by stepping each trailing leaf forward until it touches a fluence bixel with an value exceeding the threshold. From that point onwards the corresponding leading leaf is retracted, opening a gap between the trailing and leading leaf. This continues until the point where the leaf would uncover an ensemble of bixels that are all below the threshold. As a result of this approach, the leaves touch the area inside the mask with a fluence value above the threshold. Consequently, many fluence bixels may be included at the edge of the aperture with values below the threshold (figure 4.3(b)). However, these bixels may be blocked by the leaves in the other layers of the six-bank MLC. Unduly blocking of fluence bixels with intensity above the threshold would lead to an unnecessary reduction of the mask and fragmentation of the segments.

Step 2.

The product of the mask (figure 4.3(b)) from the previous layer with the input fluence (figure 4.3(a)) constitutes the input for setting up the leaves in the second layer. The procedure to set-up the leaves is the same as described in step 1.

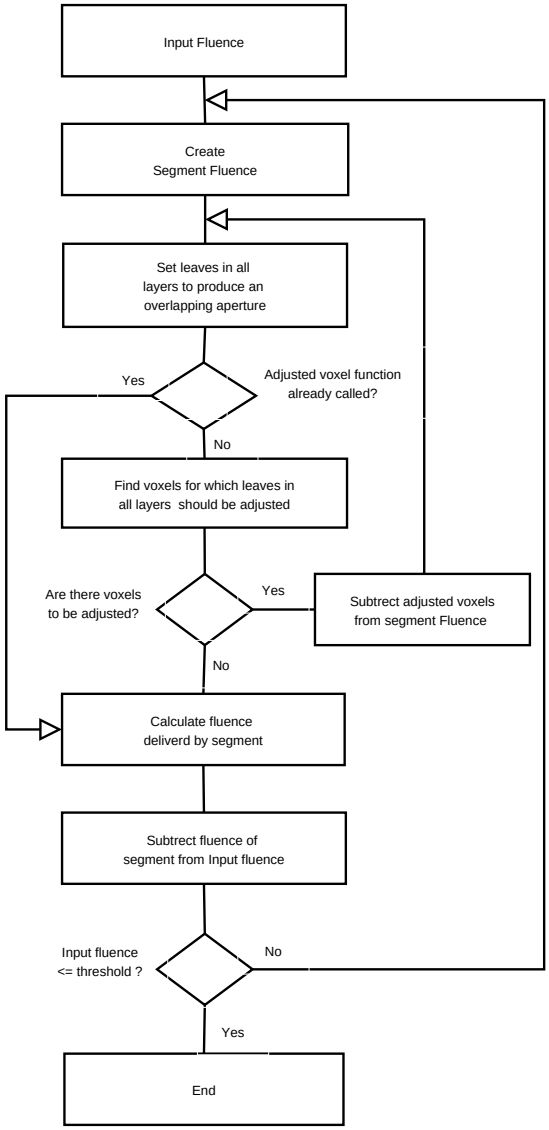

Figure 4.2: Flow diagram of an IMRT algorithm for a six-bank MLC in the high-resolution mode.

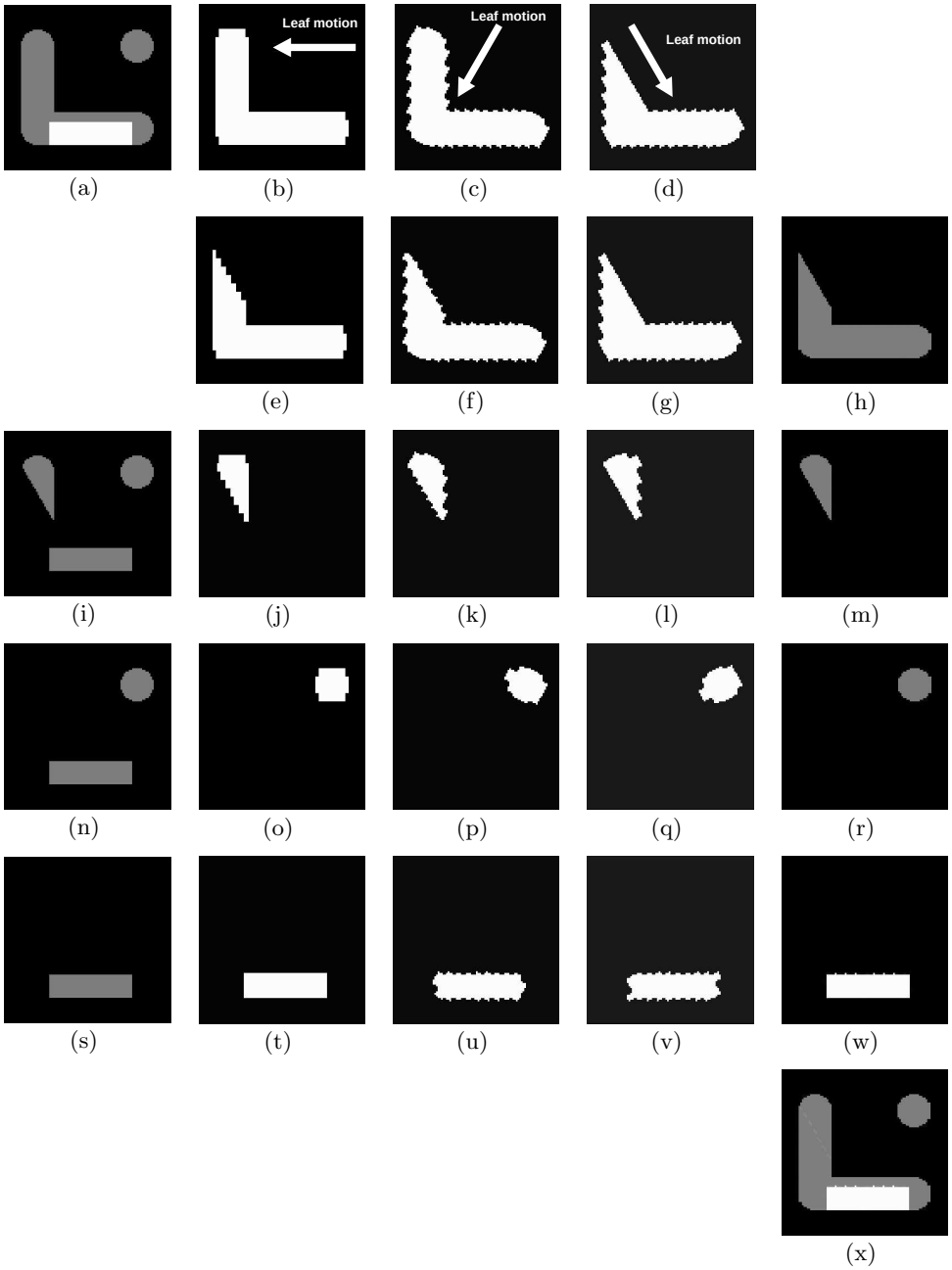

Figure 4.3: Example of high resolution sequencing; the sequencing was done using two fluence levels. (a) Input fluence, leaves positions in the (b) first, (c) second and (d) third layer after the first iteration. Further, the leaves positions in the (e) first, (f) second and (g) third layer after second iteration, (h) first segment. (i) Input fluence for the second segment, leaves positions in the (j) first, (k) second and (l) third layer, (m) second segment. (n) Input fluence for the third segment, leaves positions in the (o) first, (p) second and (q) third layer, (r) third segment. (s) Input fluence for the fourth segment, leaves position in the (t) first, (u) second and (v) third layer, (w) fourth segment. (x) All segments added together.

As the features in the fluence grid and the leaf shape are not necessarily aligned, an undulation in the field edge may occur due to the resampling of the leaf shape on the fluence grid. This undulation then shows up in the mask and thus in the input for the other layer of leaves. As a result, leaves travelling at a 60° angle relative to the previous layer, may encounter a repeating pattern of bixels that should and should not be covered. Such a pattern could lead to a fragmentation of the segment into very small parts (figure 4.4). To counter this undesirable effect, we propose to deliver these fragments in one segment if the gap between them is sufficiently small. The leading leaf is positioned as described in step 1. However, if the next step uncover an ensemble of bixels that are all below threshold, the routine will not stop. Instead, up to a predefined distance further along is probed. If within this range a fluence bixel is encountered with a value above threshold, the leading leaf is retracted so as to include this bixel in the aperture.

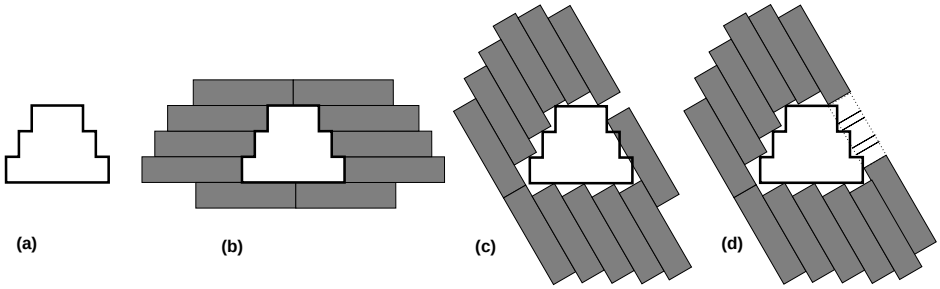

Figure 4.4: Illustrations of fragmentation due to undulating field edges in the high-resolution mode. (a) Aperture to be delivered; (b) leaf positions in the first layer; (c) leaf positions in the second layer without allowing any gap; (d) leaf positions in the second layer with allowed gap.

Another effect caused by leaves travelling at a 60° angle relative to the fluence grid, is that the leaves can not always block the whole bixel. We have made the choice that the bixel can not be partially blocked. If the center of the bixel is blocked, we consider the entire bixel to be blocked.

Figure 4.3(c) shows the position of the leaves in the second layer.

Step 3.

The product of the mask (figure 4.3(c)) from the previous layer with the input fluence (figure 4.3(a)) constitutes the input for setting up the leaves in the third layer. The procedure to set-up the leaves is the same as in step 2.

The apertures derived for the three layers now may differ considerably in size. This occurs, for example, when the first layer produces a large field, which cannot be delivered in one segment by the second or third layer of leaves (figures 4.3(b)–(d)). In this case, the non-overlapping part of the apertures will not be blocked by the first and the second layer of leaves, which is not optimal. Therefore the iteration continues. For each layer an updated mask is calculated. If the mask is changed relative to the previous iteration the leaf set-up is also adjusted. The iteration (step 1, step 2 and step 3) terminates if in two subsequent layers no adjustment of leaf set-up occurred. This procedure ensures that the optimal cooperation of the three layers of leaf banks is achieved. In the example for segment one, two iteration were needed (figures 4.3(b)–(d), (e)–(g)) to derive the final segment (figure 4.3(h)).

Step 4.

At this stage, the rough outline of the segment is established in all three layers and a stable aperture is achieved. A further improvement is now achieved by weighting the benefit for an bixel involved in a step against that at another bixel involved in the same step. Iteratively, each leaf is moved inwards by a small step if the average value of the bixels involved in the step is below the threshold.

Step 5.

When a segment is finally derived, the fluence delivered can be calculated and subtracted from the input fluence. If the input fluence is below the threshold the algorithm terminates, otherwise it will continue to make another segment.

The example in figure 4.3(a) can be sequenced in four segments (figures 4.3(h), (m), (r) and (w)). Figures 4.3(e)–(g), 4.3(j)–(l), 4.3(o)–(q) and 4.3(t)–(v) show the positions of the leaves in the first, second and the third layer, respectively,

for each segment. For this example, the further optimization of the leaf position (step 4) did not show any improvement. So, if we would had moved any leaf inward we would have created more underdose area than we would have covered overdose area. Finally, figure 4.3(x) shows the sum of all segments added.

4.2.3 Parameters for evaluating IMRT sequences

The performance of the six-bank MLC for delivering intensity-modulated fluences is compared to a mini-MLC (0.4 cm leaves) and a conventional MLC (1.0 cm leaves). We evaluate the sequences based on their accuracy and efficiency in terms of monitor units and leaf travel (LT).

The root-mean-square (RMS) indicates the accuracy to which the sequence delivers the input fluence (Bär *et al.*, 2001; Budgell, 1999). It is defined as

$$RMS = \sqrt{\frac{1}{n \cdot m} \sum_{i=1}^{n} \sum_{j=1}^{m} (F(i,j)_{or} - F(i,j)_{seq})^2} \tag{4.1}$$

where n and m are the number of elements in the row and in the column of the fluence profile respectively; F_{or} is the original and F_{seq} is the sequenced fluence.

As described above, sequencing was done using a fixed number of ten fluence levels, evenly distributed between 0 and the maximum fluence in the matrix. As a benchmark for a particular fluence matrix it was stratified to the same number of equidistant levels, and the RMS error between this stratified matrix and the input was calculated. In this way, the effect of stratification on the sequenced fluence can be distinguished from the effect of the various sequencing approaches for the six-bank and conventional MLCs.

The efficiency factor (EF) is defined as the ratio between the maximum of the input fluence matrix ($max(F_{or})$) and the total number of monitor units for a MLC ($TNMU_{MLC}$) to deliver all segments (Galvin *et al.*, 1993a; Convery and Webb, 1998).

$$EF = \frac{max(F_{or})}{TNMU_{MLC}} \tag{4.2}$$

The EF is the reciprocal of the modulation scale factor (MSF) (Xia and Verhey, 1998; Dai and Hu, 1999).

For step-and-shoot IMRT the time required for delivery depends on three parameters that can be derived from a sequence (Siochi, 1999b). The total number of monitor units bears on the time needed for actual irradiation and is reflected in the EF. The number of segments relates to the number of times the beam has to halt. The maximum leaf travel relates to the time required to set up the segments. The maximum leaf travel per segment transition is calculated by finding the maximum distance any leaf has to travel in the transition between two segments. The total maximum leaf travel is the sum of these values for all transitions.

For conventional MLCs, back-up collimators are used frequently to attenuate the transmission outside the aperture formed by the leaves of the MLC. As these collimators produce only a box around the aperture, some part of this region will be blocked by leaves only (one layer). For the six-bank MLC, field-shaping occurs by all three layers of leaves. As a result, a smaller area is expected to be blocked by leaves of only a single layer. In order to quantify the back-up collimation, we calculate for each segment the area blocked by a single leaf and the area of the bounding box around the input fluence. For each sequence, the average area of the box and the average area covered by one layer of leaves are calculated.

4.2.4 Fluence matrices

In this study, we compare the sequencing for three types of collimators of high-resolution fluence matrices: (1) a conventional MLC with 40 leaf pairs of 1 cm width, (2) a conventional mini-MLC with 100 leaf pairs of 0.4 cm width and (3) the six-bank MLC with 1 cm leaf width. Fluence matrices obtained from inverse treatment planning programs typically are adapted to the properties of the MLC: the width of a fluence bixel is equal to the leaf width. The length of a bixel is equal to the minimal step size allowed and is chosen 2 mm. For comparing the different MLC designs such an adapted fluence matrix is not practical. Therefore, we use matrices with a resolution of 2x2 mm^2 as input for the sequencers for all three types.

For the conventional MLCs with 0.4 and 1 cm leaf width we use the iterative

sequencing algorithm described above (section 4.2.1). However, because the input fluence matrix has bixels smaller than the leaf width, even a 2 mm step of a single leaf will cover multiple fluence bixels. For this reason the high-resolution fluence matrices are resampled to 2×4 and 2×10 mm^2, so that the average value of the involved bixels is considered.

For a conventional MLC the size of the area which a leaf can cover in one step is $A \cdot B$, where A is the leaf width, and B is the size of a leaf step. For a six-bank MLC the size of such area is $B^2 \cdot \sqrt{3}/4$.

We tested the capacity of the MLCs to deliver intensity modulated fluences with four geometrical examples. Fluence matrices were generated with a 2×2 mm^2 resolution and a size of 12×12 cm^2 (figures 4.5(a), 4.6(a), 4.7(a) and 4.8(a)). The maximum value was set to 100. In addition, five clinical examples were obtained for prostate (Pros) and five for head-neck (HN). IMRT plans for the clinical examples were generated in PLATO (Nucletron, Veenendaal, The Netherlands). A hypothetical MLC with 200 leaf pairs of 2 mm width was introduced, so that a fluence map could be generated with a 2×2 mm^2 resolution. The fluence matrices belonging to the prostate examples had a size of 12×12 cm^2. The fluence matrices for the head-neck cases were 16×16 cm^2. During the optimization, median filtering of the fluence was applied in order to smooth the fluence. The theoretical fluence was exported and normalized to a peak value of 100. These fluence matrices were used as input for the sequencing in this study. Figure 4.9(a) illustrates a prostate (Pros 1) example and figure 4.10(a) illustrates an example of head-neck (HN 1).

4.3 Results

4.3.1 Conventional sequencing

The geometrical fluence matrices described in section 4.2.4 were sequenced to ten intensity levels, equally spaced between zero and the maximum value of 100. For sequencing of the fluence for the conventional MLC and the six-bank MLC in conventional mode, the fluence matrices were resampled to bixels of 2×10 mm^2. The segments of the conventional MLC and the six-bank MLC were not completely identical. Because of different leaf thickness, a different fraction of fluence is transmitted outside the aperture. As a result, bixels that

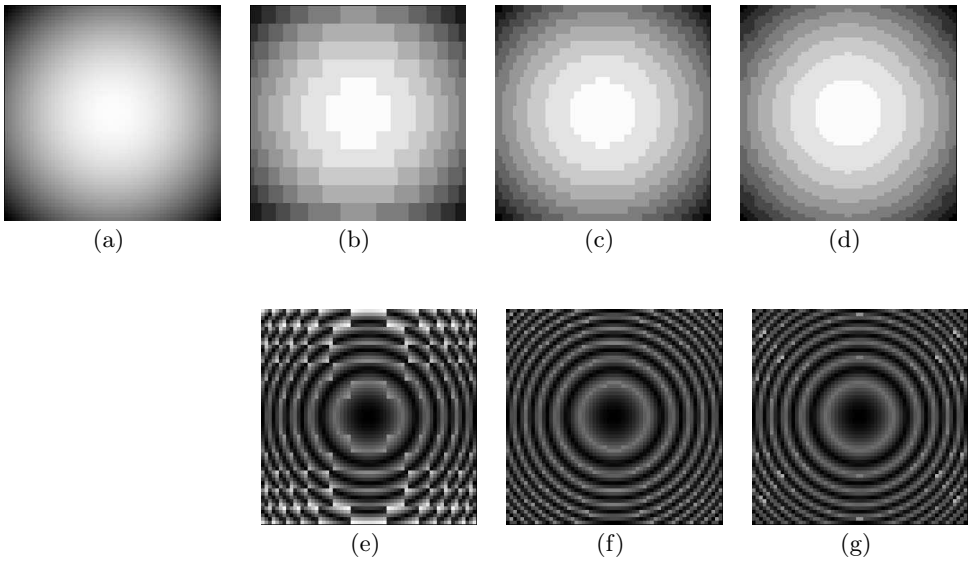

Figure 4.5: Example A ($z = -a_1(x^2+y^2)+a_2$), size 12×12 cm^2: (a) original fluence. Fluence sequenced with (b) 1 cm MLC, (c) mini-MLC and (d) six-bank (HR). Absolute difference between the original and sequenced fluence for (e) 1 cm MLC, (f) mini-MLC and (g) six-bank MLC (HR).

are initially just above the threshold for inclusion in a segment may end up just below it. This causes small variations in segments between the conventional MLC and the six-bank MLC in low-resolution mode. The effect is the biggest in the Pros 1 example with a difference of 2% in RMS error. The degree of back-up attenuation differs for the two collimator systems. The average area covered by one leaf is consistently smaller for the six-bank MLC than for the conventional MLC (table 4.1), however, at the cost of an increase in leaf travel. For the prostate (Pros 1) and head-neck (HN 1) fluence maps the same comparison was made and indeed the area covered by only a single leaf is negligible for the six-bank MLC, while it constitutes up to half the area of the bounding box for a conventional MLC.

4.3.2 High-resolution sequencing

The high-resolution sequencing of the six-bank MLC was compared to the results of the mini-MLC as well as the conventional MLC. As in the low-

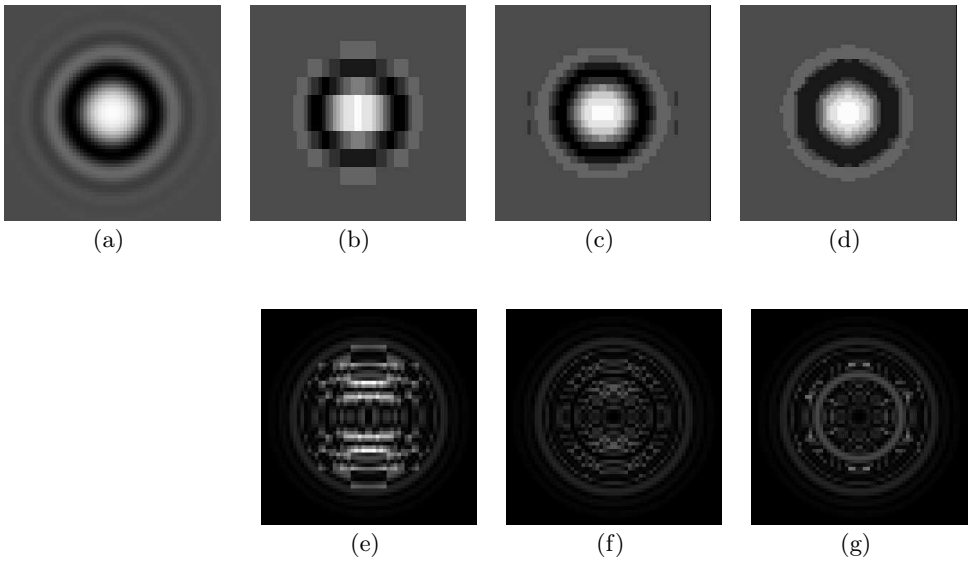

Figure 4.6: Example B ($z = b_1 cos[b_2(x^2 + y^2)]/exp[b_3(x^2 + y^2)] + b_4$), size 12 × 12 cm^2: (a) original fluence. Fluence sequenced with (b) 1 cm MLC, (c) mini-MLC and (d) six-bank (HR). Absolute difference between the original and sequenced fluence for (e) 1 cm MLC, (f) mini-MLC and (g) six-bank MLC (HR).

resolution mode, the six-bank MLC has a highly efficient back-up collimation (table 4.2). Figures 4.5(b)–(d), 4.6(b)–(d), 4.7(b)–(d), 4.8(b)–(d) show the results for geometrical examples. For geometrical examples A and D we find that the number of segments for the six-bank MLC is identical to that of the mini-MLC (table 4.3). For example B–the sinc function–a substantially larger number of segments is found. However, many of these are smaller than 1 cm^2. Removal of these segments reduces the number so that it is similar to the mini- and conventional MLCs, while the impact on RMS error is small. Nevertheless, the resulting fluence is not as good as for the mini-MLC because the concave field shapes with a small radius cannot be formed as accurately by the 1 cm leaves as by the 0.4 cm leaves of the mini-MLC.

The average area blocked with only one layer of leaves as shown in tables 4.1 and 4.2 increases when the six-bank MLC is used in high-resolution as compared to low-resolution mode (examples A and D). This is a consequence of

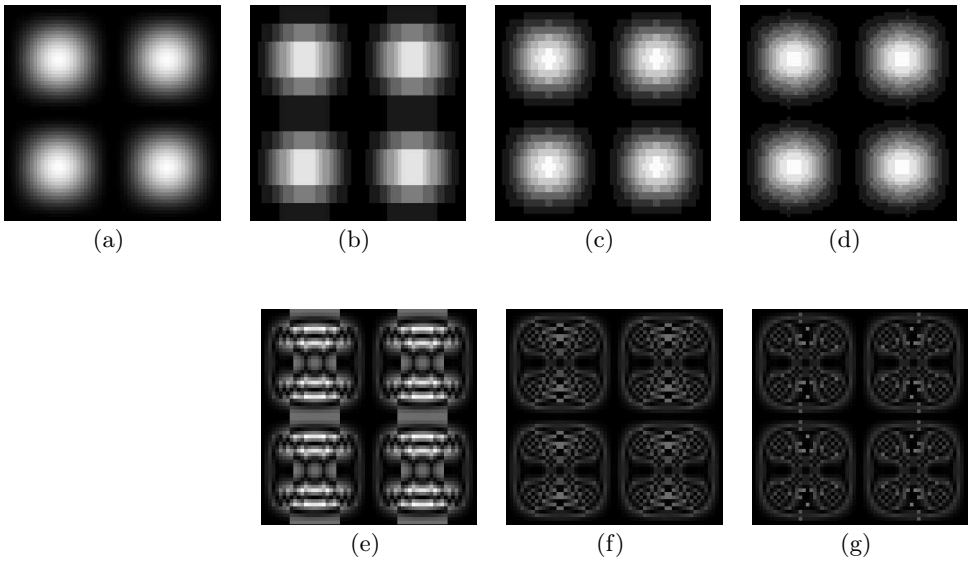

Figure 4.7: Example C ($z = c_1 sin^2(c_2|x|) sin^2(c_2|y|)$), size 12 × 12 cm^2: (a) original fluence. Fluence sequenced with (b) 1 cm MLC, (c) mini-MLC and (d) six-bank (HR). Absolute difference between the original and sequenced fluence for (e) 1 cm MLC, (f) mini-MLC and (g) six-bank (HR).

the discretization of the fluence matrices and our choice to consider a bixel as blocked entirely, if its center is blocked by a leaf. In low-resolution mode the fluence bixels are 2 × 10 mm^2 as compared to 2 × 2 mm^2 in high-resolution mode. A leaf that partially blocks the low-resolution bixel is considered to block it in full, while in high-resolution mode part of the same area is recognized as not blocked.

For geometrical example C the six-bank MLC requires twice as many segments as the mini-MLC. This is caused by the fact that the mini-MLC can deliver the two parallel peaks in one sweep. The dark line in between is covered by the leaves only. For the six-bank MLC the first step in the sequencing algorithm derives apertures for the three layers of leaf banks with similar size, so that areas outside the apertures are optimally covered by all the layers. As a result the two parallel peaks will be delivered separately.

For the geometrical examples, the RMS error of the six-bank MLC was com-

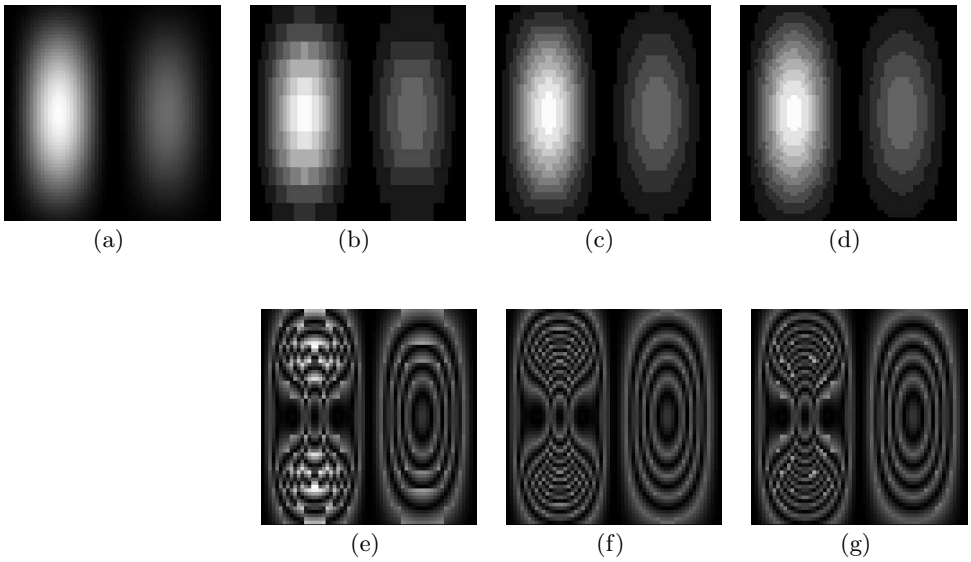

Figure 4.8: Example D ($z = d_1 sin^2(d_2|x|)cos^2(d_3|y|)$, $d_2 = d_3/2.5$), size 12×12 cm^2: (a) original fluence. Fluence sequenced with (b) 1 cm MLC, (c) mini-MLC and (d) six-bank (HR). Absolute difference between the original and sequenced fluence for (e) 1 cm MLC, (f) mini-MLC and (g) six-bank MLC (HR).

parable to that of the mini-MLC and better than the conventional MLC. In particular for examples A and D the RMS error after high-resolution sequencing is only slightly higher than the RMS error calculated from the stratified fluence maps. This shows that the RMS error is mainly caused by the stratification and not by the further sequencing.

For the ten clinical examples, we found that the number of segments for the six-bank MLC is considerably higher than for the mini-MLC. Again, this is mainly caused by a large number of very small segments in the sequence. Removal of segments and isolated areas smaller than 1 cm^2 results in a number of segments quite comparable to that of the mini-MLC except for the HN 1 and HN 4 examples. In table 4.4 the results are listed for both the full sequence and the sequence with fields and isolated areas smaller than 1 cm^2 removed (in parentheses).

For the prostate fluence maps we find that the average RMS errors for the con-

Table 4.1: Back-up collimation and leaf travel for conventional MLC with 1 cm leaf width and the six-bank MLC in conventional mode (low resolution (LR)). Data presented are the number of segments, the average size of rectangular shape around aperture (box), the average size of the area blocked by only one layer of leaves (one layer), and leaf travel (LT).

Example	MLC	Number of segments	Box (cm^2)	One layer (cm^2)	LT (m)
A	1 cm	10	107.4	13.0	0.13
	Six-bank (LR)	10	107.4	0	0.16
B	1 cm	18	35.7	11.0	0.39
	Six-bank (LR)	17	35.8	6.4	0.49
C	1 cm	18	30.4	10.4	0.19
	Six-bank (LR)	18	30.6	1.2	0.65
D	1 cm	14	26.6	4.2	0.23
	Six-bank (LR)	14	26.6	0	0.30
Pros 1	1 cm	17	32.4	9.7	0.38
	Six-bank (LR)	18	30.7	0.7	0.73
HN 1	1 cm	30	36.9	19.2	0.83
	Six-bank (LR)	30	36.6	0.4	1.83

ventional, mini- and the six-bank MLC are 14.6 ± 2.2, 8.9 ± 1.6, 7.6 ± 1.1 respectively. If we remove all segments and isolated areas smaller than 1 cm^2 the numbers are 14.7 ± 2.2, 9.5 ± 1.7, 9.3 ± 1.0. All RMS errors are substantially larger than the RMS error from the stratified fluence maps. Figures 4.9(e)–(g) show Pros 1 example where the differences are mainly located at the boundaries of the fluence. For the conventional and mini-MLCs the differences are especially large at the top and bottom end of the fluence maps (figures 4.9(b), (c)), because of the discretization of the leaf width.

The six-bank MLC for the head-neck examples can achieve a similar average RMS error as the mini-MLC (6.2 ± 0.4 mini and 6.2 ± 0.8 the six-bank MLC), but only at the cost of an unrealistically large number of small segments.

The head–neck fluence maps are 16×16 cm^2 and are substantially larger than prostate maps. Here the same effect, where the differences are mainly

Table 4.2: Back-up collimation and leaf travel for mini-MLC with 0.4 cm leaf width and the six-bank MLC in high-resolution mode (HR). Data presented are the number of segments, the average size of rectangular shape around aperture (box), the average size of the area blocked by only one layer of leaves (one layer), and leaf travel (LT). The results listed in parentheses do not include fields and isolated areas smaller than 1 cm^2.

Example	MLC	Number of segments	Box (cm^2)	One layer (cm^2)	LT (m)
A	mini	10	106.4	11.9	0.16
	Six-bank (HR)	10	107.7	2.0	0.16
B	mini	20 (18)	34.4 (38.1)	12.3 (13.6)	0.46 (0.43)
	Six-bank (HR)	32 (21)	20.4 (34.8)	0.6 (1.0)	1.14 (0.75)
C	mini	20 (18)	28.4 (31.0)	10.7 (11.3)	0.31 (0.30)
	Six-bank (HR)	42 (36)	10.6 (12.3)	0.8 (0.9)	0.6 (0.58)
D	mini	14	26.5	4.1	0.25
	Six-bank (HR)	14	26.9	1.2	0.30
Pros 1	mini	17 (11)	29.7 (41.0)	9.4 (11.6)	0.33 (0.28)
	Six-bank (HR)	45 (14)	9.1 (32.4)	0.4 (1.3)	0.80 (0.46)
HN 1	mini	32 (22)	38.9 (51.5)	22.3 (27.7)	0.99 (0.85)
	Six-bank (HR)	110 (35)	8.1 (27.8)	0.5 (1.5)	2.49 (1.59)

located at the edges shows up (figures 4.10(e)–(g)), but the discretization of the leaf width has less of an impact on the overall RMS error. Removal of segments and isolated areas smaller than smaller than 1 cm^2 results in a reasonable number of segments, but an increase in average RMS error (6.9 ± 0.6 mini-MLC and 8.6 ± 0.7 the six-bank MLC). In all cases, the high-resolution sequences produce a smaller average RMS error than the conventional MLC (10.1 ± 1.3 all segments and 10.4 ± 1.5 without segments and isolated areas smaller than 1 cm^2).

Table 4.3: RMS error and efficiency for conventional MLC, mini-MLC and the six-bank MLC in high-resolution mode (HR), for geometrical examples. Data presented are the number of segments, efficiency factor(EF), RMS error of stratification and RMS error of sequencing. The results listed in parentheses do not include fields and isolated areas smaller than 1 cm^2.

Example	MLC	Number of segments	EF	RMS (strat)	RMS (seq)
A	1 cm	10	1	2.87	3.98
	mini	10	1	2.87	3.03
	Six-bank (HR)	10	1	2.87	2.90
B	1 cm	18	0.55	2.10	5.71
	mini	20 (18)	0.50 (0.56)	2.10	2.93 (3.08)
	Six-bank (HR)	32 (21)	0.28 (0.48)	2.10	3.18 (3.55)
C	1 cm	18	0.56	2.80	8.09
	mini	20 (18)	0.50 (0.56)	2.80	4.06 (4.15)
	Six-bank (HR)	42 (36)	0.24 (0.28)	2.80	3.36 (3.54)
D	1 cm	14	0.71	2.84	3.94
	mini	14	0.71	2.84	3.06
	Six-bank (HR)	14	0.71	2.84	2.98

4.4 Discussion

For the six-bank MLC to function as a multi-purpose collimator, suitable for all types of treatment, it is important that IMRT can be delivered as well. IMRT fields can be delivered in a low-resolution (conventional), as well as in a high-resolution mode. Our goal was to present the feasibility of the six-bank MLC to deliver IMRT.

The low-resolution mode is a straightforward approach, that may be useful when relatively simple IMRT techniques are used that do no require a high-resolution. In that mode the conventional MLC and the six-bank MLC produce almost the same segments and have similar RMS errors. The back-up collimation for the six-bank MLC is significantly better than for a conventional MLC, at the cost an of increase in total leaf travel.

The high-resolution mode is more complex than the low-resolution mode as field-shaping occurs by all three layers of leaves. The three layers of leaf banks

Table 4.4: RMS error and efficiency for conventional MLC, mini-MLC and the six-bank MLC in high-resolution mode (HR), for clinical examples. Data presented: the number of segments, efficiency factor (EF), RMS error of stratification and RMS error of sequencing. The results listed between the brackets do not include fields and isolated areas smaller than 1 cm^2.

Example	MLC	number of segments	EF	RMS (strat)	RMS (seq)
Pros 1	1 cm	17 (14)	0.59 (0.71)	2.96	18.40 (18.44)
	mini	17 (11)	0.53 (0.77)	2.96	11.16 (11.44)
	6bank (HR)	45 (14)	0.17 (0.63)	2.96	8.12 (10.11)
Pros 2	1 cm	13 (10)	0.77 (1.0)	3.29	13.05 (13.07)
	mini	14 (8)	0.63 (1.11)	3.29	6.74 (7.62)
	6bank (HR)	39 (10)	0.24 (1.0)	3.29	7.88 (9.76)
Pros 3	1 cm	16 (11)	0.63 (0.91)	2.70	13.73 (13.85)
	mini	16 (11)	0.59 (0.83)	2.70	7.33 (7.70)
	6bank (HR)	47 (14)	0.18 (0.67)	2.70	6.27 (7.90)
Pros 4	1 cm	14 (10)	0.71 (1.0)	3.09	14.75 (14.91)
	mini	17 (10)	0.56 (0.91)	3.09	9.66 (10.10)
	6bank (HR)	38 (13)	0.24 (0.71)	3.09	8.88 (10.01)
Pros 5	1 cm	16 (12)	0.63 (0.83)	2.80	13.22 (13.37)
	mini	19 (13)	0.50 (0.71)	2.80	9.71 (10.06)
	6bank (HR)	40 (12)	0.20 (0.77)	2.80	6.70 (8.65)
HN 1	1 cm	30 (23)	0.33 (0.43)	2.84	10.92 (11.18)
	mini	32 (22)	0.31 (0.45)	2.84	5.99 (6.64)
	6bank (HR)	110 (35)	0.08 (0.28)	2.84	6.35 (8.30)
HN 2	1 cm	25 (16)	0.40 (0.63)	2.83	8.20 (8.41)
	mini	25 (15)	0.40 (0.71)	2.83	5.67 (6.17)
	6bank (HR)	85 (19)	0.10 (0.45)	2.83	4.87 (7.76)
HN 3	1 cm	23 (18)	0.43 (0.56)	2.86	9.77 (9.98)
	mini	26 (21)	0.37 (0.48)	2.86	6.42 (7.10)
	6bank (HR)	111 (25)	0.08 (0.40)	2.86	6.63 (8.65)
HN 4	1 cm	36 (21)	0.27 (0.48)	2.93	11.65 (12.37)
	mini	39 (24)	0.26 (0.42)	2.93	6.72 (7.77)
	6bank (HR)	148 (44)	0.06 (0.23)	2.93	7.00 (9.60)
HN 5	1 cm	23 (15)	0.42 (0.67)	2.91	10.04 (10.19)
	mini	25 (14)	0.33 (0.71)	2.91	6.0 (6.81)
	6bank (HR)	89 (18)	0.09 (0.56)	2.91	6.05 (8.70)

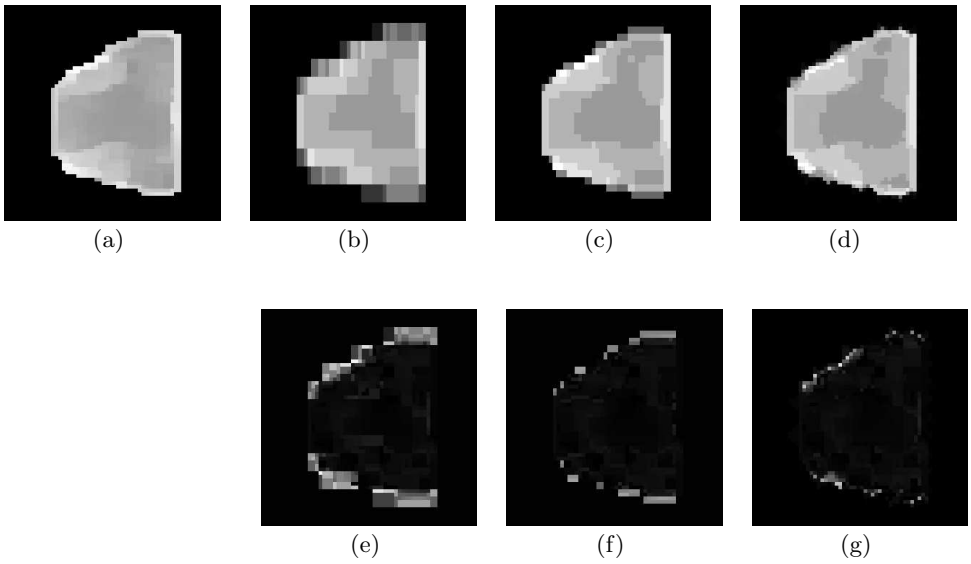

Figure 4.9: Example of prostate (Pros 1), size 12 × 12 cm^2: (a) original fluence. Fluence sequenced with (b) 1 cm MLC, (c) mini-MLC and (d) six-bank (HR). Absolute difference between the original and sequenced fluence for (e) 1 cm MLC, (f) ini-MLC and (g) six-bank MLC (HR).

cannot be sequenced independently as this might result in apertures in the three layers that do not overlap. A connection between the layers is established by use of masks for each layer of leaf banks to indicate which part of the fluence matrix is included in the aperture created by the other layers.

Overall, the performance of the six-bank MLC is comparable to that of the mini-MLC in terms of RMS error, but in particular for the head-neck examples substantially more segments are required to achieve this.

Otto and Clark (2002) investigated the enhancement of IMRT delivery through MLC rotation. Their results also show an improvement in spatial resolution. However, they present a strong correlation between the number of segments and the mean difference between realized and intended fluence. Indeed a twofold reduction in mean difference between input and result fluence comes at the cost of a doubling of the number of segments. In this study, we have chosen not to allow this collimator rotation in the conventional MLCs. Con-

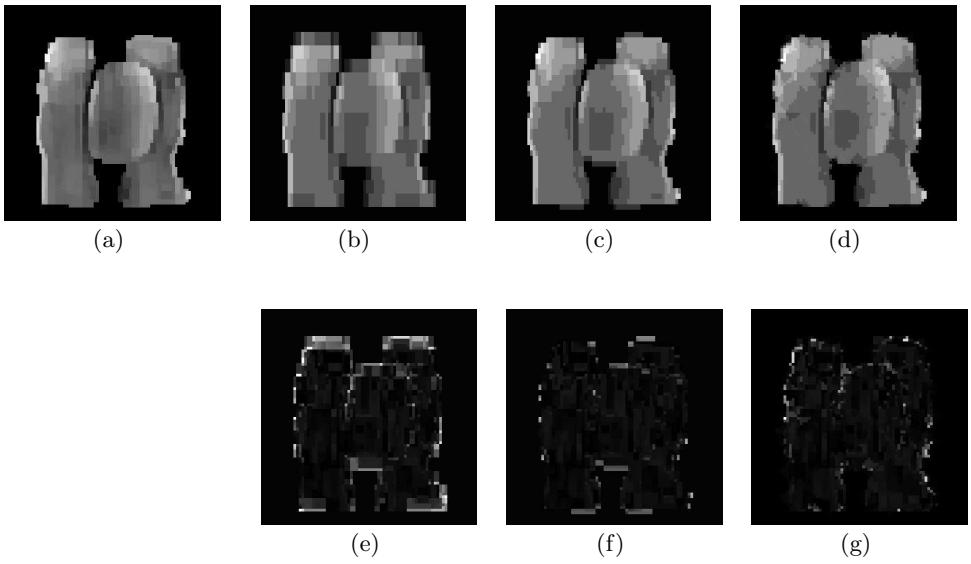

Figure 4.10: Example of head-neck (HN 1), size 16 × 16 cm^2: (a) Original fluence. Fluence sequenced with (b) 1 cm MLC, (c) mini-MLC and (d) six-bank (HR). Absolute difference between the original and sequenced fluence for (e) 1 cm MLC, (f) mini-MLC and (g) six-bank MLC (HR).

sidering the results by Otto and Clark (2002), it is reasonable to assume that for 1 cm MLC an improvement in RMS would be possible, but at the cost of increasing the number of segments. For the six-bank MLC this relation is not as clear. In particular for the simpler examples (geometrical examples A,B and D, and the prostate) the improvement in RMS error can be achieved without increasing the number of segments larger than 1 cm^2 substantially.

The large number of segments is the result of a choice that we made in the sequencer algorithm: in order to achieve optimal blocking of areas outside the aperture and the highest resolution field shaping, we repeated the segment set-up for each layer of leaf banks until their mask was stable (section 4.2.2). The consequence of this requirement is that concave shapes and segments consisting of two or more isolated areas can not be delivered. In these situations, multiple segments are required to deliver the fluence.

The choice to achieve optimal blocking by all three layers of leave banks bears

also on the design of the six-bank collimator itself. If one assumes that all three layers are required to block the beam outside the aperture, the thickness of an individual leaf may be reduced. On the other hand, if the leaves are made thicker, sufficient attenuation may be achieved with only one or two layers of leaves. In that case, a reduction of segments may be realized by allowing concave shapes and fragmented segments in the sequencing algorithm.

The high-resolution sequencer for the six-bank MLC is made for step and shoot delivery of IMRT. Dynamic IMRT delivery with the six-bank MLC may well be possible, but further work should be done to develop a suitable method. We expect the leaf travel to be significant, in particular if the requirement to use all three layers of leaves for blocking is maintained. Because the leaf banks are at sharp angles relative to each other, extremely fast leaf travel may be required in some layers.

4.5 Conclusion

In this study, we have presented two methods for delivering intensity modulated radiotherapy with a six-bank MLC system. Using either the low- or the high-resolution mode of sequencing reasonable sequences are obtained, with respect to numbers of segments, monitor unit efficiency and leaf travel.

In low-resolution mode similar segments can be delivered as with a conventional two-bank MLC with a leaf width of 1 cm.

The performance of the six-bank MLC in high-resolution mode is comparable to that of a mini-MLC with a leaf width of 0.4 cm, but a trade-off has to be made between accuracy and number of segments.

This combination of properties would make a linear accelerator equipped with a six-bank MLC suitable as a general purpose machine.

Acknowledgment

This study is supported by Elekta Ltd, Crawley, UK.

Chapter 5

MLC Leaf Design

This chapter has been submitted as:
R. Topolnjak and U. A. van der Heide. MLC Leaf Design.

Abstract
In this study, we present an analytical approach for optimizing the leaf design of a multi-leaf collimator (MLC) in a linear accelerator. To this end a model of the linac is created that includes the following parameters: the source size, the maximum field size, the distance between source and isocenter and the leaf's design parameters. First, the optimal radius of the leaf tip was found. This optimum was defined by the requirement that the fluence intensity should fall from 80% of the maximum value to 20% in a minimal distance, defining the width of the fluence penumbra. A second requirement was that this penumbra width should be constant when a leaf moves from one side of the field to the other. The geometric, transmission and total penumbra width (80-20%) were calculated depending on the design parameters.

The model is used to characterize and quantify the effect of changing the leaf's design parameters on the fluence penumbra. It is in agreement with Elekta, Varian and Siemens collimator designs. The model was also used to find the optimal design parameters for a six-bank multi-leaf system. Such a system was proposed earlier and combines a high-resolution field-shaping ability with a large field size.

5.1 Introduction

In external radiation treatment accelerators equipped with multileaf collimators (MLCs) are widely used to irradiate tumor and spare healthy tissue. Elekta, Varian and Siemens are the most popular accelerators equipped with MLCs. Jordan and Williams (1994), Galvin *et al.* (1993b) and Das *et al.* (1998) described their designs and dosimetric characteristics. To irradiate tumor and to spare healthy tissue as much as possible, it is important to have a steep dose gradient. Here, the leaf design is critical because of its impact on the penumbra (Galvin *et al.*, 1992; Yu, 1998). For optimizing the leaf design in practice, a balance must be found between the transmission of the leaves, their range of travel, the position in the collimator as well as their total volume as it relates to cost.

The easiest way to reduce the leaf's geometric penumbra and to improve the performance is by placing the collimator closer to the isocenter. However, the consequence will be a bigger leaf volume (and thus increasing cost) and possibly a reduction of leaf (over)travel. An other approach is to reduce the leaf's transmission penumbra by increasing the leaf thickness. But, in this case the leaf volume and the required space for collimator inside the accelerator head will increase.

In this paper we address the problem of deriving optimal leaf design and tip curvature. We were motivated by the following three major issues. Firstly, the leaf designs vary between vendors related to differences in the the geometric design of the linacs. This raises the question as to what is the influence of such different linac geometries on the optimal MLC? We therefore have characterized the effect of different compromises in linac design. Secondly, we want to find an optimal leaf design for our six-bank MLC (Topolnjak *et al.*, 2004a, 2005). Finally, we want to characterize and quantify the effect of different compromises which have to be made between performance parameters.

One approach of finding the optimal set of parameters is by deriving analytical expressions for the penumbra. Alternatively, a numerical trial and error approach can be used, such as ray tracing. The disadvantage of an analytical approach is that generally approximations of the system have to be made. On the other hand, the benefit is a better understanding and the opportunity of finding the theoretical limitations of the system under consideration.

In this investigation we present a simple analytical model by which a linac can be described. The model incorporates the parameters for the source size, the maximum field size, the distance between source and isocenter and the leaf's design parameters. With this model we characterize and quantify the effect of changing the leaf's design parameters on the fluence penumbra. Also, the results of the model are compared to the collimator designs of the commercially available MLCs of Elekta, Varian and Siemens. Finally, the model is used to find the optimal design parameters for a six-bank MLC (Topolnjak *et al.*, 2004a), which is an alternative design of a multi-leaf collimator that combines high-resolution field shaping with a large field size.

5.2 Materials and methods

In this investigation a simple analytical model by which a linac can be described will be made. The design parameters included in the model are: leaf thickness (lt), maximal field size (FS), source-MLC leaf distance (c), source-isocenter distance (F), coefficient of attenuation (μ), the source size (s), radius of the leaf tip (R) and leaf position (lp) projected at the isocenter. The output of the model will be the penumbra width (80-20%) (Khan, 1994; Sun and Zhu, 1995).

The leaf width is not included in the model as a parameter, because it does not influence penumbra width directly. But, the leaf width is important because it influences the maximum field size over which the penumbra should be constant. At maximum overtravel and a 'horizontal' position the leaves may bend under their weight. The displacement is proportional to the fourth power of overtravel and inversely proportional to the square of the leaf width (Shigley and Mischke, 1989). Thus, by using 0.4 cm leaves rather than 1 cm the maximum overtravel for the leaf would be decreased by a factor 0.63 without increasing the inter-leaf distance. It is important to find the optimal balance between field size and leaf width. Furthermore, our findings are applicable to any leaf width, because of a clear relation between leaf width and field size.

In intensity-modulated radiotherapy (IMRT) the maximum overtravel of the leaves (defined as the maximum distance the leaf can travel across the midline) has become an important issue. To be able to modulate an intensity of a beam

at the edges of the field, sometimes it is necessary to use leaves from the opposite bank. In this investigation the maximum field size (FS) will be a variable, or it will be set to generally accepted size of 40 x 40 cm^2. We will assume that leaves have full overtravel capability.

The coefficient of attenuation $\mu = 77.2$ m^{-1} was used, which corresponds to the attenuation of 4 MeV photons in tungsten. At this energy the attenuation exhibits a minimum (Bureau of Radiological Health, 1970).

Several physical effects contribute to the dose penumbra: scatter (P_s), geometry (P_g) and transmission (P_t) (Khan, 1994; Sun and Zhu, 1995). The scatter is primarily produced in the phantom/patient and does not depend on the specific leaf design. Furthermore, geometry and transmission of the leaves contribute to penumbra. If leaves are further away from a source, the geometry penumbra at the fluence plane will be smaller. Additionally, a thicker leaf will attenuate a ray more quickly and thus result in a smaller transmission penumbra. In our model we deal with the geometric and transmission penumbra separately.

In deriving the formula for geometric penumbra the Gaussian distribution of the source has been approximated with the flat one and size of 2 mm. Furthermore, the source was assumed to be a point in formulas for transmission penumbra and for deriving the optimal radius of the leaf tip.

5.2.1 Radius of the leaf tip.

From a clinical point of view it is important that the leaves produce a constant penumbra while moving move from one side of the field to the other. For single focus leaves this can be achieved by using a round leaf tip.

The optimal radius of the leaf tip was defined by the requirement that the fluence intensity should fall from 80% of the maximum value to 20% in a minimal distance, defining the width of the fluence penumbra. A second requirement was that this penumbra width should be constant when a leaf moves from one side of the field to the other.

The first step is to find a radius of the leaf tip for a given setup of parameters. In our model the parameters influencing the radius of the leaf tip are: lt, FS, F and μ. For a given setup of parameters we can start increasing the radius

of a leaf tip from the smallest possible value ($2 \cdot R_{\min} = lt$). Then, penumbra width 80-20% ($P_{(80-20\%)}$) will decrease in the whole region. After we achieve the optimal radius of a leaf tip, penumbra width will continue to decrease in the central part, but it will start to increase on the border of the field. This is caused by increasing transmission at the edges. In other words, bigger radius is better, but we have to be careful not to exceed maximum allowed radius of the leaf tip on the edge of fields. That means, that irradiation ray should always be able to have path going through the tip of a length which drops irradiation to 20% of the initial value (right leaf on figure 5.1).

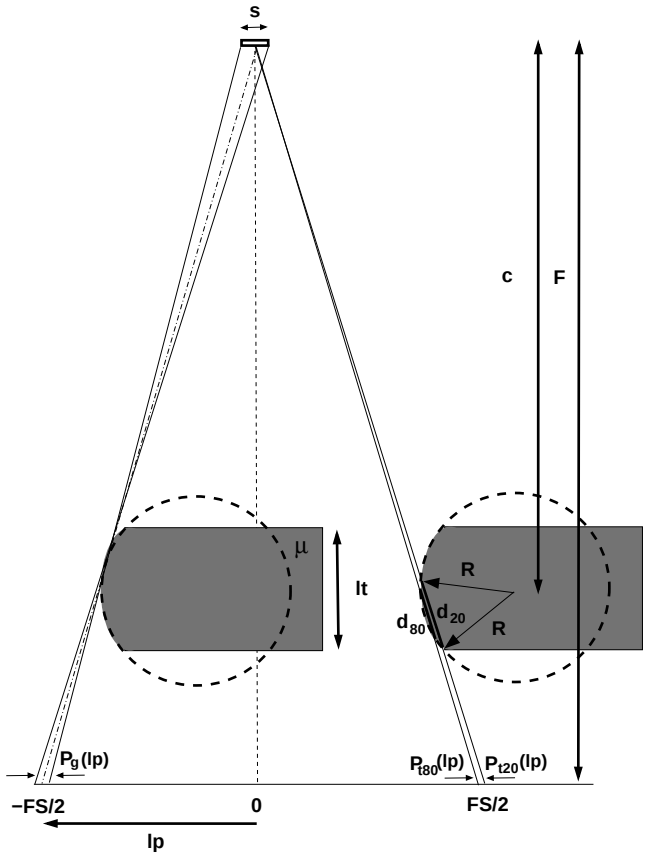

Figure 5.1: Schematic drawing of a leaf placed at the left and the right edge of a field. On the left-hand side is a leaf which presents the effect of geometric penumbra. On the right-hand side another leaf and its transmission penumbra are shown.

The optimal radius of a leaf tip which minimizes transmission penumbra if leaf is moved from the non-overtravel to the overtravel side is given by

$$R = \frac{1}{2} \cdot \sqrt{\frac{ln(0.2)^2}{\mu^2} + \frac{4 \cdot ln(0.2)^2 \cdot F^2}{\mu^2 \cdot FS^2} + \frac{4 \cdot ln(0.2) \cdot F^2 \cdot \sqrt{\frac{4 \cdot F^2 + FS^2}{F^2}} \cdot lt}{\mu \cdot FS^2} + lt^2 + \frac{4 \cdot F^2 \cdot lt^2}{FS^2}} \tag{5.1}$$

Appendix 5.A gives a description of derivation of equation (5.1). For design parameters: $F = 1$ m, $FS = 0.4$ m and $\mu(4MeV) = 77.2$ m^{-1} (Bureau of Radiological Health, 1970) equation (5.1) becomes

$$R = \sqrt{28.3 - 26.6 \cdot lt + 6.5 \cdot lt^2} \tag{5.2}$$

5.2.2 Geometric penumbra.

Now that the optimal radius of a leaf tip is found, the geometric penumbra of the leaves can be calculated. The geometric penumbra is actually a projection of the source onto the isocenter plane and linearly depends on the source size. The ratio of the distances between source and MLC leaf and between source and isocenter plane also determine the geometric penumbra. If a leaf bank is further from the source, the geometric penumbra at the isocenter plane will be smaller.

On the left side of figure 5.1 a leaf from the right bank placed at the left edge of the field can be seen. When leaf is moving from one to other side of the field it will create a geometric penumbra with different parts of the tip. Furthermore, the distance between source and leaf tip is shorter when leaf is on the right-hand side. As a consequence, geometric penumbra width will be smaller when leaf is on the right-hand side. Now, we can find an analytical expression for geometric penumbra width (80-20%) depending on the leaf position. The design parameters in our model are: R, F, s and c.

$$P_{g(80-20\%)}(lp) = \frac{0.6 \cdot s \cdot \left(F - c - R \cdot \sin\left(\arctan\left(\frac{lp}{F}\right)\right)\right)}{c + R \cdot \sin\left(\arctan\left(\frac{lp}{F}\right)\right)} \tag{5.3}$$

Appendix 5.B gives details about equation (5.3).

5.2.3 Transmission penumbra.

On the right-hand side figure 5.1 shows a schematic view of a leaf from the right bank placed at the right edge of a field. If a leaf position in the field is known, it is possible to define two ray lines through which irradiation will drop to 80% and 20% from the initial irradiation. The distance in the fluence plane between points $P_{t20}(lp)$ and $P_{t80}(lp)$ is the transmission penumbra width (80-20%).

In our model the parameters influencing transmission penumbra are distances source-MLC leaf, source-isocenter, radius of a leaf tip and coefficient of attenuation. The position of the point $P_{t20}(lp)$ is given by equation

$$\begin{aligned} P_{\mathrm{t20}}(lp) = \quad & F \cdot \tan\left(\arctan\left(\frac{c \cdot \frac{lp}{F} + R \cdot \cos\left(\arctan\left(\frac{lp}{F}\right)\right) + \frac{lp}{F} \cdot R \cdot \sin\left(\arctan\left(\frac{lp}{F}\right)\right)}{c}\right)\right) \\ & - F \cdot \tan\left(\arcsin\left(\frac{\sqrt{R^2 - \left(\frac{ln(0.2)}{2 \cdot \mu}\right)^2}}{\sqrt{c^2 + c \cdot \frac{lp}{F} + R \cdot \cos\left(\arctan\left(\frac{lp}{F}\right)\right) + \frac{lp}{F} \cdot R \cdot \sin\left(\arctan\left(\frac{lp}{F}\right)\right)}}\right)\right) \end{aligned} \tag{5.4}$$

The position of point $P_{t80}(lp)$ can been found with the same equation by applying a drop in dose to 80% instead of 20%. Appendix 5.C gives detailed description of equation (5.4).

5.3 Results

5.3.1 Radius of the leaf tip

To find the optimal radius of the leaf tip it is important to know how much leaves can travel from one side of the field to other. The leaves should produce a constant penumbra in the whole region as much as possible. Elekta (Jordan and Williams, 1994) and Varian (Galvin *et al.*, 1993b) do not produce MLCs with full overtravel leaves, but in this investigation the radius of the leaf tip was calculated assuming that leaves can fully overtravel. Furthermore, the optimal radius of the leaf tip depends on the leaf thickness and maximal field size of 40 x 40 cm^2. Table 5.1 lists real and calculated (chapter 5.2.1) values for the radius of the leaf tip for Elekta and Varian MLCs, based on the leaf thickness of 7.5 cm for Elekta and 5.5 cm for Varian.

Table 5.1: Real and calculated tip curvatures for Elekta and Varian MLCs.

tip curvature	Elekta (cm)	Varian (cm)
real	15	8
our calculation	14.0	8.9

5.3.2 Penumbra width (80-20%) for Elekta, Varian and Siemens MLCs

Elekta (Jordan and Williams, 1994) and Varian (Galvin *et al.*, 1993b) produce MLCs with round tip and single focus leaves. On the other hand, Siemens (Das *et al.*, 1998) has MLCs with straight tip and double focus leaves. The transmission through the leaf tip has contribution to the total penumbra for the Elekta and Varian MLC's but not for the Siemens MLC. However, the total penumbra for the Siemens MLC is bigger than for Varian (Huq *et al.*, 2002). This is due to the fact that the leaves are closer to the source. As a result the geometric penumbra is dominant, an effect that can not be compensated by the absence of transmission penumbra.

Figure 5.2 shows total penumbra width (80-20%) depending on the leaf position for Elekta (dashed), Varian (doted) and Siemens (solid) MLCs. The shape of the curves is consistent with experimental data presented by Huq *et al.* (2002). However, our values are lower because the scatter penumbra is not included in our equations for the fluence penumbra. In our analytical model the source has been approximated by a flat one with a size of 2 mm. Furthermore, we used $\mu(2MeV) = 84.341$ m^{-1} for mono-energetic photons, which is the maximum energy peak for 6 MV photons used in work of Huq *et al.* (2002).

5.3.3 Penumbra width (80-20%) for a general MLC

Figure 5.3(a) shows the effect of changing the distance source-MLC leaf, and the leaf thickness on the geometric penumbra (80-20%). The leaf thickness varies from 3 to 10 cm and the distance source-MLC leaf from 20 to 60 cm. Figure 5.3(b) shows the same effect but for the transmission penumbra (80-20%). The data is calculated with the leaves placed in the center of the field. From figure 5.3(a) we can see that leaves closer to the source produce a larger geometric penumbra width (80-20%) for all leaf thicknesses. Furthermore, the leaf

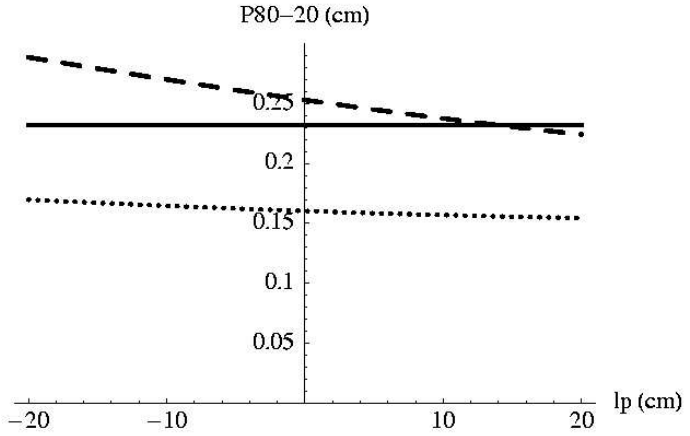

Figure 5.2: The total penumbra width (80-20%) depending on the leaf position (lp) for Elekta (dashed), Varian (doted) and Siemens (solid) MLCs.

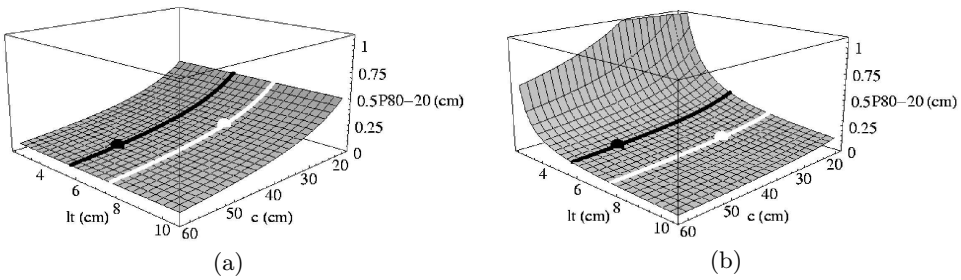

Figure 5.3: The effect of changing the distance between source and MLC leaf (c), and leaf thickness (lt) on: (a) geometric and (b) transmission penumbra width (80-20%). The white curve shows what would be the effect of changing the c for Elekta and black curve shows for Varian linac design. Note, white dot presents real Elekta design and black one presents Varian design.

thickness does not have an effect on the geometric penumbra width (80-20%). On the other hand, the transmission penumbra mainly depends on the leaf thickness and less on the distance source-leaves (figure 5.3(b)). Additionally, figure 5.3 shows the effect in our model of changing the distance source-MLC leaf on the geometric and transmission penumbras for the Elekta (white curve) and Varian (black curve) linacs. The white dot represents the Elekta design and the black one the Varian design. Changing the distance source-MLC leaf for Elekta and Varian MLCs would require a new design of the leaves, because the physical leaf width should be changed.

Figure 5.4 shows the total penumbra width (80-20%) which is the square root of the sum of the squared geometric and transmission penumbras. For leaves thicker than 4 cm the geometric penumbra plays the most dominant role. The most important parameter is the distance source-leaves. Moreover, the total

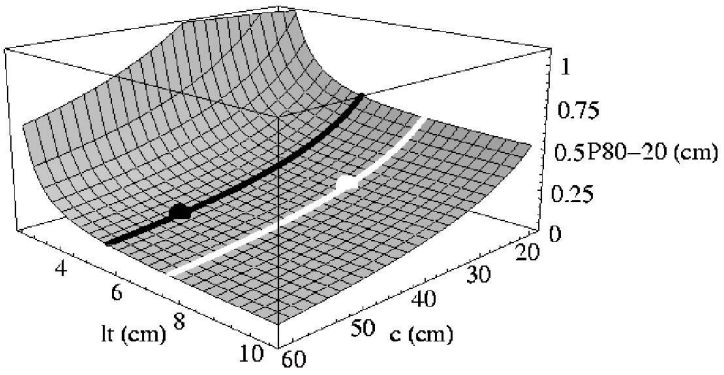

Figure 5.4: The effect of changing the distance between source and MLC leaf (c), and leaf thickness (lt) on penumbra width (80-20%). The white curve shows what would be the effect of changing the c for Elekta and black curve shows for Varian linac design. Note, white dot presents real Elekta design and black one presents Varian design.

penumbra width (80-20%) for the Varian linac design (black dot) is 1 mm smaller than for Elekta (white dot). This is mainly caused by the smaller geometric penumbra for the Varian design (black dot, figure 5.3(a)) than for Elekta (white dot, figure 5.3(a)) linac.

The radius of leaf tip is optimal in terms of achieving the smallest possible transmission penumbra that remains constant with leaf position in the field

(chapter 5.2.1). Nevertheless, a small change remains of the penumbra (80-20%) size if a leaf is moved from the non-overtravel to the overtravel side. The reason for this change is that the distance between the source and the leaf tip is different when the leaf is on the same position on non-overtravel or on the overtravel side (figure 5.8B). The same effect happens for the transmission penumbra, but it is smaller. If the leaves are positioned at $lp = +20$ cm instead of in the center of the field (figure 5.4, $lp = 0$ cm), they will produce a smaller penumbra width (80-20%) for all combinations of lt and c. Figure 5.5(a) shows this difference. The stability of the system varies depending on the design. If leaves are closer to the source and thicker, this effect become more prominent. Figure 5.5(b) shows the difference in penumbra width obtained with leaves positioned on the overtravel position at lp = -20 cm and in the center of the field ($P_{(80-20\%)}(lp = -20cm) - P_{(80-20\%)}(lp = 0cm)$). The effect is similar, but has opposite sign.

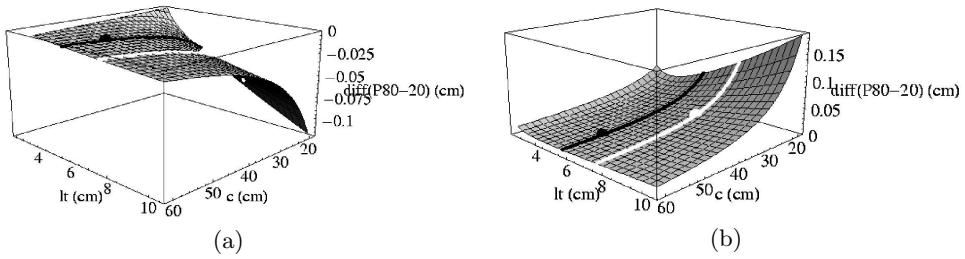

Figure 5.5: The difference in penumbra width (80-20%) obtained with leaves positioned at (a) $lp = +20$ cm or (b) lp = -20 cm and leaves positioned in the center of the field ($lp = 0$ cm). The white curve shows what would be the effect of changing the c for Elekta and black curve for Varian linac design. Also, white dot presents real Elekta design and black one presents Varian design.

5.3.4 A six-bank MLC

In a previous study, we proposed an alternative design for a multi-leaf collimator that combines high-resolution field shaping with a large field size (Topolnjak *et al.*, 2004a). The system consists of three layers of bank pairs, positioned at 60° relative to each other. The space available for a six-bank collimator

in the Elekta-accelerator geometry lies between the ionization chamber and adaptor ring (18 cm $< c <$ 50 cm). However, to avoid that the lowest pair of leaf banks become unpractically large and to be able to achieve full overtravel of the leaves we positioned the lowest layer at $c = 41.75$ cm. Furthermore, we added others layers with the condition of keeping the penumbra width (80-20%) size similar to the lowest layer as much as possible. Additionally, the space of 2.5 cm between layers should be left for the leaf motors. Table 5.2 lists the positions of the leaves, leaf thickness and penumbra width (80-20%).

Figure 5.6 shows all possible solutions for leaf width and distance source-MLC leaf with the condition that the penumbra width should lie between 3.6 mm and 4.0 mm. The black, gray and white dots represent solutions for the leaves in the highest, middle and the lowest layers of the bank pairs for the six-bank MLC, respectively. The results (table 5.2) for the penumbra width (80-20%)

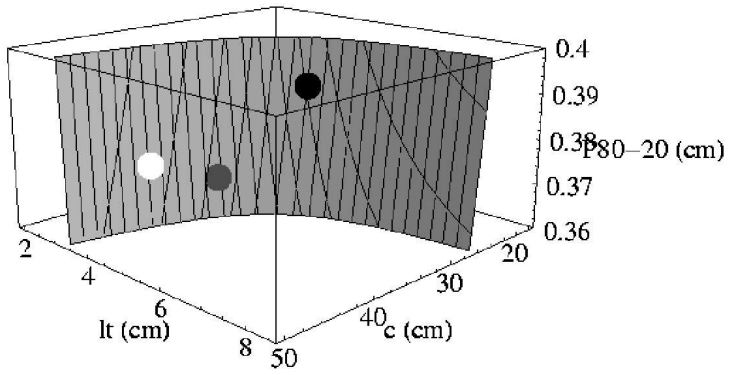

Figure 5.6: All possible solutions for leaf width and distance source-leaf with a condition that penumbra width should be in range between 3.6 mm and 4.0 mm. Black, gray and white dots represent solutions for leaves in the highest, middle and the lowest layers of the bank pairs for the six-bank MLC, respectively.

obtained from three-dimensional (3D) ray tracing (Topolnjak *et al.*, 2004a) are almost identical to the results in this investigation, when only the contribution from the primary source is considered. Finally, the radius of the tip curvature in the analytical model was set to the same value as in the 3D ray tracing model (Topolnjak *et al.*, 2004a).

Table 5.2: Penumbra width (80-20%) ($P_{(80-20\%)}(R)$) depending on the radius of the leaf tip (R) for analytical (anal) model with optimal R, with R of the six-bank MLC, and for 3D ray tracing model (ray-trac) obtained with primary source only.

Banks pair	Distance from the source (cm)	Leaf thickness (cm)	anal (optimal R) $P_{(80-20\%)}$(R) (cm)	ray-trac (6bank R) $P_{(80-20\%)}$(R) (cm)	anal (6bank R) $P_{(80-20\%)}$(R) (cm)
High	28.5	5	0.39 (7.6)	0.37 (8)	0.38 (8)
Middle	35.5	4	0.37 (5.1)	0.34 (6)	0.33 (6)
Low	41.75	3.5	0.38 (3.9)	0.37 (4)	0.37 (4)

5.4 Discussion

In this investigation a simple analytical model describing a linac has been presented. The model successfully characterizes and quantifies the effect of changing the leafs' design parameters on the fluence penumbra.

First, an optimal radius of leaf tip was found. By our choice, it was optimized to produce minimal transmission penumbra width (80-20%) if leaves travel from one side of the field to the other. The maximum field size (FS) and leaf (over)travel have influence on the optimal radius of a leaf tip as well. In the result section we used a maximum FS of 40 x 40 cm^2. Finally, in defining the optimal radius of the leaf tip the source was approximated by a point.

The concept of the geometric penumbra (chapter 5.2.2) was modelled using a source with a finite size and a flat fluence distribution. In order to simply the model for the transmission penumbra (chapter 5.2.3) the source was here approximated by a point.

In our analytical model the flattening filter is not included. It could be modelled in principle as a secondary source. However, because its size is large relative to the primary source, it is questionable if the source can be approximated by a point, or by a flat finite fluence distribution. Because the relative intensity contribution of the secondary source to the primary source is about 10% (Zhu *et al.*, 1995) we believe it is valid to neglect this contribution to the total penumbra. Indeed our model shows good agreement with results presented by Huq *et al.* (2002) for the Elekta, Varian and Siemens Linacs. We expect that the model will become unreliable when the leaves are positioned very close to the source, or when the leaf width is chosen very small.

The different setup of design parameters will result in different penumbra widths (80-20%). From figures 5.3–5.4 it can be seen that for leaves thinner than 4 cm the transmission penumbra becomes dominant and for leaves close to the source the geometric penumbra gets more important. However, thicker leaves and leaves closer to the isocenter will always produce smaller penumbra. A drawback of increasing the distance source-MLC leaves is the reduction of the maximal field size, the increase of the leaf volume and the reduction of the clearance for the patient. The increase of leaf thickness only leads to a larger leaf volume. By placing the collimator closer to the isocenter the volume of the leaf will increase as square of ratio of source-leaf distances ($V_2 = \left(\frac{c_2}{c_1}\right)^2 \cdot V_1$).

Furthermore, to achieve the same field size by doubling c the real travel of the leaves should double as well. By having the constant condition on deflection of the leaves the allowed overtravel will increase $\sqrt{\frac{c_2}{c_1}} = \sqrt{2} \approx 1.41$ times. That means that without allowing a bigger deflection the maximum field size will effectively be reduced.

By using a round leaf tip it is not possible to obtain a completely constant total penumbra width if the leaves are moving from one side of the field to the other. The penumbra width is always bigger on the overtravel side. The main reason for this is an increase of the geometric penumbra due to smaller distance between source and leaf tip. The effect of increasing the penumbra width is relatively small compared to the total penumbra width. Again, if the leaves are closer the source and thicker, this effect becomes more important. Maybe with an ellipsoid shape of the leaf tip, further improvement in the stability of the penumbra width could be archieved.

If overtravel of the leaves is limited, an assymetric situation is created. Now, the center of the curve defining the leaf tip should no longer be positioned in the middle of the leaf. We didn't study this offset further because for IMRT only leaves with full overtravel are considered.

5.5 Conclusion

In this study, we presented an analytical model by which a linac can be described. The model is able to characterize and quantify the effect of changing the leaf's design parameters on the fluence penumbra.

For leaves thinner than 4 cm, the transmission penumbra becomes dominant, and for leaves close to the source the geometric penumbra plays a role. However, thicker leaves and leaves closer to the isocenter will always produce smaller penumbra. A drawbacks of increasing the distance source-MLC leaves are a reduction of maximal field size, an increase of leaf volume and a decrease of the clearance for the patient. The increase of leaf thickness increases only leaf volume.

Finally, the analytical model was used to find the optimal leaf design parameters for a six-bank MLC. By choosing the leaf thickness of 3.5 cm, 4 cm and

5 cm from the lowest to the highest bank respectively, the similar total fluence penumbra width (80-20%) for all layers was achieved.

Acknowledgment

This study is supported by Elekta Ltd, Crawley, UK.

Appendix

5.A Radius of the leaf tip

Attenuation in leaves can be described by formula (5.5A) and it has the following parameters: d is path length through the leaf tip, μ is a coefficient of attenuation, I_o is an initial irradiation, and I is irradiation on the fluence plane (after attenuation).

$$I = I_o \cdot e^{-\mu d} \tag{5.5A}$$

If we want the initial irradiation to drop to 20% of its initial value, the path length (d_{20}) can be found from the equation (5.5A) as follows:

$$I(20\%) = 0.2 \cdot I_o \quad \Longrightarrow \quad d_{20} = -\frac{ln(0.2)}{\mu} \tag{5.6A}$$

Figure 5.7A shows a schematic view of a leaf placed at the edge of a field. Let B, be an input point where of the irradiation ray which passes through the leaf tip. Let A be an output point of that ray. The distance between points A and B is d_{20}. To simplify, the origin of the coordinate system is placed at point A. Now B has coordinates $(-d_{20} \cdot \sin(\alpha),\ d_{20} \cdot \cos(\alpha))$ where $\alpha = \arctan(\frac{FS}{2F})$

Further, a circle approximating a leaf tip, and passing through A and B has a center at D(D_x, $lt/2$) determined by:

$$\begin{aligned} (A_x - D_x)^2 + (A_y - D_y)^2 &= R^2 \\ (B_x - D_x)^2 + (B_y - D_y)^2 &= R^2 \end{aligned} \tag{5.7A}$$

and after substituting

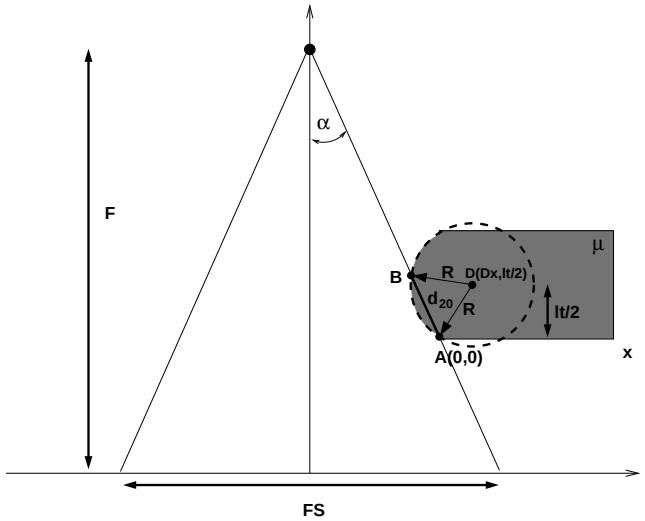

Figure 5.7A: Schematic view of a leaf placed at the edge of a field. Point C is the position of the source, point A is point at the edge of a filed. d_{20} is the distance between points A and B, and R is a radius of a tip.

$$(D_x)^2 + \left(\frac{lt}{2}\right)^2 = R^2$$

$$\left(-d_{20} \cdot \sin\left(\arctan\left(\frac{FS}{2F}\right)\right) - D_x\right)^2 + \left(d_{20} \cdot \cos\left(\arctan\left(\frac{FS}{2F}\right)\right) - \frac{lt}{2}\right)^2 = R^2 \tag{5.8A}$$

From the equations 5.6A and 5.8A, R can be found and it is given in equation 5.1.

5.B Geometric penumbra

Figure 5.8B shows a schematic view of a leaf of the right bank, placed at the left, or the right edge of a field. Now, an angle $\alpha(lp)$ defined by a tangent of the tip and the central axis can be defined. Let lp be a position of the leaf tip projected at Iso-center, F be a distance between the source and the Iso-center, c a distance between the source and the center of the leaf, and s a source size. Finally, a distance *y(lp)* can be defined:

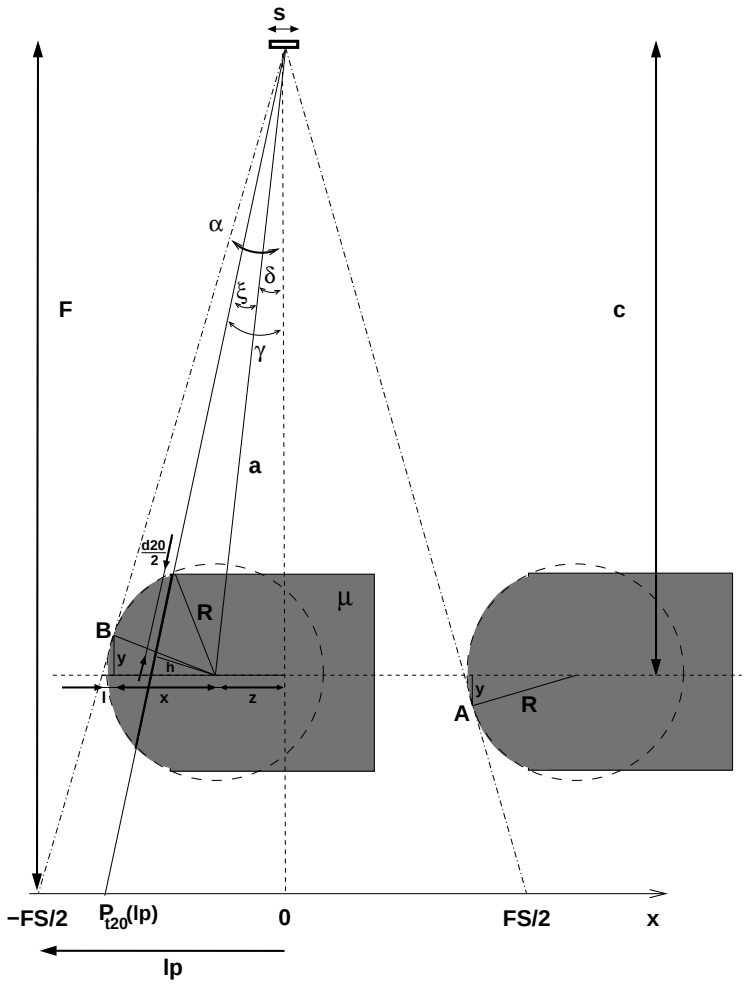

Figure 5.8B: Schematic drawing of a leaf placed at the left and the right edge of a field. All necessary variables to find geometric and transmission penumbra are shown.

$$\alpha(lp) = \arctan\left(\frac{lp}{F}\right), \qquad y(lp) = R \cdot \sin(\alpha(lp)) \tag{5.9B}$$

Geometric penumbra is defined by 5.10B (Khan, 1994),

$$P_{\mathrm{g}} = \frac{s \cdot (F - c)}{c} \tag{5.10B}$$

and penumbra width 80-20% is given by 5.11B

$$P_{\mathrm{g}(80-20\%)}(lp) = 0.6 \cdot P_{\mathrm{g}}(lp) \tag{5.11B}$$

Finally, $P_{\mathrm{g}(80-20\%)}(lp)$ is described in 5.12B

$$\begin{aligned} P_{\mathrm{g}(80-20\%)}(lp) &= \frac{0.6 \cdot s \cdot (F - (c + y(lp)))}{c + y(lp)} \\ &= \frac{0.6 \cdot s \cdot \left(F - c - R \cdot \sin\left(\arctan\left(\frac{lp}{F}\right)\right)\right)}{c + R \cdot \sin\left(\arctan\left(\frac{lp}{F}\right)\right)} \end{aligned} \tag{5.12B}$$

From 5.12B the size of a geometric penumbra while leaf is moving from one side of the field to another is known. In the formulae above the Gaussian distribution of the source was approximated with the flat one.

5.C Transmission penumbra

In this section analytical formula of transmission penumbra depending on leaf position will be presented. On the right hand side of the figure 5.1 a schematic view of a leaf from the right bank placed at the right edge of a field is shown. If a leaf position (lp) in the field space is known, two ray lines through which irradiation will drop to 80% and 20% from the initial irradiation can be defined. If the distance in the fluence plane between points $P_{t20}(lp)$ and $P_{t80}(lp)$ is considered, transmission penumbra 80-20% is known.

$P_{\mathrm{t}(80-20\%)}(lp)$ is the distance between points $P_{t20}(lp)$ and $P_{t80}(lp)$:

$$P_{\mathrm{t}(80-20\%)}(lp) = P_{t20}(lp) - P_{t80}(lp) \tag{5.13C}$$

Figure 5.8B shows all variables relevant for finding position of point $P_{t20}(lp)$:

$$P_{t20}(lp) = F \cdot \tan(\gamma_{20}(lp)) \tag{5.14C}$$

where $\gamma_{20}(lp)$ is an angle between 20% ray line and the central axis,

$$\gamma_{20}(lp) = \delta(lp) - \xi_{20}(lp) \tag{5.15C}$$

$\delta(lp)$ is an angle between ray line connecting center of a tip curvature and the central axis, and $\xi_{20}(lp)$ is an angle between 20% ray line and the center tip ray line,

$$\delta(lp) = \arctan\left(\frac{z(lp)}{c}\right), \quad \xi_{20}(lp) = \arcsin\left(\frac{h_{20}(lp)}{a(lp)}\right) \tag{5.16C}$$

$z(lp)$ is the distance between the center of a tip and the central axis, $a(lp)$ is the distance between the source and the center of tip, c is the distance source-center of a leaf and $h_{20}(lp)$ is the distance between 20% ray line and the center of the tip.

$$h_{20}(lp) = \sqrt{R^2 - \left(\frac{d_{20}}{2}\right)^2}, \quad d_{20} = -\frac{\ln 0.2}{\mu} \tag{5.17C}$$

R is a radius of the tip, d_{20} is a path length through the tip, and μ is a coefficient of attenuation.

Further, from the equation (5.16C) *a(lp)* and *z(lp)* are

$$\begin{aligned} a(lp) &= \sqrt{z(lp)^2 + c^2} \\ z(lp) &= c \cdot \frac{lp}{F} + x(lp) + l(lp) \end{aligned} \tag{5.18C}$$

Figure 5.8B shows variables $x(lp)$, $y(lp)$ and $l(lp)$

$$\begin{aligned} l(lp) &= y(lp) \cdot \frac{lp}{F} \\ y(lp) &= R \cdot \sin(\alpha(lp)) \\ x(lp) &= R \cdot \cos(\alpha(lp)) \end{aligned} \tag{5.19C}$$

Finally, $\alpha(lp)$ is an angle between the tangent of a leaf tip and the central axis

$$\alpha(lp) = \arctan\left(\frac{lp}{F}\right) \tag{5.20C}$$

Now, by substitution of all variables in equation 5.14C the position of the point $P_{20}(lp)$ is given in equation 5.4. Position of the point $P_{80}(lp)$ can be found the same way as the position of the point $P_{20}(lp)$.

Chapter 6

Summary and general discussion

The aim of this **thesis** was to investigate the influence of linac/MLC design on intensity-modulated radiotherapy (IMRT). Also, an alternative multi-leaf collimator (MLC) design and IMRT sequencer were developed. Finally, an analytical model of the optimal MLC leaves design was made.

The motivation for this work was given by the fact that a conventional linac/MLC, currently available on the market, has not been designed for IMRT. It has initially been designed for conformal radiotherapy. The MLCs were constructed for beam shaping, but now they are also used for IMRT. A step-and-shoot approach of delivering IMRT usually produces a large number of segments. Therefore, MLCs should be able to quickly deliver multiple segments, to have small transmission, and to produce a sharp penumbra. With the advent of imaging in radiotherapy and of IGRT, a higher precision of treatments can be achieved. Thus, to benefit from this optimally, the resolution and performance of an MLC should also be improved.

In **chapter 2** the impact of linac/MLC design parameters on IMRT treatment plans have been quantified. The investigated parameters were: leaf width of the MLC, leaf transmission related to the thickness of the leaves, and penumbra related primarily to the source size. Seven head-and-neck patients with stage T1-T3N0-N2cM0 oropharyngeal cancer were studied. For each patient nine plans were made with a different set of linac/MLC parameters. The plans were optimized in Pinnacle^3 v7.6c and PLATO RTS v2.6.4, ITP v1.1.8. A hypothetical ideal linac/MLC was introduced to investigate the influence of one parameter at the time without the interaction of other parameters. When any of the three parameters was increased from the ideal setup values (leaf

width 2.5 mm, transmission 0%, penumbra 3 mm), the mean dose to the parotid glands increased, given the same tumor coverage. The largest increase was found when increasing the leaf transmission. The investigation showed that by changing more than one parameter of the ideal linac/MLC setup, the increase in the mean dose was smaller than the sum of the dose increments for each parameter separately. As a reference to clinical practice, we also optimized the plans of the seven patients with the clinically used Elekta SLi 15, equipped with a standard MLC with a leaf width of 10 mm. As compared to the ideal linac this resulted in an increase of the average dose to the parotid glands of 5.8 Gy. The clinical impact of dose differences can be assessed by observing the normal tissue control probability (NTCP) curves as proposed by Roesink *et al.* (2001) and Eisbruch *et al.* (1999). A complication is defined as a reduction of the stimulated parotid flow rate one year after a radiotherapy treatment to less than 25% of the of flow before the treatment. Depending on the model used (Roesink *et al.* (2001) or Eisbruch *et al.* (1999)), the dose reduction found between the Elekta and the ideal linac/MLC results in an average decrease of the NTCP between 8% and 17%. **Chapter 2** concludes that the MLC leaf width, MLC leaf transmission and linac's source size have a large impact on IMRT treatment plans of patients with head-neck cancer. That motivated us to propose an alternative multi-leaf collimator (MLC) designed according to those findings.

The resolution of an MLC can be improved by decreasing the leaf width. A drawback is that the maximum field size will decrease as well, because at maximum overtravel and in a 'horizontal' position, the leaves may bend under their weight. The displacement is proportional to the fourth power of overtravel and inversely proportional to the square of the leaf width (Shigley and Mischke, 1989). Thus, by using 0.4 cm leaves rather than 1 cm the maximum overtravel for the leaf would be decreased by a factor 0.63 without increasing the inter-leaf distance. It is important to find the optimal balance between field size and leaf width. Another approach of increasing resolution of an MLC is by adding more layers of leaves which was proposed and presented in **chapter 3**. A six-bank multi-leaf system, presented here, is an alternative MLC that allows high precision shaping of large fields. The MLC system consists of three layers of two opposing leaf banks. The layers are rotated 60° relative to each other. The leaves in each bank have a standard width of 1 cm projected at the isocenter. Because of the symmetry of the collimator set-up it is expected that collimator

rotation will not be required, thus simplifying the construction considerably. Furthermore, inter-leaf transmission in one leaf bank would be blocked by the two other banks. For this reason a tongue-and-groove design would not be required. The total thickness of all three layers would be 12.5 cm. That would decrease transmission of the MLC in comparison with MLCs available on the market and would improve characteristics of the MLC considerably. A 3D ray tracing computer program was developed in order to simulate the fluence profile for a given collimator. It was used to optimize the design and investigate its performance. The simulations showed that a six-bank collimator would afford field shaping of fields of about 40 cm diameter with a precision comparable to that of existing mini-MLCs with a leaf width of 4 mm.

For the six-bank multi-leaf system, which would function as a multi-purpose collimator suitable for all types of treatments, the delivery of IMRT is also an important task. A sequencer for delivering step-and-shoot IMRT using a six-bank MLC has been described in **chapter 4**. A low-resolution mode of sequencing was achieved by using one layer of leaves as primary MLC, while the other two were used to improve back-up collimation. For high-resolution sequencing an algorithm was presented that creates segments shaped by all six banks. Using either the low- or the high-resolution mode of sequencing reasonable sequences were obtained with respect to the number of segments, monitor unit efficiency and leaf travel. In a low-resolution mode similar segments could be delivered as with a conventional two-bank MLC with a leaf width of 1 cm. The performance of the six-bank MLC in high-resolution mode was comparable to that of a mini-MLC with a leaf width of 0.4 cm, but a trade-off had to be made between accuracy and number of segments. This combination of properties would make a linear accelerator equipped with a six-bank MLC suitable as a general purpose machine.

To irradiate the tumor and to spare healthy tissue as much as possible, it is important to have a steep dose gradient. Here, the leaf design is critical because of its impact on the penumbra. For optimizing the leaf design in practice, a balance must be found between the transmission of the leaves, their range of travel, the position in the collimator as well as their total volume as it relates to cost. In **chapter 5** an analytical approach for optimizing the leaf design of an MLC in a linear accelerator has been given. To this end a model of the linac has been created that includes the following parameters: the source size, the

maximum field size, the distance between source and isocenter and the leaf's design parameters. First, the optimal radius of the leaf tip was found. This optimum was defined by the requirement that the fluence intensity should fall from 80% of the maximum value to 20% in a minimal distance, defining the width of the fluence penumbra. A second requirement was that this penumbra width should be constant when a leaf moves from one side of the field to the other. The geometric, transmission and total penumbra width (80-20%) were calculated depending on the design parameters. The model is used to characterize and quantify the effect of changing the leaf's design parameters on the fluence penumbra. It is in agreement with Elekta, Varian and Siemens collimator designs. **Chapter 5** concludes that for leaves thinner than 4 cm the transmission penumbra becomes dominant, and for leaves close to the source the geometric penumbra is more important. However, thicker leaves and leaves closer to the isocenter will always produce a smaller penumbra. A drawback of increasing the distance source-MLC leaves is the reduction of the maximal field size, the increase of the leaf volume and the reduction of the clearance for the patient. The increase of leaf thickness only leads to a larger leaf volume. Finally, the analytical model was used to find the optimal leaf design parameters for a six-bank MLC. By choosing the leaf thickness of 3.5 cm, 4 cm and 5 cm from the lowest to the highest bank respectively, the similar total fluence penumbra width (80-20%) for all layers was achieved.

In conclusion, linac/MLC design is of great importance for IMRT treatment of patients. The effect of different setup of linac/MLC design parameters has been characterized and quantified. As result of those findings, a new design of an MLC has been proposed. By further improvement of IGRT and application of on-line position verification on a daily basis, additional reduction of margins will be possible. This would lead to a great benefit enhancement of a six-bank MLC over the conventional MLCs.

Hoofdstuk 7

Samenvatting

Radiotherapie is een methode voor de behandeling van patienten met kanker waarbij straling wordt toegepast. Voor dit doel wordt in de meeste gevallen een lineare versneller (linac) gebruikt. Dit apparaat deponeert hoog-energetische ioniserende straling (fotonen of electronen) in de tumor in de patient. De absorptie van deze straling in het weefsel beschadigt cellen. Intensiteitsgemoduleerde radiotherapie (IMRT) is een geavanceerde vorm van radiotherapie, waarbij een niet-uniforme bundelintensiteit wordt gebruikt. Met deze extra vrijheidsgraad is het mogelijk de vorm van de dosisverdeling nauwkeurig te sturen.

De motivatie voor dit werk werd gegeven door het feit dat een conventionele linac met multi-leaf collimator (MLC), zoals nu op de markt beschikbaar, niet is ontworpen voor IMRT. In dit onderzoek is de invloed van het ontwerp van de linac/MLC op IMRT bestudeerd. Ook werd een alternatieve MLC ontworpen en een bijbehorende IMRT sequencer. Tot slot werd een analytisch model opgesteld voor een optimaal ontwerp van MLC leaves.

In **hoofdstuk 2** is de invloed van ontwerp parameters van de linac/MLC op IMRT bestralingsplannen gekwantificeerd. De onderzochte parameters zijn: de leaf breedte van de MLC; de transmissie van een leaf, gerelateerd aan de dikte ervan; en de penumbra, vooral gerelateerd aan de grootte van het focus van de stralingsbundel. Zeven patienten met kanker in het hoofd-hals gebied (T1-T3N0-N2cM0 oropharynx tumoren) werden bestudeerd. Voor elke patient werden 9 bestralingsplannen gemaakt met een verschillende combinatie van linac/MLC parameters. De plannen werden geoptimaliseerd in Pinnacle^3 v7.6c en PLATO RTS v2.6.4, ITP v1.1.8. Een hypothetische ideale linac/MLC

werd geintroduceerd als referentie om de invloed van een van de parameters te onderzoeken zonder interactie van de andere parameters. Wanneer een van de drie parameters vergroot werd ten opzichte van de ideale waarde (leaf breedte 2.5 mm, transmissie 0%, penumbra 3 mm), dan leidde dit tot een verhoging van de gemiddelde dosis op de parotis speekselklieren bij een gelijke bestraling van de tumor. De grootste toename werd gevonden bij een verhoging van de leaf transmissie. Het onderzoek liet zien dat bij verandering van meer dan een parameter ten opzichte van de ideale linac/MLC de toename in parotis dosis geringer was dan de som van de afzonderlijke componenten. Als referentie naar de klinische praktijk hebben we voor de zeven patienten ook plannen geoptimaliseerd met de klinisch gebruikte Elekta Sli 15, met een standaard MLC met leaves van 1 cm breedte. Vergeleken met de ideale versneller leverde dit een toename in gemiddelde dosis op de parotis klieren op van 5.8 Gy.

In **hoofdstuk 3** wordt het ontwerp gepresenteerd van een alternatieve multi-leaf collimator, de zes-bank MLC waarmee van grote velden de vorm met een hoge-resolutie gemaakt kan worden. Het MLC systeem bestaat uit drie lagen van twee tegenover elkaar liggende leaf banken. Deze lagen zijn 60 graden gedraaid ten opzichte van elkaar. De leaves in elk van de banken hebben een standaardbreedte van 1 cm, geprojecteerd in het isocentrum. Vanwege de symmetrie van deze geometrie wordt verwacht dat rotatie van de collimator niet nodig zal zijn, wat het ontwerp van de kop van de versneller sterk vereenvoudigt. Een 3D ray tracing computer programma is ontworpen om het fluentieprofiel van een gegeven collimator te simuleren. Dit programma werd gebruikt om het ontwerp te optimaliseren en de prestaties ervan te bestuderen. De simulaties toonden aan dat een zes-bank collimator nauwkeurige veldvorming mogelijk maakt van velden met een diameter van ongeveer 40 cm, waarbij de precisie vergelijkbaar is met die van bestaande mini-MLCs met leaves van 4 mm breed.

Om mogelijk te maken dat het zes-bank multi-leaf systeem voor alle typen bestraling bruikbaar is, is het van belang dat ook IMRT kan worden uitgevoerd. Een sequencer voor het afstralen van step-and-shoot IMRT met de zes-bank MLC is beschreven in **hoofdstuk 4**. Een lage-resolute methode van sequencing werd ontwikkeld door een van de lagen van de MLC te gebruiken als primaire collimator, terwijl de andere twee uitsluitend werden gebruikt om de transmissie buiten de apertuur van de primaire collimator te beperken.

Voor hoge-resolutie sequencing wordt een algoritme gepresenteerd waarmee de segment vorm door een combinatie van alle zes banken wordt gemaakt. Zowel met de lage als de hoge resolutie methode werden goede sequenties verkregen wat betreft aantal segmenten, efficientie van monitor eenheden en afstand waarover de leaves moeten bewegen. Met de lage-resolutie methode werden vergelijkbare segmenten gemaakt als met een conventionele MLC met 1 cm leaves. De prestaties van hoge-resolutie methode van de zes-bank MLC zijn vergelijkbaar met die van een mini-MLC met leaves van 0.4 cm breed, maar hier moet wel een afweging worden gemaakt tussen nauwkeurigheid en aantal segmenten. Deze combinatie van eigenschappen maakt een lineaire versneller met een zes-bank MLC geschikt als algemeen bruikbare machine voor alle typen externe radiotherapie.

Om de tumor te bestralen en gezond weefsel maximaal te sparen, is het belangrijk steile dosisgradienten te kunnen maken. Het ontwerp van de leaf van de multi-leaf collimator is van groot belang vanwege de invloed op de penumbra. Om het ontwerp van een leaf te optimaliseren is het in de praktijk nodig een balans te vinden tussen de transmissie van de leaves, de afstand waarover ze in het veld kunnen bewegen, de positie in de collimator en het totale volume, gerelateerd aan de kosten van het apparaat. In **hoofdstuk 5** is een analytische aanpak gegeven voor het optimaliseren van het leaf ontwerp van een MLC in een lineare versneller. Hiervoor is een model van de linac gemaakt waarin de volgende parameters zijn opgenomen: de grootte van de stralingsbron, de maximale veldgrootte, de afstand tussen bron en isocentrum en de ontwerpparameters van de leaves. Met de keuze van een dikte van de leaves van respectievelijk 3.5, 4 en 5 cm voor de laagste, middelste en hoogste leaf banken, werd een vergelijkbare totale fluentie penumbra bereikt voor alle lagen.

Het ontwerp van een linac/MLC is van groot belang voor de IMRT behandeling van patienten. Het effect van de verschillende keuze van linac/MLC parameters is gekarakteriseerd en gekwantificeerd. Als resultaat van deze bevindingen is een nieuw ontwerp voor een MLC voorgesteld. Door verdere verbetering van beeldgestuurde radiotherapie (IGRT) en de dagelijkse toepassing van on-line positieverificatie zal een verdere reductie van marges mogelijk zijn. Hiermee kan de zes-bank MLC grote voordelen hebben ten opzichte van conventionele MLCs.

References

Austin-Seymour M, Chen G T Y, Rosenman J, Michalski J, Lindsley K and Goitein M 1995 Tumor and target delineation: current research and future challenges *International Journal of Radiation Oncology, Biology and Physics* **33** 1041–1052

Bär W, Albert M and Nüssilin F 2001 A variable fluence step clustering and segmentation algorithm for step and shoot imrt *Physics in Medicine and Biology* **46** 1997–2007

Bortfeld T, Bürkelbach J, Boesecke R and Schlegel W 1990 Methods of image reconstruction from projections applied to conformation radiotherapy *Physics in Medicine and Biology* **35** 1423–1434

Bortfeld T, Oelfke U and Nill S 2000 What is the optimum leaf width of a multileaf collimator? *Medical Physics* **27** 2494–2502

Bortfeld T, Schlegel W and Rhein B 1993 Decomposition of pencil beam kernels for fast dose calculations in three-dimensional treatment planning *Medical Physics* **20** 311–318

Bortfeld T R, Kahler D L, Waldron T J and Boyer A L 1994 X-ray field compensation with multileaf collimators *International Journal of Radiation Oncology, Biology and Physics* **28** 723–730

Budgell G J 1999 Temporal resolution requirements for intensity modulated radiation therapy delivered by multileaf collimators *Physics in Medicine and Biology* pp. 1581–1596

Bureau of Radiological Health (ed.) 1970 *Radiological Health Handbook* (U.S. Department of Health, Education, and Welfare) revised edn.

Burmeister J, McDermott PN, Bossenberger T, Ben-Josef E, Levin K and Forman JD 2004 Effect of MLC leaf width on the planning and delivery of SMLC IMRT using the CORVUS inverse treatment planning system *Medical Physics* **31** 3187–3193

Chen Y, Boyer A L and Ma C M 2000 Calculation of x-ray transmission through a multileaf collimator *Medical Physics* **27** 1717–1726

Chui C, Chan M F, Yorke E, Spirou S and Ling C C 2001 Delivery of intensity-modulated radiation therapy with conventional multileaf collimator: Comparison of dynamic and segmental methods *Medical Physics* **28** 2441–2449

Convery D J and Webb S 1998 Generation of discrete beam-intensity modulation by dynamic multileaf collimation under minimum leaf separation constraints *Physics in Medicine and Biology* **43** 2521–2538

Cosgrove V P, Jahn U, Pfaender M, Bauer S, Budach V and Wurm R E 1999 Commissioning of micro multi-leaf collimator and planning system for stereotactic radiosurgery *Radiotherapy and Oncology* **50** 325–336

Cruz M, Tsuda K, Narumi Y, Kuroiwa Y, Nose T, Kojima Y, Okuyama A, Takahashi S, Aozasa K, Barentsz J O and Nakamura H 2002 Characterization of low-intensity lesions in the peripheral zone of prostate on pre-biopsy endorectal coil MR imaging *European Radiology* **12** 357–365

Dai J R and Hu Y M 1999 Intensity-modulation radiotherapy using independent collimators: An algorithm study *Medical Physics* **26** 2562–2570

Das I J, Desobry G E, McNeeley S W and Cheng E C 1998 Beam characteristics of a retofitted double-focused multileaf collimator *Medical Physics* **25** 1676–1684

Eisbruch A, Ten Haken R K, Kim H M, Marsh L H and Ship J A 1999 Dose, volume, and function relationships in parotid salivary glands following conformal and intensity-modulated radiation of head and neck cancer *International Journal of Radiation Oncology, Biology and Physics* **45** 577–587

Evans P M and Partridge M 2000 A method of improving the spatial resolution of treatments that involve a multileaf collimator *Physics in Medicine and Biology* **45** 609–622

Fiveash JB, Murshed H, Duan J, Hyatt M, Caranto J, Bonner JA and Popple RA 2002 Effect of multileaf collimator leaf width on physical dose distributions in the treatment of CNS and head and neck neoplasms with intensity modulated radiation therapy *Medical Physics* **29** 1116–1119

Galvin J M, Chen X G and Smith R M 1993a Combining multileaf fields to modulate fluence distributions *International Journal of Radiation Oncology, Biology and Physics* **27** 697–705

Galvin J M, Han K and Cohen R 1998 A comparison of multileaf-collimator and alloy-block field shaping *International Journal of Radiation Oncology, Biology and Physics* **40** 721–731

Galvin J M, Smith A R and Lally B 1993b Characterization of a multi-leaf collimator system *International Journal of Radiation Oncology, Biology and Physics* **25** 181–192

Galvin J M, Smith A R, Moeller R D, Goodman R L, Powlis W D, Rubenstein J, Solin L J, Michael B, Needham M, Huntzinger C J and Kligerman M M 1992 Evaluation of multileaf collimator design for a photon beam *International Journal of Radiation Oncology, Biology and Physics* **23** 789–801

Hartmann G H and Föhlisch F 2002 Dosimetric characterization of a new miniature multileaf collimator *Physics in Medicine and Biology* **47** N171–N177

Huch Böni R A, Meyenberger C, Pok Lundquist J, Trinkler F, Lutolf U and Krestin G P 1996 Value of endorectal coil versus body coil MRI for diagnosis of recurrent pelvic malignancies *Abdominal Imaging* **21** 345–352

Huq M S, Das I J, Steinberg T and Gavin J M 2002 A dosimetric comparison of various multileaf collimators *Physics in Medicine and Biology* **47** N159–N170

Jaffray D A, Battista J J, Fenster A and Munro P 1993 X-ray sources of medical linear accelerators: Focal and extra-focal radiation *Medical Physics* **20** 1417–1427

Jaffray D A, Siewerdsen J H, Wong J W and Martinez A A 2002 Flat-panel cone-beam computed tomography for image-guided radiation therapy *International Journal of Radiation Oncology, Biology and Physics* **53** 1337–1349

Jaffray D A, Yan D and Wong J W 1999 Managing geometric uncertainty in conformal intensity-modulated radiation therapy *Seminars in Radiation Oncology* **9** 4–19

Jordan T J and Williams P C 1994 The design and performance characteristics of a multileaf collimator *Physics in Medicine and Biology* **39** 231–251

Khan F M 1994 *The Physics of Radiation Therapy* (Baltimore, USA: Williams & Wilkins) 2nd edn.

Killoran J H, Giraud J Y and Chin L 2002 A dosimetric comparison of two multileaf collimator designs *Medical Physics* **29** 1752–1758

Kubo H D, Wilder R B and Pappas C T E 1999 Impact of collimator leaf width on stereotactic radiosurgery and 3D conformal radiotherapy treatment plans *International Journal of Radiation Oncology, Biology and Physics* **44** 937–945

Lagendijk J J W and Bakker C J G 2000 MRI guided radiotherapy: a MRI based linear accelerator in *ESTRO-2000: Abstracts* Istanbul European Society for Therapeutic Radiation Oncology

Lagendijk J J W, Raaymakers B W, Van Der Heide U A, Topolnjak R, Dehnad H, Hofman P, Nederveen A J, Schulz I M, Welleweerd J and Bakker C J G 2002 Mri guided radiotherapy: Mri as position verification system for imrt in *Radiotherapy and Oncology* vol. 64 (Suppl. 1) p. abstract 224 Prague, Czech Republic European Society for Therapeutic Radiation Oncology

Langen K M and Jones D T L 2001 Organ motion and its management *International Journal of Radiation Oncology, Biology and Physics* **50** 265–278

Leal A, Sanchez-Doblado F, Arrans R, Capote R, Lagares J I, Pavon E C and Rosello J 2004 MLC leaf width impact on the clinical dose distribution: a Monte Carlo approach *International Journal of Radiation Oncology, Biology and Physics* **59** 1548–1559

Ling C C, Humm J, Larson S, Amols H, Fuks Z, Leibel S and Koutcher J A 2000 Towards multidimensional radiotherapy (MD-CRT): biological imaging and biological conformality *International Journal of Radiation Oncology, Biology and Physics* **47** 551–560

Liu H H, Mackie T R and McCullough E C 1997 A dual source photon beam model used in convolution/superposition dose calculations for clinical megavoltage x-ray beams *Medical Physics* **24** 1960–1974

Loewenthal E, Loewinger E, Bar-Avraham E and Barnea G 1992 Measurement of the source size of a 6- and 18-MV radiotherapy linac *Medical Physics* **19** 687–690

Mackie T R, Ahnesjö A, Dickof P and Snider A 1987 Development of a convolution/superposition method for photon beams in *The Use of Computers in Radiation Therapy* pp. 107–110 ICCR

Mackie T R, Holmes T, Swerdloff S, Reckwerdt P, Deasy J O, Yang J, Paliwal B. and Kinsella T 1993 Tomotherapy: a new concept for the delivery of dynamic conformal radiotherapy *Medical Physics* **20** 1709–1719

Martinez A A, Di Yan F A C R, Lockman D, Brabbins D, Kota K, Sharpe M, Jaffray D A, Vicini F and Wong J 2001 Improvement in dose escalation using the process of adaptive radiotherapy combined with three-dimensional conformal or intensity-modulated beams for prostate cancer *International Journal of Radiation Oncology, Biology and Physics* **50** 1226–1234

Meeks S L, Bova F J, Kim S, Tomé W A, Buatti J M and Friedman W A 1999 Dosimetric characteristics of a double-focused miniature multileaf collimator *Medical Physics* **26** 729–733

Mohan R, Wu Q, Manning M and Schmidt-Ullrich R 2000 Radiobiological considerations in the design of fractionation strategies for intensity-modulated radiation therapy of head and neck cancers *International Journal of Radiation Oncology, Biology and Physics* **46** 619–630

Nederveen A J, Van der Heide U A, Hofman P, Welleweerd H and Lagendijk J J W 2001 Partial boosting of prostate tumours *Radiotherapy and Oncology* **61** 117–126

Nill S, Tücking T, Münter M W and Oelfke U 2005 Intensity modulated radiation therapy with multileaf collimators of different leaf widths: a comparison of achievable dose distributions *Radiotherapy and Oncology* **75** 106–111

Otto K and Clark B G 2002 Enhancement of IMRT delivery through MLC rotation *Physics in Medicine and Biology* **47** 3997–4017

Otto K, Clark B G and Huntzinger C 2002 Exploring the limits of spatial resolution in radiation dose delivery *Medical Physics* **29** 1823–1831

Raaymakers B W, Lagendijk J J W, Van der Heide U A, Overweg J, Brown K, Topolnjak R, Dehnad H, Jurgenliemk-Schulz I M, Welleweerd J and Bakker C J G 2004 Integrating a MRI scanner with a radiotherapy accelerator: a new concept of precise on line radiotherapy guidance and treatment monitoring in *The Use of Computers in Radiation Therapy*, eds. B Yong, S Do, E Kyung and W Sung pp. 89–92 ICCR Jeong Publishing

Raaymakers B W, Lagendijk J J W, Van der Heide U A and Topolnjak R 2003 The development of a linac-MRI combination for on-line position verification *European journal of medical physics* **XIX** 45

Raaymakers B W, Lagendijk J J W, Van Der Heide U A, Topolnjak R and Welleweerd J 2002 Imrt fluency compensation of heterogeneous beam transmission through an mri cryostat and gradient coils in *Radiotherapy and Oncology* vol. 64 (Suppl. 1) p. abstract 703 Prague, Czech Republic European Society for Therapeutic Radiation Oncology

Roesink J M, Moerland M A, Battermann J J, Hordijk G J and Terhaard C H J 2001 Quantitative dose-volume response analysis of changes in parotid gland function after radiotherapy in the head-and-neck region *International Journal of Radiation Oncology, Biology and Physics* **51** 938–946

Shepard D M, Olivera G, Angelos L, Sauer O and Reckwerdt P 1999 A simple model for examining issues in radiotherapy optimization *Medical Physics* **26** 1212–1221

Shigley J E and Mischke C R 1989 *Mechanical Engineering Design* (McGraw Hill) 5th edn.

Siochi R 1999a Virtual Micro-IMRT *Medical Physics* **26** 1096

Siochi R A C 1999b Minimizing static intensity modulation delivery time using an intensity solid paradigm *International Journal of Radiation Oncology, Biology and Physics* **43** 671–680

Spiessl B, Hermanek P, Scheibe O and Wagner G 1985 *TNM-Atlas* (Berlin, Germany: Springer-Verlag) 2nd edn.

Stroom J C, de Boer J C J, Huizenga H and Visser A G 1999 Inclusion of geometrical uncertainties in radiotherapy treatment planning by means of coverage probability *International Journal of Radiation Oncology, Biology and Physics* **43** 905–919

Sun J and Zhu Y 1995 Study of dosimetric penumbra due to multileaf collimation on a medical linear accelerator *International Journal of Radiation Oncology, Biology and Physics* **32** 1409–1417

Topolnjak R, van der Heide U A and Lagendijk J J W 2005 IMRT sequencing for a six-bank multi-leaf system *Physics in Medicine and Biology* **50** 2015–2031

Topolnjak R, van der Heide U A, Raaymakers B W, Kotte A N T J and Lagendijk J J W 2003a IMRT sequencing for a six banks multi-leaf system in *Radiotherapy and Oncology* vol. 68 (Suppl. 1) p. abstract 330 Geneva, Switzerland European Society for Therapeutic Radiation Oncology

Topolnjak R, van der Heide U A, Raaymakers B W, Kotte A N T J, Welleweerd J and Lagendijk J J W 2002 Six banks multi-leaf system, high resolution and large field size MLC in *Radiotherapy and Oncology* vol. 64 (Suppl. 1) p. abstract 107 Prague, Czech Republic European Society for Therapeutic Radiation Oncology

Topolnjak R, van der Heide U A, Raaymakers B W, Kotte A N T J, Welleweerd J and Lagendijk J J W 2003b Six-bank multi-leaf system for IMRT *European journal of medical physics* **XIX** 59

Topolnjak R, van der Heide U A, Raaymakers B W, Kotte A N T J, Welleweerd J and Lagendijk J J W 2004a A six-bank multi-leaf system for high precision shaping of large fields *Physics in Medicine and Biology* **49** 2645–2656

Topolnjak R, Van der Heide U A and W Lagendijk J J 2004b IMRT sequencing for a six-bank multi-leaf collimator system in *The Use of Computers in Radiation Therapy*, eds. B Yong, S Do, E Kyung and W Sung pp. 322–324 ICCR Jeong Publishing

Van Herk M, Remeijer P, Rasch C and Lebesque J V 2000 The probability of correct target dosage: dose-population histograms for deriving treatment margins in radiotherapy *International Journal of Radiation Oncology, Biology and Physics* **47** 1121–1135

Van Santvoort J P C and Heijmen B J M 1996 Dynamic multileaf collimation without 'tongue-and-groove' underdosage effects *Physics in Medicine and Biology* **41** 2091–2105

Van Vulpen M, Field C, Raaijmakers C P, Parliament M B, Terhaard C H, MacKenzie M A, Scrimger R, Lagendijk J J W and Fallone B G 2005 Comparing step-and-shoot IMRT with dynamic helical tomotherapy IMRT plans for head-and-neck cancer *International Journal of Radiation Oncology, Biology and Physics* **62** 1535–9

Vicini F A, Abner A, Baglan K L, Kestin L L and Martinez A A 2001 Defining a dose-response relationship with radiotherapy for prostate cancer: is more really better? *International Journal of Radiation Oncology, Biology and Physics* **51** 1200–1208

Wang L, Hoban P, Paskalev K, Yang J, Li J, Chen L, Xiong W and Ma CC 2005 Dosimetric advantage and clinical implication of a micro-multileaf collimator in the treatment of prostate with intensity-modulated radiotherapy *Medical Dosimetry* **30** 97–103

Wang L, Movsas B, Jacob R, Fourkal E, Chen L, Price R, Feigenberg S, Konski A, Pollack A and Ma C 2004 Stereotactic IMRT for prostate cancer: dosimetric impact of multileaf collimator leaf width in the treatment of prostate cancer with IMRT **5** 29–41

Webb S 2001a Concepts for shuttling multileaf collimators for intensity-modulated radiation therapy *Physics in Medicine and Biology* **46** 637–651

Webb S 2001b *Intensity-modulated radiation therapy* Medical Sience Series (Bristol, UK: IOP Publishing Ltd)

Webb S 2002 Intensity-modulated radiation therapy using only jaws and a mask *Physics in Medicine and Biology* **47** 257–275

Williams P C and Cooper P 2000 High-resolution field shaping utilizing a masked multileaf collimator *Physics in Medicine and Biology* **45** 2313–2329

Wu Y, Yan D, Sharpe M B, Miller B and Wong J W 2001 Implementing multiple static field delivery for intensity modulated beams *Medical Physics* **28** 2188–97

Xia P, Geis P, Xing L, Ma C, Findley D, Forster K and Boyer A 1999 Physical characteristics of a miniature multileaf collimator *Medical Physics* **26** 65–70

Xia P and Verhey L J 1998 Multileaf collimator leaf sequencing algorithm for intensity modulated beams with multiple static segments *Medical Physics* **25** 1424–1434

Yu C X 1998 Design considerations for the sides of multileaf collimator leaves *Physics in Medicine and Biology* **43** 1335–1342

Zelefsky M J, Fuks Z, Happersett L, Lee H J, Ling C C, Burman C M, Hunt M, Wolfe T, Venkatraman E S, Jackson A, Skwarchuk and Leibel S A 2000 Clinical experience with intensity modulated radiation therapy (IMRT) in prostate cancer *Radiotherapy and Oncology* **55** 241–249

Zhu T C, Bjärngard B E and Shackford H 1995 X-ray source and the output factor *Medical Physics* **22** 793–798

Zhu X R, Klein E E and Low D A 1998 Geometric and dosimetric analysis of multileaf collimation conformity *Radiotherapy and Oncology* **47** 63–68

Zhu X R, Prado K, Liu H H, Guerrero T M, Jeter M, Liao Z, Rice D, Forster K and Stevens C W 2005 Intensity-modulated radiation therapy for mesothelioma: impact of multileaf collimator leaf width and pencil beam size on planning quality and delivery efficiency *International Journal of Radiation Oncology, Biology and Physics* **62** 1525–1534

Publications

Papers in international journals

- Topolnjak R, van der Heide U A, Raaymakers B W, Kotte A N T J, Welleweerd J and Lagendijk J J W 2004 A six-bank multi-leaf system for high precision shaping of large fields *Phys. Med. Biol.* **49** 2645–2656
- Topolnjak R, van der Heide U A and Lagendijk J J W 2005 IMRT sequencing for a six-bank multi-leaf system *Phys. Med. Biol.* **50** 2015–2031
- Topolnjak R, van der Heide U A, Meijer G, van Asselen B, Raaijmakers C R J and Lagendijk J J W Influence of the Linac design on IMRT **(submitted)**
- Topolnjak R and van der Heide U A MLC Leaf design **(submitted)**

Papers in conference proceedings

- Topolnjak R, Van der Heide U A and W Lagendijk J J 2004b IMRT sequencing for a six-bank multi-leaf collimator system in *The Use of Computers in Radiation Therapy*, eds. B Yong, S Do, E Kyung and W Sung pp. 322–324 ICCR Jeong Publishing
- Raaymakers B W, Lagendijk J J W, Van der Heide U A, Overweg J, Brown K, Topolnjak R, Dehnad H, Jurgenliemk-Schulz I M, Welleweerd J and Bakker C J G 2004 Integrating a MRI scanner with a radiotherapy accelerator: a new concept of precise on line radiotherapy guidance and treatment monitoring in *The Use of Computers in Radiation Therapy*, eds. B Yong, S Do, E Kyung and W Sung pp. 89–92 ICCR Jeong Publishing

Abstracts in conference proceedings

- Topolnjak R, van der Heide U A, Raaymakers B W, Kotte A N T J, Welleweerd J and Lagendijk J J W 2002 Six banks multi-leaf system, high resolution and large field size MLC in *Radiotherapy and Oncology* vol. 64 (Suppl. 1) p. abstract 107 Prague, Czech Republic European Society for Therapeutic Radiation Oncology

- Lagendijk J J W, Raaymakers B W, Van Der Heide U A, Topolnjak R, Dehnad H, Hofman P, Nederveen A J, Schulz I M, Welleweerd J and Bakker C J G 2002 MRI guided radiotherapy: MRI as position verification system for IMRT in *Radiotherapy and Oncology* vol. 64 (Suppl. 1) p. abstract 224 Prague, Czech Republic European Society for Therapeutic Radiation Oncology
- Raaymakers B W, Lagendijk J J W, Van Der Heide U A, Topolnjak R and Welleweerd J 2002 IMRT fluency compensation of heterogeneous beam transmission through an MRI cryostat and gradient coils in *Radiotherapy and Oncology* vol. 64 (Suppl. 1) p. abstract 703 Prague, Czech Republic European Society for Therapeutic Radiation Oncology
- Topolnjak R, van der Heide U A, Raaymakers B W, Kotte A N T J, Welleweerd J and Lagendijk J J W 2003 Six-bank multi-leaf system for IMRT *European journal of medical physics* **XIX** 59
- Raaymakers B W, Lagendijk J J W, Van der Heide U A and Topolnjak R 2003 The development of a linac-MRI combination for on-line position verification *European journal of medical physics* **XIX** 45
- Topolnjak R, van der Heide U A, Raaymakers B W, Kotte A N T J and Lagendijk J J W 2003a IMRT sequencing for a six banks multi-leaf system in *Radiotherapy and Oncology* vol. 68 (Suppl. 1) p. abstract 330 Geneva, Switzerland European Society for Therapeutic Radiation Oncology
- Topolnjak R, van der Heide U A, Raaijmakers C P J, Meijer G J and Lagendijk J J W 2005b Influence of the linac design on IMRT in *Radiotherapy and Oncology* vol. 76 (Suppl. 2) p. abstract 197 Lissabon, Portugal European Society for Therapeutic Radiation Oncology

Patent

- Topolnjak R, van der Heide U A and Lagendijk J J W 24 October 2003 Multi-leaf Collimator *The United Kingdom Patent Office* Patent Application Number 0315909.2

Acknowledgments

The years I have spent doing my PhD were tough at times, but still maybe the most beautiful I had. Not only because I was doing work I liked, but also because of the nice colleagues and enjoyable atmosphere at the department. Therefore, I would like to thank the people I worked with, and those who have contributed in writing this book in one way or another.

First of all, I would like to thank professor Jan Lagendijk whose enormous enthusiasm and positive thinking were always inspiring. Jan, you knew how to motivate me and give me back hope when I did not know in which direction my research should go. Your understanding for my (private) obligations, which were sometimes conflicting with my work, was essential in finishing this thesis. Thank you for giving me the opportunity to work on such an interesting and challenging project.

A word of thanks goes to Uulke van der Heide, my supervisor. Uulke, scientific discussions with you were at times really tough, but fruitful. I am grateful for the numerous corrections of my English, especially of 'a' and 'the' articles, the purpose and use of which I hope to understand one day. I would also like to mention all the nice dinners we had, with hope that there are more to come.

The reason why my stay at the department was so enjoyable is definitely because of the people who were my officemates over the past years. First, a word of thanks goes to Jeroen van de Kamer. Jeroen, you were incredibly patient with my Dutch.
Following is my thanks to Bas Raaymakers, Gijsbert Bol and Anna Petoukhova. Bas, I have learnt a lot from you and have truly enjoyed our discussions. Gijs, you were my software guru. Anna, thanks for the numerous advices on parenting. In the last year, my officemates was Alexander Raaijmakers with whom I had many passionate political discussions. Alexander, it was a great fun!

I need to thank Alexis Kotte who patiently spent days helping me with programming problems. He also opened the door of object oriented programming to me, from where there is no way back. I always had 'one small question', but we both knew that we might be searching for some hours or days for the answer. Alexis, it was nice to work with you.
I performed a part of the experiments in the Catharina Hospital in Eindhoven. I would like to thank Gert Meijer who always had time for my questions and was always incredibly kind.

I would also like to acknowledge other (ex)PhD students and Post-Docs at the department with whom I had nice coffee breaks, occasional drinks and quite a bit of fun. Those are Aart Nederveen, Bob van den Berge, Cécile Jeukens, Eleftheria Astreinidou, Ellen Otten, Hugo Kroeze, Marion van Gellekom, Vera Lagerburg and Veronica Flyckt. Here, special thanks to Nico van den Berg. Nico, lunch discussion about the topic of the day were a great fun. Thanks for being my paranimf.
Clinical physicists (in training) that I would like to add to this acknowledgement are Astrid de Leeuw, Bram van Asselen, Danny Schuring, Hans Welleweerd, Martijn Ketelaars, Niels Raaijmakers and Rien Moerland. I would also like to add here doctors Marco van Vulpen and Homan Dehnad with whom I have had interesting discussions.

Colleagues from abroad with whom I have shared some homesick times were Maria Sastre Padro, Cemile Ceylan, and Boxue Liu.
The people in charge of ICT should definitely not to be forgotten: Kees Imhof, Ric Exterkate and Rob Uittenbogaard. I need to add here the Plato gurus who made my experiments possible: Theo van Soest and Ties Timmers. It was also pleasure to work and to cooperate with Bernard Klok and Jan Kok. A thanks also goes to administrative staff: Joke van Randwijk, Monique Slagter and Therese Vogel.
I would also like to thank Elekta co-workers for very constructive and critical discussions about the six-bank MLC, especially Kevin Brown for answering many questions about MLC design.
Thanks to Erik-Jan Rijkhorst, my new roommate at the Dutch Cancer Institute for helping me with the cover page of this book.

For different reasons I would also like to thank Joes Staal, Nicole Alkemade, Caroline Collard, Dieter Hauwaerts, Meindert Niemeijer, Davorka Ruškač,

Bart Seesing, Sanja and Marjano Budimir. They made me want to integrate. I would especially like to thank Ivan Rehak, my 'paraninf' and the only friend I have in the Netherlands from my student days in Zagreb. I hope that we will continue to have, together with our families, a lot of fun together, and many more football matches to watch (and not only those when Croatia loses). Damir Kovačić, the best friend from my student days, whose long-distance support and optimism were very important. Here, I would like to add Marin Soljačić, a friend since my high school days, whose experience and advices from his PhD student days abroad were of great help. Another friend since those days that I would like to acknowledge is Darija Buljan, a person I can always count on.

Finally, I would like to thank my family. Many thanks go to my dad, and mum who is always in my thoughts. Big thanks to my parents-in-law. You have always been a great support and without your grand parenting, writing this book would have been a lot more difficult.
At the end, I would like to thank my wife Ivana and my daughter Ema. My dear Ivana, it is impossible to express, how enormous and important your help and support were during all our years together. Without you, finishing this journey would certainly have been impossible. Ema, you make me happier than I have ever imagined I could be. I am proud to be your dad.

Curriculum Vitae

Rajko Topolnjak was born in 1974 in Zagreb, Croatia. From 1988-1992 he attended the High School for Mathematics and Computer Sciences in Zagreb. After graduation he decided to study Physics at the Faculty of Natural Sciences and Mathematics of the University of Zagreb. Three years later he chose to continue his education in Theoretical Physics. He graduated in the year 2000 with the work entitled 'State density of even-odd nucleus core'. Later that year he moved to The Netherlands to work at Silicon Biomedical Instruments BV in Arnhem. His work there was related to the analysis of Electroencephalograph data based on chaos theory and Fourier analysis. One year later he started as a PhD student at the Radiotherapy Department of the University Medical Center Utrecht, where he investigated the design of 'The six-bank multi-leaf system'. The results of the work are described in this thesis.